

# ABSTRACT

$\delta$ -CATENIN: IMPLICATIONS IN PROSTATE CANCER PROGRESSION

BY JONGDEE NOPPARAT

APRIL, 2014

DIRECTOR: DR. YAN-HUA CHEN

CO-DIRECTOR: DR. QUN LU

DEPARTMENT OF ANATOMY AND CELL BIOLOGY

Prostate cancer (PCa) is the most commonly diagnosed cancer and the second most common cause of cancer death among men in the US. Due to the advances in research, the ability to detect and cure PCa has improved and led to significant reductions in PCa patients' mortality. Therefore, determining and understanding specific molecular mechanisms involved in PCa progression is a pivotal step towards the potentially better and more accurate diagnosis and intervention of PCa in the future.

$\delta$ -Catenin is a unique armadillo (Arm) domain containing protein in that it is neural specific and primarily expressed in the brain. However,  $\delta$ -catenin alterations have been implicated in pathogenesis ranging from neuronal deficits, genetic disorders, to cancers. In particular,  $\delta$ -catenin expression is shown to increase in primary human prostatic adenocarcinomas corresponding with PCa progression. Although overexpressed  $\delta$ -catenin in PCa has been reported over a decade ago, few studies have been undertaken to identify how  $\delta$ -catenin promotes PCa progression and what other significant molecules are relevant to its expression. Studies presented in this dissertation explore the effects of a truncated variant of  $\delta$ -catenin involved in promoting PCa using both *in vitro* PCa culture systems and *in vivo* mouse models of

PCa. Additionally, we aim to test the hypothesis that  $\delta$ -catenin mutations promote PCa progression by interacting with multiple cancer-specific pathways including  $\beta$ -catenin/LEF-1-mediated transcription and HIF-1 $\alpha$ .

Information presented in this dissertation demonstrates that ectopic  *$\delta$ -catenin* gene is susceptible to mutagenesis when overexpressed in PCa cells, CWR22Rv-1 and PC-3, leading to sequence disruptions predicting functional alterations. It is shown that PCa cells overexpressing mutant  $\delta$ -catenin increase  $\beta$ -catenin translocation to the nucleus and HIF-1 $\alpha$  expression when cultured under glucose deprived condition. These results suggest that  $\delta$ -catenin mutations provide a survival advantage upon overgrowth and glucose deprivation over the control cells. Furthermore, we demonstrate that  *$\delta$ -catenin* mutations promote tumor development in mouse prostate with probasin promoter (ARR<sub>2</sub>PB)-driven, prostate specific expression of *Myc* oncogene. Additional investigations indicate that  $\delta$ -catenin mutations in *Myc* transgenic mice not only promote  $\beta$ -catenin expression leading to dramatically elevated *Myc* expression but HIF-1 $\alpha$  is also increased in a  *$\delta$ -catenin* gene-dosage dependent manner. Overall, we reveal that the introduction of  $\delta$ -catenin mutations is an important step in metabolic adaptation by modulating  $\beta$ -catenin and HIF-1 $\alpha$  signaling in order to magnify its tumor promoting effect.

$\delta$ -CATENIN: IMPLICATIONS IN PROSTATE CANCER PROGRESSION

A Dissertation

Presented to

The Academic Faculty of the Department of  
Anatomy & Cell Biology

by

Jongdee Nopparat

In Partial Fulfillment

of the Requirements for the Degree

Doctor of Philosophy in Anatomy & Cell Biology

East Carolina University

April, 2014

©Copyright 2014

Jongdee Nopparat

**δ-CATENIN: IMPLICATIONS IN PROSTATE CANCER PROGRESSION**

by

Jongdee Nopparat, B.S.

**APPROVED BY:**

DIRECTOR OF DISSERTATION: \_\_\_\_\_  
Yan-Hua Chen, Ph.D.

CO-DIRECTOR OF DISSERTATION: \_\_\_\_\_  
Qun Lu, Ph.D.

COMMITTEE MEMBER: \_\_\_\_\_  
Warren Knudson, Ph.D.

COMMITTEE MEMBER: \_\_\_\_\_  
Edward L. Apetz, M.D.

COMMITTEE MEMBER: \_\_\_\_\_  
Heng Hong, M.D, Ph.D.

CHAIR OF THE DEPARTMENT OF ANATOMY & CELL BIOLOGY:  
\_\_\_\_\_  
Cheryl B. Knudson, Ph.D.

DEAN OF THE GRADUATE SCHOOL:  
\_\_\_\_\_  
Paul Gemperline, Ph.D.



## **DEDICATION**

To my parents Panida and Wijarn Nopparat

## ACKNOWLEDGEMENTS

First and foremost, I would like to thank my parents Panida and Wijarn Nopparat for their unwavering love, support, and encouragement throughout this process. Without them and all their encouragement, I could never have pursued my academic and professional goals.

I would like to gratefully and sincerely thank my mentors Dr. Yan-Hua Chen and Dr. Qun Lu for their guidance, understanding, patience, and most importantly, their encouragement during my graduate studies. Dr. Lu has been my role model and has patiently taught me to truly appreciate the intricacies of the scientific process. From him I have learned to perform my work to the best of my ability. I consider it an honor to work with and learn from him.

I also wish to acknowledge the faculty and staff of the Department of Anatomy and Cell Biology for providing a friendly environment and giving me the opportunity to pursue this degree. Appreciation is also extended to my precandidacy committee: Dr. Donald Fletcher, Dr. Yan-Hua Chen, Dr. John Smith, and Dr. Walter Jenkins for the support in the early days of my graduate career. To my candidacy committee: Dr. Yan-Hua Chen, Dr. Qun Lu, Dr. Warren Knudson, Dr. Edward L. Apetz, and Dr. Heng Hong, I truly appreciate all of your critical suggestions and time spent advising and encouraging me to think scientifically. Every committee meeting proved significant in advancing my dissertation.

Additionally, I am grateful for the experience and time of working with Dr. Cheryl B. Knudson, Dr. Ann B. Sperry, and Dr. Yan-Hua Chen early in my graduate work. I have broadened and gained the knowledge in other significant research fields. Your guidance has also been very helpful throughout my graduate studies.

It is with immense gratitude that I acknowledge the love and support of Dr. Donald Fletcher who has always treated me like I was part of his family. Everything he has done has meant so much to me, especially since I am far from home. So I sincerely thank you, Dr. Fletcher and I would like to extend my gratitude to his wife, Elaine Fletcher, for her kindness as well.

To the past and present members of the Lu lab: Dr. Jiao Zhang, Dr. Amy Friesland, Christi Boykin, and Yi (Neo) Zhu, who have made the lab a wonderful place to work. To Joani Zary-Oswald and to Chen Lab members, especially, Rodney Tatum, who have been very generous and assisted me on both academic and non-academic issues.

Finally, to all the past and present graduate students in the Department of Anatomy and Cell Biology: Dr. Kristjan Thompson, Dr. Na Luo, and Dr. Lilliana Mellor, thanks for all the support in the early days. To Dr. Zhe (Wendy) Lu, Dr. Amy Friesland, and Nicole DeVaul, you have been such wonderful friends to me. To Ben Danielson and Jonathan Busada, you have provided much needed humor and entertainment. You all have made it a pleasure to come to school every day. I have shared my good days, and more importantly the bad days with you and I am truly grateful for friendship, encouragement, and moments of laughter. I wish you all the best in whatever your future holds.

# TABLE OF CONTENTS

	<b>PAGE</b>
LIST OF FIGURES .....	vii
LIST OF TABLES .....	x
LIST OF SYMBOLS AND ABBREVIATIONS .....	xi
CHAPTER I. Introduction .....	1
A. Prostate .....	1
Human prostate.....	1
Mouse prostate .....	1
B. Prostate cancer.....	2
C. Mouse model of prostate cancer.....	4
D. Regulation of epithelial cell architecture.....	6
Adherens junction.....	6
Cadherin-catenin complex.....	6
$\beta$ -Catenin subfamily .....	8
p120-Catenin subfamily .....	10
$\delta$ -Catenin .....	11
E. $\delta$ -Catenin and prostate cancer .....	13
Evidence for $\delta$ -catenin involvement in PCa.....	13
Regulation of $\delta$ -catenin in PCa.....	16
$\delta$ -Catenin: potential cross-regulation in Wnt/ $\beta$ -catenin signaling in PCa...	17
Mutation-induced metabolic adaptation in cancer .....	18

F. Rational for current studies .....	20
G. Statement of hypothesis and specific aims.....	22
H. Significance .....	25
CHAPTER II. $\delta$ -Catenin: a Wnt/ $\beta$ -catenin modulator, reveals inducible	
mutagenesis promoting cancer cell survival adaptation and metabolic	
reprogramming.....	
	45
A. Summary .....	45
B. Introduction.....	46
C. Experimental procedures .....	47
C1. Antibodies and reagents.....	47
C2. Cell culture, mutagenesis, and transfection .....	48
C3. Genomic DNA extraction from tissue and PCR amplification of	
$\delta$ -catenin gene .....	49
C4. PCR products sequence analysis.....	52
C5. Genomic DNA extraction from cultured cell line and PCR	
amplification of mouse $\delta$ -catenin cDNA sequence .....	52
C6. Immunofluorescent light microscopy .....	53
C7. Western blot with ECL detection.....	54
C8. Chromosome spread preparation .....	54
C9. Fluorescence in situ hybridization (FISH).....	55
C10. Cell growth with high glucose or with glucose deprivation.....	56
C11. Metabolic measurement .....	57
C12. Preparation of nuclear and cytoplasmic protein fractions.....	57

D. Results.....	58
D1. Ectopically expressed $\delta$ -catenin is invariably mutated in prostate cancer cells.....	58
D2. There are hot-spot mutation cluster regions in <i>CTNND2</i> exons in human primary prostatic adenocarcinomas .....	60
D3. <i>CTNND2</i> mutations are not locus-selective.....	60
D4. $\delta$ -Catenin mutations lead to survival adaptation under glucose deprivation and reprogram energy utilization.....	61
E. Discussion.....	64
F. Acknowledgements.....	91
CHAPTER III. Mutations of $\delta$ -catenin contribute to mouse prostate tumorigenesis through enhanced $\beta$ -catenin-mediated oncogenic signals leading to increased cell proliferation and survival thereby promoting prostate tumor growth.....	
	92
A. Summary.....	92
B. Introduction.....	93
C. Experimental procedures .....	96
C1. Generation of transgenic mouse models.....	96
C2. DNA extraction and genotyping PCR-based analysis .....	96
C3. Mouse tissue preparation .....	97
C4. Histopathological analysis of mouse prostate tissue.....	98
C5. Immunofluorescent analysis of prostate tissue .....	98
C6. Protein analysis of prostate tissue .....	99

C7. Statistical analysis .....	100
D. Results .....	100
D1. Generation of Myc/ $\delta$ -cat double transgenic mouse model of PCa ...	100
D2. Gross anatomy of Myc/ $\delta$ -cat double transgenic mouse prostate displays mild phenotype .....	101
D3. Myc/ $\delta$ -cat double transgenic mouse prostate exhibits mouse prostatic intraepithelial neoplasia (mPIN) lesions .....	101
D4. Generation of Myc/ $\delta$ -catenin mutant mouse model of PCa .....	103
D5. Gross anatomy of Myc/ $\delta$ -catenin mutant mice display significant increased prostate size.....	104
D6. Myc/ $\delta$ -catenin mutant mice promote prostate tumor development in a mutation dose-dependent manner .....	104
D7. $\delta$ -Catenin mutations promote cell proliferation and apoptosis in Myc/ $\delta$ -catenin mutant mice .....	105
D8. Myc/ $\delta$ -catenin mutant mice reveal a dramatic increase in cells overexpressing Myc .....	107
D9. Myc overexpression does not mediate apoptosis in Myc/ $\delta$ -catenin mutant mice.....	107
D10. $\delta$ -Catenin mutations enhance $\beta$ -catenin and Myc expressions in Myc/ $\delta$ -catenin mutant mice .....	108
D11. $\delta$ -Catenin mutations promote HIF-1 $\alpha$ leading to metabolic adaptation.....	110
E. Discussion.....	111

F. Acknowledgements.....	145
CHAPTER IV. Characterization of prostatic epithelial cell lines established from	
$\delta$ -catenin mutant mice overexpressing <i>Myc</i> oncogene .....	146
A. Summary .....	146
B. Introduction .....	146
C. Experimental procedures.....	148
C1. Establishment of cell lines from <i>Myc</i> / $\delta^{+/+}$ and <i>Myc</i> / $\delta^{+/-}$ mouse	
PCa models .....	148
C2. PCR genotyping.....	149
C3. RNA isolation and reverse-transcription PCR.....	150
C4. Immunofluorescent analysis .....	151
C5. Western blot analysis .....	151
C6. Statistical analysis.....	152
D. Results.....	152
D1. Characterization of the novel murine prostate tumor cell lines .....	152
D2. Reverse-transcription PCR reveals phenotypic difference in	
C1- <i>Myc</i> / $\delta^{+/+}$ and C2- <i>Myc</i> / $\delta^{+/-}$ cell lines.....	153
D3. C1- <i>Myc</i> / $\delta^{+/+}$ and C2- <i>Myc</i> / $\delta^{+/-}$ cell lines are prostatic epithelial	
in origin.....	154
D4. Loss or altered distribution of E-cadherin and $\beta$ -catenin in	
C2- <i>Myc</i> / $\delta^{+/-}$ in comparison to that of C1- <i>Myc</i> / $\delta^{+/+}$ .....	154
D5. Altered Wnt/ $\beta$ -catenin signaling pathway elements in	
C2- <i>Myc</i> / $\delta^{+/-}$ in comparison to that of C1- <i>Myc</i> / $\delta^{+/+}$ .....	156

D6. C2-Myc/ $\delta^{+/-}$ promotes HIF-1 $\alpha$ and PKM <sub>2</sub> expression level.....	157
E. Discussion.....	157
CHAPTER V. Conclusions and general discussion .....	173
REFERENCES .....	179
APPENDIX A: Animal use protocol .....	191
APPENDIX B: Permission policy from NPG .....	192

## LIST OF FIGURES

	<b>PAGE</b>
1.1 Illustration of the anatomy and histology of mouse prostate.....	26
1.2 Pathway for mouse prostate tumor progression.....	28
1.3 Dendrogram showing sequence relationship between several members of the catenin family proteins.....	30
1.4 Schematic representation of the classical cadherin-catenin complex .....	32
1.5 Schematic representation of the canonical Wnt/ $\beta$ -catenin signaling pathway....	34
1.6 Comparisons of sequence analysis between $\delta$ -catenin, $\beta$ -catenin, and p120 <sup>ctn</sup> ...	36
1.7 Linear structural representation of full-length human $\delta$ -catenin .....	40
1.8 Schematic illustration represents the driving-force of abnormal metabolic phenotype of tumor cells .....	42
2.1 Mutations and formation of $\delta$ -catenin variants.....	69
2.2 Targeted mutation of <i><math>\delta</math>-catenin</i> cDNA generated the truncated protein with predicted size on SDS-gel.....	71
2.3 Mutation cluster regions (MCRs) of <i><math>\delta</math>-catenin</i> coding sequences in human prostate cancer .....	73
2.4 Summary of mutation cluster regions (MCRs) of <i><math>\delta</math>-catenin</i> coding regions in human prostate adenocarcinoma tissues.....	75
2.5 Cancer cells are capable of altering ectopic <i><math>\delta</math>-catenin</i> gene sequence and function .....	77
2.6 $\delta$ -Catenin truncation variant promotes overgrowth <i>in vitro</i> .....	79

<b>2.7</b>	$\delta$ -Catenin mutations promote metabolic reprogramming to increase cancer cell survival and adaptation under glucose deprivation.....	81
<b>2.8</b>	$\delta$ -Catenin mutations promote metabolic adaptation under glucose deprivation.	83
<b>2.9</b>	$\delta$ -Catenin mutations lead to survival adaptation under glucose deprivation .....	85
<b>2.10</b>	$\delta$ -Catenin mutations alter protein expression and distribution in the Wnt/ $\beta$ -catenin and hypoxia pathways .....	87
<b>2.11</b>	MCR of <i><math>\delta</math>-catenin</i> showing functional impacts .....	89
<b>3.1</b>	Production and analysis of Myc/ $\delta$ -cat double transgenic mice.....	116
<b>3.2</b>	Gross anatomy of Myc/ $\delta$ -cat double transgenic mouse prostate .....	118
<b>3.3</b>	Characteristic features of Myc/ $\delta$ -cat double transgenic mice .....	120
<b>3.4</b>	$\delta$ -Catenin overexpression in ectopically expressed <i>Myc</i> oncogene does not promote tumor progression in transgenic mice.....	122
<b>3.5</b>	Production and analysis of Myc/ $\delta$ -catenin mutant mice.....	124
<b>3.6</b>	Gross anatomy of Myc/ $\delta$ -catenin mutant mouse prostate.....	126
<b>3.7</b>	Characteristic features of Myc/ $\delta$ -catenin mutant mice .....	128
<b>3.8</b>	Histopathology analysis (H&E) of Myc/ $\delta^{-/-}$ mice .....	130
<b>3.9</b>	An increase in cell proliferation and apoptosis labeling index in Myc/ $\delta$ -catenin mutant mice .....	132
<b>3.10</b>	$\delta$ -Catenin mutations promote histone-H3 activity.....	134
<b>3.11</b>	$\delta$ -Catenin mutations promote number of cells overexpressing Myc .....	136
<b>3.12</b>	Myc does not mediate apoptosis in Myc/ $\delta$ -catenin mutant mice.....	138
<b>3.13</b>	$\delta$ -Catenin mutations enhance $\beta$ -catenin and Myc protein expression .....	140

<b>3.14</b>	$\delta$ -Catenin mutations induce HIF-1 $\alpha$ activity and affect expression profiles of Glut-1 and PKM <sub>2</sub> .....	142
<b>3.15</b>	Proposed model of $\delta$ -catenin-induced PCa progression in mouse model.....	144
<b>4.1</b>	Characterization of the C1-Myc/ $\delta^{+/+}$ and C2-Myc/ $\delta^{+/-}$ cell lines .....	161
<b>4.2</b>	C1-Myc/ $\delta^{+/+}$ and C2-Myc/ $\delta^{+/-}$ cell lines are epithelia in origin.....	163
<b>4.3</b>	C2-Myc/ $\delta^{+/-}$ reveals the reductions of E-cadherin and $\beta$ -catenin immunoreactivities.....	165
<b>4.4</b>	C2-Myc/ $\delta^{+/-}$ cells reveal increased cell apoptosis .....	167
<b>4.5</b>	$\delta$ -Catenin mutations in C2-Myc/ $\delta^{+/-}$ are correlated with upregulated Myc and cyclin D1 .....	169
<b>4.6</b>	$\delta$ -Catenin mutations in C2-Myc/ $\delta^{+/-}$ promote HIF-1 $\alpha$ and PKM <sub>2</sub> expressions...	171

## LIST OF TABLES

	<b>PAGE</b>
<b>1.1</b> $\delta$ -Catenin binding partners and outcomes of their interactions .....	40
<b>2.1</b> Specific primer sets for human <i><math>\delta</math>-catenin</i> .....	50
<b>2.2</b> Specific primer sets for mouse <i><math>\delta</math>-catenin</i> .....	52
<b>4.1</b> Primer sets used in PCR-based analysis .....	149
<b>4.2</b> Primer sets used in reverse transcription PCR-based analysis .....	150

## LIST OF SYMBOLS AND ABBREVIATIONS

Abl	Abelson tyrosine kinase
AD	Alzheimer's disease
AMPA	Alpha-amino-3-hydroxy-5-methyl-4 isoxazole propionate
AP	Anterior prostate
APC	Adenomatosis polyposis coli
AMPK	Adenosine monophosphate (AMP)-activated protein kinase
AR	Androgen receptor
Arm	Armadillo
ARR <sub>2</sub> PB	Two androgen response elements of the probasin promoter
ARVCF	Armadillo repeat gene deleted in Velo-cardio-facial syndrome
Bcl-2	B-cell lymphoma 2
BPH	Benign prostatic hyperplasia
BSA	Bovine serum albumin
CAM	Chick chorioallantoic membrane
CBD	Catenin binding domain
CC	Coiled-coil domain
CDCS	Cri-du-Chat syndrome
Cdk1	Cyclin-dependent kinase 1
Cdk5	Cyclin-dependent kinase 5
CDKN1B-p27	Cyclin-dependent kinase inhibitor 1B (p27, Kip1)
cDNA	Complementary deoxyribose nuclei acid

CNS	Central nervous system
Ctn	Catenin
CZ	Central zone
DLP	Dorsal lateral prostate
DMEM	Dulbecco's modified Eagle's medium
DNA	Deoxyribose nucleic acid
DP	Dorsal prostate
DRE	Digital rectal exam
DVL	Dishevelled
ECAR	Extracellular acidification rate
ECL	Enhanced chemiluminescence
EDTA	Ethylendiamine tetra acetic acid
FISH	Fluorescence in situ hybridization
FITC	Fluoresceine isothiocynate
FBS	Fetal bovine serum
Fz	Frizzled
GABA	Gamma-aminobutyric acid
GAP	GTPase activating protein
GAPDH	Glyceraldehyde 3-phosphate dehydrogenase
G418	Geneticin-418
GEF	Guanine nucleotide exchange factor
GFP	Green fluorescent protein
GDI	Guanine nucleotide dissociation inhibitor

GDP	Guanosine-diphosphate
GLS	Glutaminase
GluR1	Glutamate receptor 1
Glut-1	Glucose transporter 1
GRIP	Glutamate receptor-interacting protein
GSK-3	Glycogen synthase kinase 3
GSK-3 $\beta$	Glycogen synthase kinase 3 beta
HEPES	4-(2-hydroxyethyl)-1-piperazineethanesulfonic acid
Hes1	Human homolog of Drosophila Hairy and enhancer of split 1
HIF-1 $\alpha$	Hypoxia-inducible factor 1 isoform alpha
HK2	Hexokinase 2
JMD	Juxtamembrane domain
kDa	Kilodalton
LEF	Lymphoid enhancing factor
LP	Lateral prostate
LRP	Low density lipoprotein receptor related protein
MCR	Mutation cluster region
MDCK	Madin-Darby canine kidney
mGluR1a	Metabotropic glutamate receptor 1 alpha
mPIN	Mouse prostatic intraepithelial neoplasia
mRNA	Massager ribose nucleic acid
Myc	Myelocytomatosis virus oncogene cellular homolog
NF- $\kappa$ B	Nuclear factor kappa-light-chain-enhancer of activated B cells

NLS	Nuclear localization sequence
NPRAP	Neural plakophilin-related arm-repeat protein
NR2	N-methyl-D-aspartic acid receptor 2A
OCR	Oxygen consumption rate
OXPHOS	Oxidative phosphorylation
PAGE	Polyacrylamide gel electrophoresis
Pax6	Paired box 6
PARP	Poly Adenosine diphosphate ribose polymerase
PBS	Phosphate buffered saline
PCa	Human prostate cancer
PDZ	PSD-95/Dlg-A/ZO-1 PDZ
PI3K	Phosphoinositide-3 kinase
PIN	Prostatic intraepithelial neoplasia
PKM <sub>2</sub>	Pyruvate kinase isoform 2
PSA	Prostate specific antigen
PS-1	Presenilin-1
PSD-95	Postsynaptic density-95
PTEN	Phosphatase and tensin homolog
PZ	Peripheral zone
RB1	Retinoblastoma 1
Rheb	Ras homolog enriched in brain
Rho	Ras homologous
RhoA	Ras homologous member A

RhoGEF	Ras homologous guanine nucleotide exchange factors
RhoGTPase	Ras homologous activating proteins
RIPA	Radioimmuno precipitation assay
rPB	Rat probasin promoter
RPMI	Roswell Park Memorial Institute medium
SDS	Sodium dodecyl sulfate
SH3	Src homology 3
SNP	Single nucleotide polymorphism
S-SCAM	Synaptic scaffolding molecule
TCF	T-cell factor
TM	Transmembrane
TRAMP	Transgenic adenocarcinoma of the mouse prostate
TSC2	Tuberous sclerosis 2
TUNEL	Terminal deoxynucleotidyl transferase dUTP nick end labeling
TZ	Transition zone
VEGF	Vascular endothelial growth factor
VP	Ventral prostate
UV	Ultraviolet

## CHAPTER I: INTRODUCTION

### A. Prostate

#### *Human prostate*

In adult humans, the prostate is a small, walnut-shaped gland that encircles the upper urethra at the base of the bladder. As described in original work of McNeal (1988) the human prostate has one lobe divided into 3 distinct morphological zones; namely the periurethral transition zone (TZ), the peripheral zone (PZ), and the central zone (CZ). Histologically, the prostate consists of two major compartments, the stroma and the epithelium. The stromal component is comprised of smooth muscle cells, fibroblasts and endothelial cells. Five cell subtypes constitute the epithelium including basal epithelium, secretory epithelium, transit amplifying cells, neuroendocrine cells, and stem cells (Abate-Shen and Shen, 2000; Shen and Abate-Shen, 2010). The primary function of the prostate gland, which contracts with ejaculation, is to provide enzymes to maintain the fluid nature of seminal fluid and to nourish sperm as they pass through the prostatic and penile urethra to the outside of the body (McNeal, 1988).

#### *Mouse prostate*

In contrast with humans, the rodent prostate gland is divided into four distinct lobes; the anterior prostate (AP), also referred to as the coagulating gland, the ventral prostate (VP), the dorsal prostate (DP), and the lateral prostate (LP). The DP and LP are often grouped together as the dorsolateral prostate or DLP. Each lobe is surrounded and separated from the others by fibrous and adipose connective tissue. The VP is located below the ventral aspect of the bladder neck. The DLP lies in the triangular area between urethra and seminal vesicle (Fig. 1.1A).

Despite the anatomical differences, several studies have asserted that the mouse DLP is most similar to the PZ of human prostate, where prostate cancer usually develops. However, evidence supporting these analogies is primarily descriptive (Abate-Shen and Shen, 2000; Shen and Abate-Shen, 2010).

## **B. Prostate cancer**

Prostate cancer (PCa) is the most commonly diagnosed cancer and the second most common cause of cancer death among men in the US behind only lung cancer. The latest American Cancer Society estimates show that about 1 in 6 men in the US will be diagnosed with PCa during their lifetime and 1 in 36 will die from this disease (American Cancer Society, 2013). As described previously, the prostate consists of three major zones, the TZ is particularly associated with benign prostatic hyperplasia (BPH) which is a non-cancerous enlargement of the prostate and is very common in men as they age. The PZ, the outermost and most voluminous zone of the prostate, is also the most frequent site of PCa origin (Shappell et al., 2004).

Almost all PCa develop from the gland cells, termed adenocarcinoma (American Cancer Society, 2013). Shen et al (2010) propose a pathway for PCa progression including 4 stages; normal epithelium, Prostatic Intraepithelial Neoplasia (PIN), invasive adenocarcinoma, and metastasis. The primary precursor of PCa known as PIN can be classified into four common features: tufting, micropapillary, cribriform, and flat. The cytological features of PIN closely resemble those of invasive adenocarcinoma. This includes reduced expression of the cell adhesion protein E-cadherin. However, the PIN lesions display an intact basement membrane, and thus do not invade the stroma (Shen and Abate-Shen, 2010). Many PCa are slow-growing and may stay localized (entirely contained within the prostate) for many years and they are

unlikely to cause noticeable symptoms. The symptoms begin to emerge when the tumor mass grows large enough to constrict the urethra. This can cause symptoms such as: frequent urination, especially nocturia; a weak or interrupted urine stream; pain or burning upon urination or ejaculation; and discomfort in the lower back, pelvis, or upper thighs (Harvard Medical School 2013 annual report on prostate diseases).

The current non-invasive diagnostic approach of detecting PCa is to test the amount of prostate-specific antigen (PSA) in serum. Unfortunately, PIN lesions do not produce high levels of PSA. Moreover, PSA cannot accurately differentiate between PCa and BPH, which require different treatment methods (Burger et al., 2002). This leads to the massive efforts of research to find new diagnostic markers in order to detect PCa more efficiently and accurately than PSA. Clinically, digital rectal exam (DRE) is another conventional procedure for PCa detection. Suspected PCa is typically confirmed by prostate biopsy. One way of grading PCa is called the Gleason system. This system uses a Gleason score of 2 to 10 to grade PCa. A tumor with a low Gleason score is likely to be slow-growing, while one with a high score is more likely to grow aggressively or to have already metastasized to other sites, most commonly to bone. Patients with localized PCa can be treated by surgery or radiation therapy. For patients with advanced disease, hormonal ablation therapy is initially successful as most of the tumors are androgen-dependent. However, the disease will eventually progress to an androgen-independent state with metastases (Carlsson et al., 2012; Das and Zain, 2011; Mikuz, 1997).

At present, the exact triggers for PCa development have not been fully elucidated, however epidemiological studies have shown links to both environmental and genetic contributors. A variety of growth factors and cytokines have been shown to influence the growth rate and development of PCa, and a number of proteins and genes have been identified whose

regulation and/or function are altered between malignant and benign states. The common genetic changes found in PCa include deletions of regions harboring putative tumor suppressors on chromosome 8p (*NKx3.1*), 10q23 (*PTEN*), 12p13 (*CDKN1B-p27*), 13q (*RBI*) and 17q (*TP53*); gains in regions of oncogenes on chromosome 8q24 (*MYC*) and Xq (*AR*); and point mutations, i.e., *TP53* and *AR* (Abate-Shen and Shen, 2000; Elo and Visakorpi, 2001; Gopalkrishnan et al., 2001; Hartsock and Nelson, 2008; Pan et al., 2001; Shen and Abate-Shen, 2007, 2010). Several of these proteins and genes have been marked as potential biomarkers and therapeutic targets for PCa.

### **C. Mouse models of prostate cancer**

Although PCa is a common and serious health problem for humans, this cancer rarely occurs in other animal species. The lack of natural animal models for the disease has slowed the research of prostate biology and for finding new, more effective therapies (Greenberg et al., 1995). However, transgenic technology has been useful in this regard. Through recombinant DNA procedures and embryonic manipulation, one can construct artificial genes in which DNA promoter elements from one gene product are fused to the coding region of a different gene product. To date, the characterization of promoter elements that primarily target gene expression in the prostate has led to the generation of numerous mouse models of PCa. In particular, promoter elements of the rat probasin (rPB), androgen- and zinc-regulated protein, have proven to be successful in targeting gene expression in the VP and DLP lobes (Abate-Shen and Shen, 2002; Ellwood-Yen et al., 2003; Koh et al., 2010).

Myc is an oncogenic transcription factor overexpressed in a variety of tumor types. Particularly, the region encompassing the Myc locus (8q24) is amplified in late state/aggressive

PCa; therefore, it is widely held that *Myc* is involved in the disease progression (Abate-Shen and Shen, 2000; Iwata et al., 2010; Koh et al., 2010). Hi-*Myc* mice are a transgenic mouse model that uses the modified probasin ( $ARR_2/PB$ ) promoter to overexpress human *Myc* in a prostate-specific manner. These mice develop mouse PIN (mPIN) by 2 weeks of age and invasive adenocarcinoma of the prostate by 6-9 months (Ellwood-Yen et al., 2003). The phenotypes of Hi-*Myc* share a number of similarities with the human disease. For example, histological features of mPIN recapitulate stereotypical findings in human PIN, adenocarcinoma cells, and atypical changes in nuclear morphology. In addition, the phenotype of the cancer lesions in these *Myc*-based models is exclusively adenocarcinoma, with no evidence for the neuroendocrine carcinoma phenotype observed in tumor models based upon T antigen overexpression (i.e., TRAMP and LADY mouse models) (Abate-Shen and Shen, 2000, 2002; Iwata et al., 2010; Shen and Abate-Shen, 2010).

The histopathology of *Myc* transgenic mouse prostate generated in our laboratory can be classified into 3 stages, progressing from normal, to mPIN, and then to invasive adenocarcinoma. Our *Myc* transgenic animals display normal prostate gland at a young age (6 weeks old). A normal prostate gland is composed of 1 to 2 layers of columnar epithelium with basally located nuclei (Fig. 1.2A). As the *Myc* mice age, mPIN lesions develop and can be characterized by hyper-proliferation of epithelial cells within preexisting glandular spaces with a well-defined basement membrane. In addition to multi-layering of cells, these changes in mPIN lesions are accompanied by prominent nucleoli, nuclear shape variability, and intraepithelial space formation (Fig. 1.2B). The prostate adenocarcinoma in *Myc* mice is recognized histologically by the penetration of malignant cells through the basement into the surrounding stroma (Fig. 1.2C). Although the transgenic mouse models fail to recapitulate all features of human PCa initiation

and progression, they are a very helpful tool in gaining a better understanding of molecular genetic alterations in PCa, and they can also be conveniently used for testing pre-clinical therapeutic strategies.

#### **D. Regulation of epithelial cell architecture**

##### *Adherens junction*

It is well documented that interaction of cell-cell contact known as the adherens junction is essential for the maintenance of epithelial integrity and polarity (Hartsock and Nelson, 2008; Makrilia et al., 2009). Adherens junctions occur in various forms. In many non-epithelial tissues, they take the form of small punctate or streak-like attachments that indirectly connect the cortical actin filaments beneath the plasma membranes of two interacting cells. However, the prototypical examples of adherens junctions occur in epithelia, where they often form a continuous adhesion belt, or zonula adherens, just below the tight junctions, encircling each of the interacting cells in the sheet (Hartsock and Nelson, 2008). The core molecular components of the adherens junction include interactions among transmembrane glycoproteins of the classical cadherin family and the catenin family members. Through this interaction, they perform multiple functions including initiation and stabilization of cell-cell adhesion, regulation of the actin cytoskeleton, intracellular signaling, and transcriptional regulation (Anastasiadis and Reynolds, 2000; Bussemakers et al., 2000; Davis et al., 2003; Gumbiner, 2005; Hartsock and Nelson, 2008; Paredes et al., 2007).

##### *Cadherin-catenin complex*

Cadherins represent a multigene family, encoding cell surface glycoproteins that connect

adjacent cells via calcium-dependent homophilic interactions between the cadherin extracellular domains. The most extensively studied cadherins are of the classical type, i.e., E-(epithelial), N-(neural), and P-(placental) cadherins. The classical cadherins are characterized by five conserved extracellular cadherin (EC) repeat domains, a single transmembrane segment, and an intracellular domain containing the juxtamembrane region and carboxyl-terminal domain. The carboxyl-terminus interacts with the microfilament cytoskeleton through the catenin complex (Bussemakers et al., 2000; Hartsock and Nelson, 2008).

The catenins are a family of cell adhesion molecules that share several structural and functional characteristics. The most noticeable features of the catenins are their central armadillo (Arm) repeats, a domain composed of 42-43 amino acid repeating sequences originally described in the *Drosophila* segment polarity gene *Armadillo* (Peifer et al., 1994). Such repeats fold to produce a super-helix of helices that bears a positively charged groove and crucial binding interfaces (Harrison et al., 2011; Huber et al., 1997). Based on the armadillo domains, protein and gene structure analysis revealed that the catenins (with the exception of the structurally unrelated  $\alpha$ -catenin) can be categorized into 3 subfamilies, which are as follow:  $\beta$ -catenin subfamily (12 armadillo repeats), p120-catenin subfamily (10 armadillo repeats), and plakophilin subfamily (10 armadillo repeats) (Fig. 1.3) (Hatzfeld, 2005; McCrea and Park, 2007).

$\beta$ - and  $\gamma$ -catenins can bind directly to the cadherin cytoplasmic domain, termed the catenin binding domain (CBD);  $\alpha$ -catenin, in turn, interacts with  $\beta$ - or  $\gamma$ -catenin and bridges the cadherin-catenin complex to the actin-filaments of the cytoskeleton (Makrilia et al., 2009). p120-Catenin and  $\delta$ -catenin bind to the so-called juxtamembrane domain (JMD), the proximal region of the cytoplasmic domain of E-cadherin (Lu et al., 1999). Through such associations, catenins participate in junctional assembly and maintenance, and assist with cadherin dependent

morphogenesis (Fig. 1.4). Numerous studies have demonstrated that loss of expression and/or abnormal function of cadherin-catenin complex leads to loss of cell polarity and derangement of normal tissue architecture, and thus association with many pathological processes. In most cancers of epithelial origin (i.e., prostate cancer, bladder cancer, and colorectal cancer) cell-cell adhesion is aberrant concomitantly with the gain of an invasive and aggressive phenotype (Jeanes et al., 2008; Makrilia et al., 2009; Reynolds and Carnahan, 2004). Therefore unraveling the molecular mechanisms that control cadherin-catenin expression and their regulation is an important element in understanding structural changes associated with cancer progression.

### *$\beta$ -Catenin subfamily*

$\beta$ -Catenin subfamily consists of  $\beta$ -catenin and  $\gamma$ -catenin (plakoglobin). Both  $\beta$ -catenin and  $\gamma$ -catenin are associated directly to CBD of E-cadherin and are interchangeable (Makrilia et al., 2009). Perhaps  $\beta$ -catenin (encoded by the gene *CTNNB1*) is the most widely characterized of these catenin proteins, likely due to its various biological functions which include essential roles in embryogenesis, maintenance of cell-adhesion, signal transducer, and cancer progression (Logan and Nusse, 2004; Willert and Jones, 2006; Yu et al., 2011). The signaling activity of  $\beta$ -catenin is intensely investigated as a member of the Wnt/Wingless signaling pathway. Briefly, in the absence of the Wnt ligand in the canonical signaling pathway, free cytoplasmic  $\beta$ -catenin is destabilized by the intracellular multiprotein complex (composed of Glycogen Synthase Kinase 3/GSK-3 $\beta$ , Axin, and Adenomatous Polyposis Coli/APC). Upon the binding of the multiprotein complex to the Axin/conductin, Axin interacts with GSK-3 $\beta$  in the complex and facilitates efficient phosphorylation of  $\beta$ -catenin by GSK-3 $\beta$ , most likely at serine and threonine residues in its amino-terminus. The phosphorylated  $\beta$ -catenin thus marks it for ubiquitination and

subsequent proteasome degradation. In the presence of the Wnt ligand, it binds to the membrane receptor Frizzled (Fz) and co-receptor Low density lipoprotein receptor related protein (LRP). Fz then interacts with and activates the cytoplasmic protein Disheveled (Dsh in *Drosophilla* and Dvl in vertebrates) leading to an inactivation of the multiprotein complex and thereby preventing GSK-3 $\beta$  phosphorylation of  $\beta$ -catenin. This allows the signaling pool of  $\beta$ -catenin to accumulate in the cytoplasm. The stabilized  $\beta$ -catenin will then translocate into the nucleus and bind to members of T-cell factor (TCF)/Lymphoid enhancing factor (LEF) transcription factor elements resulting in activation of Wnt target genes (Fig. 1.5). To date, more than 50 Wnt target genes have been identified in *Drosophilla* and vertebrates (Logan and Nusse, 2004; Yu et al., 2011). A comprehensive list of this pathway can be found at <http://stanford.edu/~rnusse/wntwindow.html>. These genes are involved in numerous processes namely development, cell proliferation, cell-cell interactions, and cell-matrix interactions (Logan and Nusse, 2004).

In PCa development,  $\beta$ -catenin mutations have been reported. Approximately 5% of primary PCa samples revealed mutations at exon 3 of *CTNNB1* gene which is a hot spot for mutation found in a wide variety of human tumors (i.e., colorectal cancers, ovarian cancer, pancreatic cancer, and hepatoblastoma). This exon encodes the critical serine and threonine residues, which are sites for phosphorylation by GSK-3 $\beta$ ; therefore, mutations within this exon increase cytoplasmic/nuclear accumulation of  $\beta$ -catenin (Chesire and Isaacs, 2003; Yu et al., 2011). As discussed earlier, APC is closely associated with Wnt/ $\beta$ -catenin signaling as a member of a multiprotein complex, and it can directly interact with  $\beta$ -catenin (Anastasiadis and Reynolds, 2000). In fact, APC has 6 armadillo domains and it has been well established as a tumor suppresser. Inactivating mutations in APC, or activating mutations in  $\beta$ -catenin, also cause the accumulation of  $\beta$ -catenin in the nucleus. Studies have reported that increased nuclear  $\beta$ -catenin

is associated with advance PCa since the binding of nuclear  $\beta$ -catenin to TCF/LEF causes the upregulation of the target genes (i.e., Myc, c-jun, Cdk-1 and CDK4) resulting in an increase of cell proliferation and thus mediating PCa progression. In addition, nuclear  $\beta$ -catenin has the ability to cross-talk with other significant cancer-related mechanisms including AR, PTEN/Akt, COX-2/PGE2, PDGF, and NF- $\kappa$ B pathways (Chesire and Isaacs, 2003; Lamberti et al., 2001; Willert and Jones, 2006; Yu et al., 2011).

#### *p120-Catenin subfamily*

Members of p120-catenin (or p120, hereafter p120<sup>ctn</sup>) subfamily (10 Arm repeat units) are p120<sup>ctn</sup>,  $\delta$ -catenin (Neuroplakofilin Related Armadillo Protein (NPRAP)/Neurojungin), ARVCF (Armadillo Repeat gene deleted in VeloCardio-Facial syndrome), and p0071 (plakophilin-4) (Hatzfeld, 2005). Despite overall structural similarities between  $\delta$ -catenin and p120<sup>ctn</sup>, a more detailed structural comparison of  $\beta$ -catenin, p120<sup>ctn</sup>, and  $\delta$ -catenin revealed greater sequence identity between  $\delta$ -catenin and  $\beta$ -catenin within their flanking sequences than between  $\delta$ -catenin and p120<sup>ctn</sup> (Fig. 1.6) (Kosik et al., 2005). These conserved sequences identified at amino- and carboxyl-terminal domains indicate that  $\delta$ -catenin could be regulated in a similar fashion to that of  $\beta$ -catenin.

Unlike  $\beta$ -catenin, members of p120<sup>ctn</sup> bind to JMD of E-cadherin and do not interact with  $\alpha$ -catenin, which implies that p120<sup>ctn</sup> members have functions in the cadherin complex that  $\beta$ -catenin lacks. Previous studies reported that p120<sup>ctn</sup> members mediate cell-cell adhesion by regulating cadherin turnover rather than anchoring cadherins to actin filaments as  $\beta$ -catenin does. In other words, the interaction of p120<sup>ctn</sup> members to E-cadherin directly influences adhesive strength by controlling the amount of E-cadherin available at the cell surface (Hatzfeld, 2005).

Other p120<sup>ctn</sup> members' functional distinction is their ability to modulate the activity of Rho family GTPases (Anastasiadis, 2007; Hatzfeld, 2005). When bound to cadherins at the plasma membrane, p120<sup>ctn</sup> subfamily members prevent cadherins from endocytosis and degradation by lysosomes, therefore enhancing cell adhesion. In contrast, when not bound to cadherins, p120<sup>ctn</sup> subfamily members associate with GEFs and GAPs to facilitate small-GTPase activation leading to both reduced cell adhesion and increased cell migration. These findings indicate that p120<sup>ctn</sup> subfamily members can have affects extending from developmental morphogenesis (e.g., neural crest migration) to pathological events (e.g., the primary tumor cells losing cadherin-mediated polarity together with the gain of cell motility to metastasize distally) (Wildenberg et al., 2006).

### *δ-Catenin*

δ-Catenin is encoded by the gene *CTNND2*, located on chromosome 5 (p15.2). It consists of a 1,225 amino acid, with a predicted molecular weight of 132,544.86 and a pI of 7.94 (Fig. 1.7) (Lu et al., 1999). Of note, five *δ-catenin* transcript variants have been reported which lead to variation of amino acid sequences (as references published in GenBank database provided by the NCBI). A significant portion of the molecular mass lies at amino- and carboxyl-terminal sequences flanking the Arm domain that can potentially participate in protein-protein interaction, protein-lipid interaction, and protein phosphorylations (Jones et al., 2002; Kim et al., 2008a; Lu et al., 1999). Indeed, several phosphorylated sites have been documented. Cdk 5, proline-directed serine/threonine protein kinase, phosphorylates δ-catenin at residues Ser191, Ser246 (Munoz et al., 2007), Ser300, and Ser357 (Poore et al., 2010). The residual at Thr454 is phosphorylated by Akt1 for the interaction between δ-catenin and p190RhoGEF (Kim et al., 2008a). Furthermore, δ-catenin shows a very high probability of being phosphorylated by Abelson tyrosine kinase

(Abl) at tyrosine residues 292 and 429 (Lu et al., 2002; Lu et al., 1999). These features suggest that  $\delta$ -catenin may be a scaffolding/adaptor protein that can modulate signal transduction pathways.

In addition, in the amino-terminal domain the segment of amino acids 49-85 contain a high probability of forming a coiled-coil  $\alpha$ -helical structure, favoring protein-protein interaction, followed by a proline rich motif at residues 216-226. Amino acids 532-1013 correspond to the 10 armadillo repeats. The repeat units 4, 5, and 6 of  $\delta$ -catenin are extended by spacers of 7-18 amino acids with arm-unrelated sequences. The spacer following the sixth repeat, amino acids 811-817, represent a lysine rich motif that is a potential nuclear localization signal (NLS) sequence (Lu et al., 1999; Paffenholz and Franke, 1997). Moreover, a number of studies have implicated a family of proteins containing PDZ domains (for PSD-95/Discs-large/ZO-1) in establishing epithelial cell polarity (Hatzfeld, 2005; Paffenholz and Franke, 1997).  $\delta$ -Catenin, p0071 and ARVCF but not p120<sup>ctn</sup> (with the exception of the *C. elegans* homolog of p120<sup>ctn</sup>) share such a carboxyl-terminal PDZ-binding motif suggesting possible roles of  $\delta$ -catenin in maintaining cell polarity (Fig. 1.7).

$\delta$ -Catenin is unique from  $\beta$ -catenin and all other catenin family members due to its most exclusive expression in neuronal cells of the central nervous system (CNS) of healthy individuals, while other catenins are ubiquitously expressed in many tissues. Indeed, a partial sequence of  *$\delta$ -catenin* was cloned first using a yeast two-hybrid system to search for interactions with the Alzheimer gene *presenilin 1* (Zhou et al., 1997). Since then  $\delta$ -catenin's function and its protein partners have been investigated, particularly in neurons. What is known from the cloning, characterization, and identification of binding partners of  $\delta$ -catenin is (i) its highly polarized localization to dendrites in mature neurons where it defines a unique constellation of interaction

partners; (ii) its location between the adherens junction and the synapse; (iii) its powerful, autonomous role in inducing morphological change in neurons; (iv) its regulation in dendrogenesis; and (iv) its crucial role in normal synaptic function. (Abu-Elneel et al., 2008; Ho et al., 2000; Jones et al., 2002; Kim et al., 2002; Kosik et al., 2005; Lu et al., 2002; Lu et al., 1999; Munoz et al., 2007; Tanahashi and Tabira, 1999; Zhou et al., 1997). The functional outcomes of  $\delta$ -catenin interacting with its binding partner proteins are summarized in Table 1.1.

Aberration of  $\delta$ -catenin expression implicates in several pathological events. Hemizygous deletion of the human chromosomal region (5p15.2) containing  $\delta$ -catenin is associated with mental retardation of Cri-du-Chat syndrome (CDCS) (Medina et al., 2000). More evidence regarding  $\delta$ -catenin's neural functions was obtained from mouse model studies where targeted deletion of  $\delta$ -catenin in mice resulted in severe impairments in brain cognition and abnormal synaptic plasticity. Functions of  $\delta$ -catenin in epithelial cells were discovered in the early studies by Lu et al (1999). The authors showed that exogenous expression of  $\delta$ -catenin in MDCK cells induced morphological alterations, process elaborations, and increased cell scattering in response to growth factor treatment (Lu et al., 1999). This finding was supported in other cell systems, where it was shown that overexpression of  $\delta$ -catenin induced dendrite-like branching of 3T3 fibroblast cells and enhanced branching in primary hippocampal neurons (Kim et al., 2002).

## **E. $\delta$ -Catenin and prostate cancer**

### *Evidence for $\delta$ -catenin involvement in PCa*

Although  $\delta$ -catenin was discovered over a decade ago, the exact role of  $\delta$ -catenin aside from neuronal functions has yet to be elucidated. Burger et al (2002) demonstrated for the first time that messenger RNA (mRNA) for  $\delta$ -catenin is expressed in PCa samples with the  $\delta$ -catenin

transcripts being localized to the glandular secretory cells (Burger et al., 2002). Since then  $\delta$ -catenin has increasingly gained interest as a potential molecular marker for PCa with additional studies pointing to a role for  $\delta$ -catenin in carcinogenesis of other cancer types. In fact, not only the overexpression of  $\delta$ -catenin has been observed in PCa, but it has also been best established in lung cancer and breast cancer (Burger et al., 2002; Dai et al., 2011; Lu et al., 2005; Zhang et al., 2010c; Zheng et al., 2004).

Our previous studies revealed  $\delta$ -catenin protein expression is increased in PCa cells. Lu et al (2005) compared the expression level of  $\delta$ -catenin in 4 different prostate cell lines by immunoblotting. The authors first compared human marrow stromal cells HS-5 and noncancerous human prostate epithelial cells PZ-HPV-7 with CWR-R1, a cell line derived from a recurrent CWR22 human prostate tumor xenograft. The data showed that  $\delta$ -catenin was expressed in all cells, but was distinctly higher in CWR-R1 than HS-5 and PZ-HPV-7 cells. Additionally, in order to determine whether the increased level of  $\delta$ -catenin protein in cancer cells detected by Western blot could be due to an increased mRNA expression of  $\delta$ -catenin gene, the authors applied RT-PCR and found that CWR-R1 cells showed increased amounts of  $\delta$ -catenin mRNA when compared with PZ-HPV-7 cells. Taken together, these results indicated that  $\delta$ -catenin protein is overexpressed in PCa cells *in vitro*. Subsequent *in vivo* examination with immunohistochemical analysis of the  $\delta$ -catenin protein expression in human adenocarcinomas was conducted using Tissue Micro-array (TMA). Immunostaining of anti  $\delta$ -catenin was very weak in benign tissues and became stronger in the high-grade tumor. In the prostatic adenocarcinomas with low tumor grade,  $\delta$ -catenin staining was localized to the secretory glandular epithelial cells. Moreover, in PCa an increased expression of  $\delta$ -catenin was found to be accompanied by the reduction of immunoreactivity of E-cadherin and p120<sup>ctn</sup> at the plasma membrane and their

redistribution is concomitant with prognostically significant increased Gleason scores. Collectively, these findings strongly support that  $\delta$ -catenin expression is increased in primary human prostatic adenocarcinomas correlated to PCa progression (Lu et al., 2005).

Studies *in vitro* further supported this hypothesis. Zeng et al (2009) found that the ectopic expression of  $\delta$ -catenin into human PCa cells promoted PCa cell growth and tumorigenesis by upregulating cyclin D1 and cdc34, increasing phosphorylated histone-H3, and promoting the entry of mitosis. In addition,  $\delta$ -catenin overexpression resulted in increased expression of cell survival genes Bcl-2 and survivin while reducing the cell cycle inhibitor p21<sup>Cip1</sup> (Zeng et al., 2009).  $\delta$ -Catenin accumulation in the urine of PCa patients has also been reported (Lu et al., 2009). Recent studies have demonstrated that  $\delta$ -catenin can be expressed in vascular endothelium and its haplo-insufficiency impaired pathological angiogenesis (DeBusk et al., 2010). These results were further confirmed by He et al (2013b). The authors found that  $\delta$ -catenin overexpressed in PCa cells (CWR22Rv-1 cells) displaying higher angiogenic potential than their match control cells in a CAM assay (He et al., 2013b).

p120<sup>ctn</sup>, a close member of  $\delta$ -catenin, is shown to be downregulated concomitant with the reduction of E-cadherin expression in PCa. Because E-cadherin is well known as a tumor suppressor, p120<sup>ctn</sup> may therefore function similarly as a tumor suppressor through its ability to stabilize and/or regulate E-cadherin. Since  $\delta$ -catenin and p120<sup>ctn</sup> share the same binding site (JMD) at E-cadherin, the question whether these two molecules compete with each other for E-cadherin arose. There are contradicting results depending on models used for the studies. Earlier studies by Yang et al (2010) found that the PCa cells overexpressing  $\delta$ -catenin contain less E-cadherin-bound p120<sup>ctn</sup> than the control cells, causing the re-localization of p120<sup>ctn</sup> from the plasma membrane to the cytosol (Yang et al., 2010). These finding are consistent with the

results of Zhang I. et al (2013) in colorectal cancer cells. However, Zhang H. et al (2010) showed that  $\delta$ -catenin promotes a malignant phenotype in non-small cell lung cancer by non-competitive binding to E-cadherin with p120<sup>ctn</sup> in the cytoplasm. The underlying reasons for these differences are unclear and may be related to tissue-specific differences (Zhang et al., 2010c).

### *Regulation of $\delta$ -catenin in PCa*

Growing evidence supports that increased expression of  $\delta$ -catenin in PCa is modulated by multiple mechanisms, including gene amplification, transcriptional activation, and mutation in its non-coding region (Logan and Nusse, 2004; Wang et al., 2009; Yu et al., 2011). It was reported that E2F1, a transcription factor promoting both proliferation and apoptosis activated by *Myc* and *Ras* oncogenes, positively regulates the expression of  $\delta$ -catenin in PCa cells (Kaseb et al., 2007; Kim et al., 2008c; Lu et al., 2010; Wang et al., 2009). In an effort to identify the potential transcriptional factors for upregulating  $\delta$ -catenin expression, Kim et al (2008c) analyzed the putative promoter sequences of human  $\delta$ -catenin using the Genomatix program (<http://www.Genomatix.de/>). Many proteins were listed as potential binding factors to the putative promoter region of human  $\delta$ -catenin including Pax6, RBP-Jkappa, LEF-1, and E2F. Among these proteins, the authors claimed that E2F1 drew special attention because it is involved in cell cycle regulation, interacting with Retinoblastoma (Rb) and p107 protein. The release of E2F from Rb triggers the shift from G1 to S phase in the cell cycle, and persistent activation of E2F-driven transcription occurs as a result of Rb mutation in many tumors including PCa, retinoblastoma, and bladder cancer. It is worth mentioning here that Pax6, previously identified as a positive regulator for  $\delta$ -catenin expression in the central nervous system, enhances  $\delta$ -catenin

expression in PCa cells (Zhang et al., 2010b). However, further studies are needed to reveal how Pax6 regulates  $\delta$ -catenin expression and functions in this context.

On the other hand, a human homolog of Drosophila Hairy and enhancer of split 1 (Hes1) was described as a transcriptional repressor for  $\delta$ -catenin and regulates  $\delta$ -catenin expression in human PCa cells and mouse models of prostate tumors by coordinating with transcription activator E2F1 (Lu et al., 2010). Other potential negative transcriptional regulators of the  *$\delta$ -catenin* promoter region have been revealed by the Genomatix program (<http://www.Genomatix.de/>) namely RBP-Jkappa, and p53.

Recently, an alternative model of Kaiso (Poxvirus Zinc Finger/POZ zinc finger protein) function in the context of Wnt signaling has arisen. Kaiso has been identified as a p120<sup>ctn</sup> and  $\delta$ -catenin-interacting protein, implicating a role for p120<sup>ctn</sup> and  $\delta$ -catenin in nuclear signaling activity in addition to its cell-cell adhesion function. However functional consequences of these interactions remains to be elucidated. In the nuclear compartment, p120<sup>ctn</sup> binds and relieves the transcription repression of Kaiso. A majority of candidate Kaiso target genes identified thus far, including *CDH1* (E-cadherin), *MMP7*, *MTA2*, and *Wnt 11*, have been linked with development and/or cancer progression. An intriguing observation is that  $\delta$ -catenin and Kaiso form a complex that is associated with poor prognosis in non-small-cell lung cancer, but they co-distributed mainly in the cytoplasm (Dai et al., 2011). The authors claimed that the failure to detect nuclear  $\delta$ -catenin is possibly due to its rapid and efficient export from the nucleus.

#### *$\delta$ -Catenin: potential cross-regulation in Wnt/ $\beta$ -catenin signaling in PCa*

Previous studies have primarily compared  $\delta$ -catenin to other p120<sup>ctn</sup> subfamily members. Fewer studies have directly addressed the shared functional properties between  $\delta$ -catenin and

$\beta$ -catenin. The data from Kim et al (2012) demonstrated that PCa cells overexpressing  $\delta$ -catenin promotes E-cadherin processing by recruiting PS-1/ $\gamma$ -secretase complex to the plasma membrane. In addition, these cells displayed an elevation of total  $\beta$ -catenin level and an increase of nuclear distribution resulting in the activation of  $\beta$ -catenin/LEF-1 mediated transcription and their target genes including cyclin D1, CDK4, Myc, and c-jun (Kim et al., 2012). Although the exact mechanism of how increased  $\delta$ -catenin could contribute to the elevation of nuclear  $\beta$ -catenin translocation is not well understood, these findings provide new insight into the positive relationship between  $\delta$ -catenin and  $\beta$ -catenin in PCa progression.

Additionally, a number of studies have identified GSK-3 $\beta$  as a strong negative regulator of  $\delta$ -catenin. It was shown that  $\delta$ -catenin is associated with and is phosphorylated by GSK-3 $\beta$ , which tags  $\delta$ -catenin for ubiquitination leading to proteasome-mediated degradation in PCa cells CWR22Rv-1 and primary cortical neurons (Bareiss et al., 2010; Oh et al., 2009). The studies by Bareiss et al (2010) also provided evidence that overexpression of  $\delta$ -catenin in neuronal cells caused an increased interaction between  $\beta$ -catenin and GSK-3 $\beta$ , leading to enhanced ubiquitination and degradation of  $\beta$ -catenin (Bareiss et al., 2010). Taken together, these data suggest that the regulation of  $\delta$ -catenin through GSK-3 $\beta$  signaling complex is similar to that of  $\beta$ -catenin and  $\delta$ -catenin could participate in the regulation of  $\beta$ -catenin levels by increasing the GSK-3 $\beta$ / $\beta$ -catenin interactions, suggesting  $\delta$ -catenin as a new member of the canonical Wnt/ $\beta$ -catenin signaling pathway.

#### *Mutation-induced metabolic adaptation in cancer*

Mutations in oncogenes or tumor suppressor genes lead to abnormalities of multiple cellular signaling pathways and processes, which are crucial for tumorigenesis. A well-

established capability of mutated cancer is their rapidly dividing cells. The higher rate of proliferation in solid tumor is accompanied with the higher demands for energy generation for biogenesis of macromolecules: carbohydrates, proteins, lipids, and nucleic acids (Cairns et al., 2011). However, it has become clear that many key oncogenic signaling pathways have an effect on tumor cell metabolism and reengineer the cells to allow enhanced survival and growth in the tumor microenvironment (i.e., hypoxia, low pH, low nutrients, and autophagy) (Fig. 1.8) (Patiar and Harris, 2006; Poon et al., 2009; Powis and Kirkpatrick, 2004; Vander Heiden et al., 2009).

One observation by Otto Heinrich Warburg in the 1920s found that cancer cells tend to convert most glucose to lactate regardless of whether oxygen is present. This property is shared by normal proliferative tissues (Warburg, 1956). A proposed explanation for Warburg's observation is that the hypoxia condition and homeostatic system is programmed to fit the requirements for cell proliferation, and cancer cells are capable of adapting their cellular metabolism in favor of such a hypoxic tumor microenvironment. Hence, their metabolism is often referred to as "aerobic glycolysis" or "Warburg effect" (Bensinger and Christofk, 2012; Koppenol et al., 2011; Vander Heiden et al., 2009). Recently, reprogramming of energy metabolism is considered as a novel hallmark capability of cancer (Cairns et al., 2011; Hanahan and Weinberg, 2011; Yeung et al., 2008).

Hypoxia-inducible factor 1, isoform  $\alpha$  (HIF-1 $\alpha$ ) transcription factor is an important modulator identified and activated in hypoxic cancer cells, i.e., brain, bladder, breast, colon, ovarian, and prostate (Dang et al., 2008; Dang et al., 2009; Podar and Anderson, 2010; Poon et al., 2009). Upon the activation of HIF-1 $\alpha$ , it can regulate the transcription of several genes involved in biological processes, such as angiogenesis (*VEGF*), cell proliferation (*cyclin G2*, *p21*, *WAF1*) and survival (*IGF-1*), apoptosis (*NIX*), metastasis (*Lox*), and glucose metabolism

(HK2). With respect to the glycolytic pathway, HIF-1 $\alpha$  upregulates the expression of glucose transporters and most of the glycolytic enzymes under hypoxia, increasing the capacity of the cell to carry out glycolysis (Patiar and Harris, 2006; Poon et al., 2009; Powis and Kirkpatrick, 2004). In addition, several studies have reported that in human cancers, HIF-1 $\alpha$  cooperates with Myc to enhance the expression of shared targets in the glycolytic pathway including hexokinase 2 (HK2), glucose transporter-1 (Glut-1), and pyruvate kinase 2 (PKM<sub>2</sub>) (Bensinger and Christofk, 2012; Dang et al., 2008; Dang et al., 2009; Podar and Anderson, 2010). These findings further support the hypothesis that the *Myc* oncogene, besides its well documented role in controlling cell proliferation, alters the metabolic phenotype in favoring tumorigenesis.

#### **F. Rational for current studies**

Given that the  $\delta$ -catenin protein is involved in a variety of regulatory functions within neurons and is implicated in a multitude of human pathological conditions, particularly human PCa, it is a very attractive and exploitable marker for PCa therapeutics. Our laboratory has become interested in understanding the mechanisms involved in  $\delta$ -catenin and PCa progression. More precisely, our studies aim to elucidate what other major oncogenic signaling pathways involve and/or regulate  $\delta$ -catenin and contribute to PCa progression.

Evidence established in our laboratory revealed that  $\delta$ -catenin is overexpressed *in vitro* and *in vivo* and its overexpression is correlated with PCa progression. Striking findings of  $\delta$ -catenin involvement in PCa have been reported when Lu et al (2009) demonstrated for the first time that  $\delta$ -catenin can be detected in human PCa stromal tissues, and that it is present in the voided urines in a notable association with disease occurrence. Recently, we have revealed that  $\delta$ -catenin displays frequent mutations in primary prostatic adenocarcinomas which are highly

inducible and predictive of altering functions when overexpressed in cells derived from prostate tumor xenograft (Nopparat et al., 2014). In this report, we also demonstrate that  $\delta$ -catenin mutant cells promote cancer cell survival and metabolic adaptation during densely-packed tumorigenesis. Collectively, our findings further support that  $\delta$ -catenin is (i) closely involved in PCa progression; (ii) highly inducible for mutagenesis when overexpressed; and (iii) a potential novel therapeutic target for PCa. However, it remains unclear how  $\delta$ -catenin contributes to PCa. Therefore, the thoroughly dissecting  $\delta$ -catenin involvement in the cellular signaling pathway will enable us to translate this knowledge to design PCa screening and treatment strategies more effectively.

Finally, although the human cancer cell culture models are very helpful in gaining a better understanding of  $\delta$ -catenin and its associated proteins, they cannot recapitulate the complex cellular interactions within the tumor microenvironment. This has led us to further study the function of  $\delta$ -catenin *in vivo* mouse models. We have successfully generated novel mouse models of PCa which are Myc/ $\delta$ -cat double transgenic and Myc/ $\delta$ -catenin mutant mouse models. In order to generate a model system for more detailed of PCa studies, we established novel murine prostate tumor cell lines derived from our existing mouse models. Our identification of  $\delta$ -catenin and other related protein expression profiles in these models will allow further dissection of  $\delta$ -catenin-mediated signaling pathways and mechanisms by which  $\delta$ -catenin contributes to PCa progression.

## **G. Statement of hypothesis and specific aims**

Hypothesis: Overexpressed  $\delta$ -catenin is susceptible for mutagenesis in PCa. Its mutations lead to alterations of the  $\beta$ -catenin-mediated oncogenic signaling pathway and energy reprogramming *in vitro* and *in vivo* with significant implication in PCa progression.

Specific Aim I: To investigate the effects of  $\delta$ -catenin overexpression in human PCa cell lines on the canonical Wnt/ $\beta$ -catenin/LEF-1-mediated signaling pathway and metabolic reprogramming.

*Overall approach:*

In this specific aim, we took advantage of an unexpected and serendipitous discovery of induced  $\delta$ -catenin mutations in PCa cells. We initially intended to generate stable CWR22-Rv1 cells, derived from human primary prostatic tumor xenografts, and PC-3 cells from PCa bone metastasis, by transfected with either full-length  $\delta$ -catenin (named as Rv/ $\delta$ ) or GFP vector alone (named as Rv/C). However, we found that cancer cells expressing truncated  $\delta$ -catenin (named as Rv/M1) were present and became predominant in cell populations. After selecting and cloning the mutant cells, we will perform analyses as listed:

- a) Characterization of  $\delta$ -catenin variants in Rv/M1 cells by SDS-PAGE and protease inhibitor analyses;
- b) Detection of  $\delta$ -catenin genetic alterations by PCR and sequencing;
- c) Determination of integration of ectopic  $\delta$ -catenin gene in host chromosome by chromosome spread preparation and fluorescence in situ hybridization (FISH) assay;
- d) Determination of cell death and apoptosis by flow cytometry method;
- e) Characterization of other adherens junction-associated proteins, i.e., E-cadherin and p120<sup>ctn</sup> by immunofluorescent analysis;

- f) Measurement of cell metabolism by measuring the cell glycolysis (ECAR) and mitochondrial oxidative phosphorylation (OCR) using Seahorse Bioscience XF24 Extracellular Flux Analyzer;
- g) Analysis of protein expression profiles in different cell compartments by cell fractionation protocol;
- h) Analysis of protein expression, particularly proteins involved in Wnt/ $\beta$ -catenin pathway, and glycolytic pathway, by Western blot.

Specific Aim II: To investigate the effects of  $\delta$ -catenin transgene and  $\delta$ -catenin mutation in Myc transgenic mouse models of PCa on the canonical Wnt/ $\beta$ -catenin/LEF-1-mediated signaling pathway and metabolic reprogramming.

*Overall approach:*

We have successfully generated two genetically engineered mouse models of PCa. These mouse models are Myc/ $\delta$ -cat double transgenic by cross-breeding Myc transgenic lines with  $\delta$ -catenin transgenic lines. Additionally, Myc transgenic mice were cross-bred with  $\delta$ -catenin heterozygous mutant mice in order to generate Myc/ $\delta$ -catenin mutant mice. The following aspects will be investigated in our mouse models of PCa:

- a) Determination of mouse genotypes by genomic DNA extracted from tail-snips followed by PCR-based screening assay for genotyping;
- b) Analysis of mouse prostate tissue morphology by serial sections of paraffin-embedded blocks followed by Hematoxylin and Eosin staining;
- c) Determination of cell proliferation and cells undergoing apoptosis by immunofluorescent analysis using anti-Ki67 antibody and TUNEL assay;

- d) Determination of Myc expression profile by immunofluorescent analysis;
- e) Analysis of protein expression, particularly proteins involved in Wnt/ $\beta$ -catenin pathway and glycolytic pathway, by Western blot.

Specific Aim III: To characterize mouse prostate tumor cell lines established from Myc/ $\delta^{+/+}$  and Myc/ $\delta^{+/-}$ .

*Overall approach:*

We aim to generate a model system that can represent different stages of PCa progression. This system may provide extensive data on protein expression correlating to cancer grade, as well as, a therapeutic model for an effective treatment. After isolation and generation of these immortalized cells in culture, the following aspects will be investigated in our mouse prostate tumor cell lines:

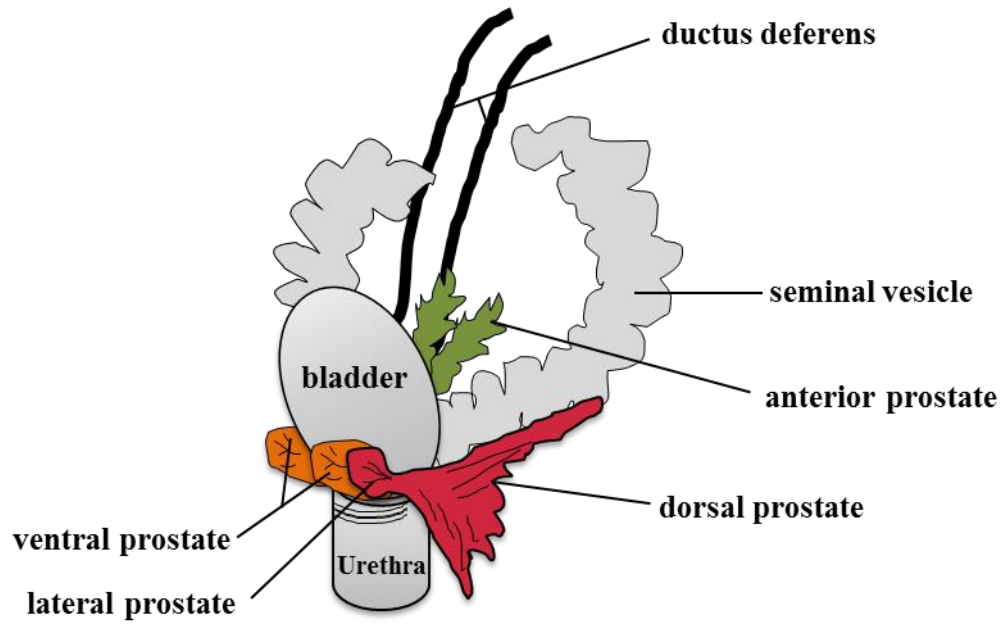
- a) Characterization of mouse cell line morphology by bright field microscopy;
- b) Determination of mouse cell line genotypes by genomic DNA extracted from cells followed by PCR-based screening assay for genotyping;
- c) Determination of epithelial characteristic in mouse prostate cell lines by immunofluorescent analysis using PSA, vimentin, E-cadherin and  $\beta$ -catenin antibodies;
- d) Analysis of protein expression, particularly proteins involved in Wnt/ $\beta$ -catenin pathway and glycolytic pathway, by Western blot.

## H. Significance

PCa accounts for about 1 in 6 newly diagnosed cancers each year among US men. With an estimated 29,720 deaths in 2013, PCa is the second-leading cause of cancer death in men (American Cancer Society, 2013). Most PCa patients are diagnosed before symptoms develop through PSA screening. Unfortunately, PSA screening has several limitations. Many men, who do not have PCa, will be screened as positive (known as false positive results) and require a biopsy for diagnosis, and some men with PCa do not have elevated PSA levels (known as false negative results). In addition, PSA screening lacks the ability to distinguish between PCa and benign prostate hyperplasia (BPH) (Burger et al., 2002). Therefore, there is a need for specific, reliable, and less invasive diagnostic tests for early detection of this disease.

At the level of histochemical studies, anti- $\delta$ -catenin is capable of distinguishing between PCa and BPH and has become a potentially promising diagnostic marker for PCa (Burger et al., 2002; Lu et al., 2005). However, the mechanism of  $\delta$ -catenin in PCa progression remains unclear. Thus, it is important to understand potential roles of  $\delta$ -catenin in PCa such that  $\delta$ -catenin could be utilized as a new and reliable biomarker for PCa screening and intervention. Our findings presented in this dissertation provide strong evidence of supporting  $\delta$ -catenin in PCa progression through its engagement with other crucial oncogenic signaling pathways. Importantly, we have now succeeded in generating innovative human and murine cancer cell lines as well as mouse models. These *in vitro* and *in vivo* model systems established in our laboratory will be beneficial for elucidating  $\delta$ -catenin induced-PCa mechanisms.

**A.**



**B.**

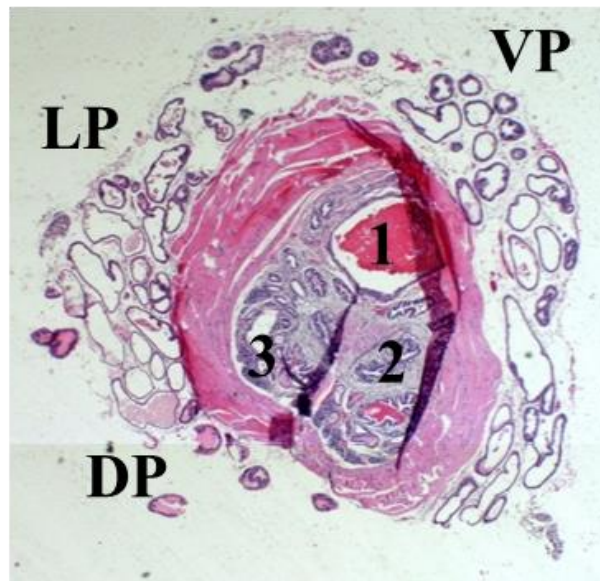
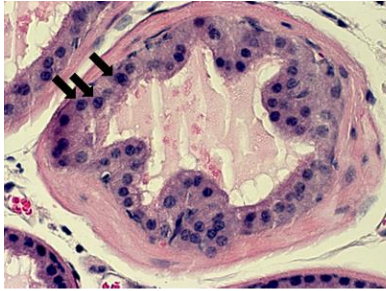
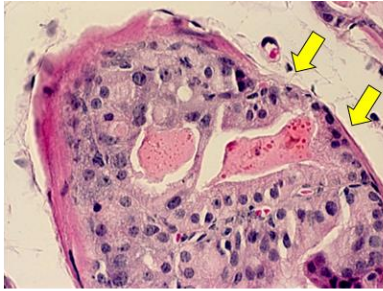


**Figure 1.1 Illustration of anatomy and histology of mouse prostate. (A).** Schematic represents the anatomy of mouse genitourinary structures showing the lobular nature of the prostate. **(B).** Histology of 6 month-old-mouse prostate. Cross section of mouse prostate tissue illustrates morphologically distinct regions including dorsal prostate (DP), lateral prostate (LP), and ventral prostate (VP) related to 1, urethra; 2, paired ductus deferens; and 3, paired ampullary glands. Original magnification: 50x.

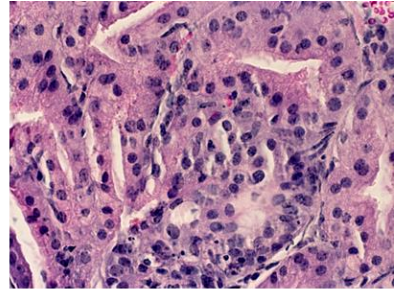
**A.**



**B.**



**C.**



Normal epithelial



Mouse Prostatic  
Intraepithelial Neoplasia  
(mPIN)



Invasive adenocarcinoma

**Figure 1.2 Pathway for mouse prostate tumor progression.** (A). Normal appearance of the prostate gland in Myc transgenic animal at 6 weeks of age is characterized by single layer with basal located nuclei (black arrows). (B). 8 month-old Myc transgenic mouse prostate represents mouse prostatic intraepithelial neoplasia (mPIN) lesions which is a precursor for prostate tumor. mPIN is defined by luminal epithelial hyperplasia filling almost entirely the lumen, enlargement of nuclei and nucleoli accompanied by well-defined basement membranes (yellow arrows). (C). Illustration of prostate tumor in transgenic mouse tissue at 8 months of age. Note that invasive adenocarcinoma cells extend into the surrounding stroma. Original magnification: 400x.

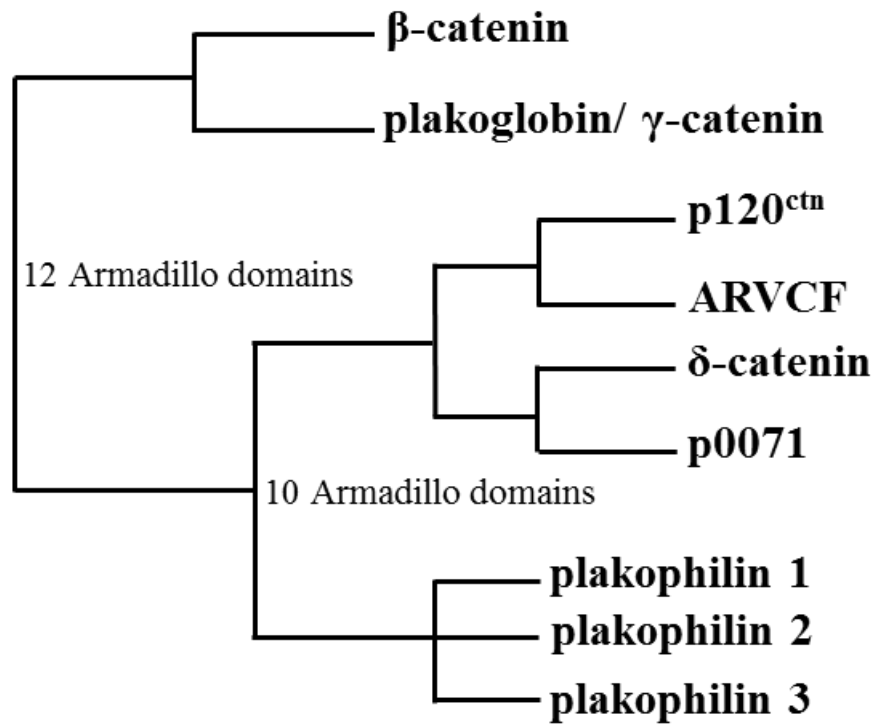


**Figure 1.3 Dendrogram showing sequence relationship between several members of the catenin family proteins.** Note that the salient characteristic distinguishing subfamily members is the number of armadillo domains. This central domain is associated with the greatest sequence homology between subfamily members and accounts for their phylogenic classification.

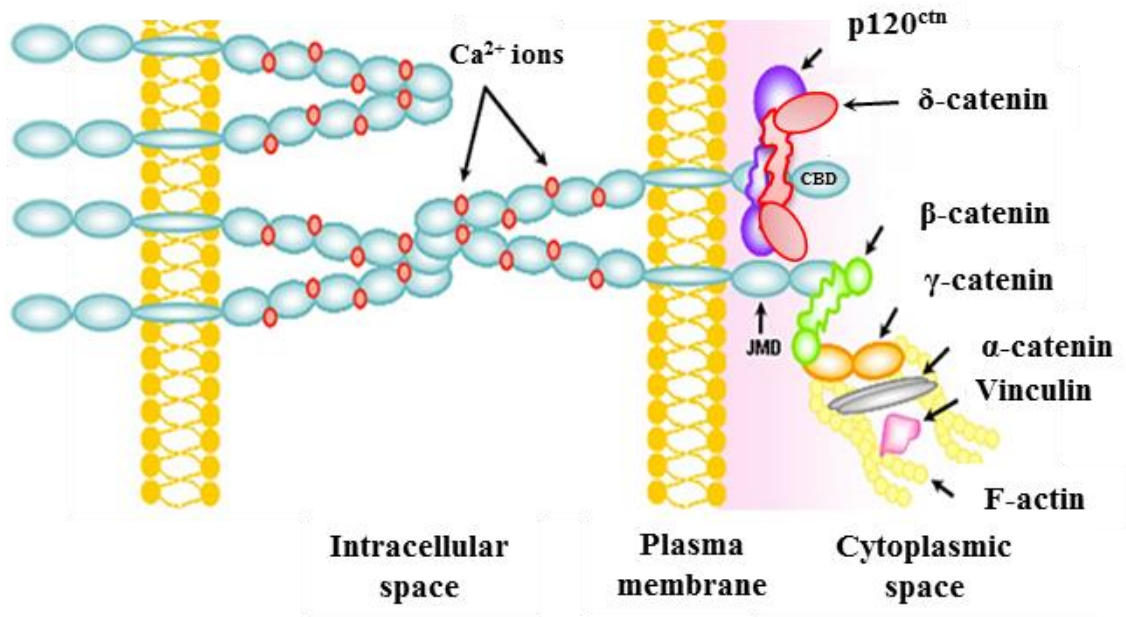


**Figure 1.4 Schematic representation of the classical cadherin-catenin complex.** Classical cadherins (blue), which mediate calcium-dependent (red) intercellular adhesion, are composed of extracellular domain, a transmembrane domain and a cytoplasmic domain. This latter domain comprises a juxtamembrane domain (JMD), which binds p120<sup>ctn</sup> (violet) and  $\delta$ -catenin (dark red), and a catenin-binding domain (CBD), which binds  $\beta$ -catenin (green), which in turns binds  $\gamma$ -catenin (grey).  $\alpha$ -Catenin (orange),  $\gamma$ -catenin and vinculin (pink) establish a direct link between the cadherin-catenin complex and the actin cytoskeleton (yellow). This schematic was modified from Paredes et al (2007).

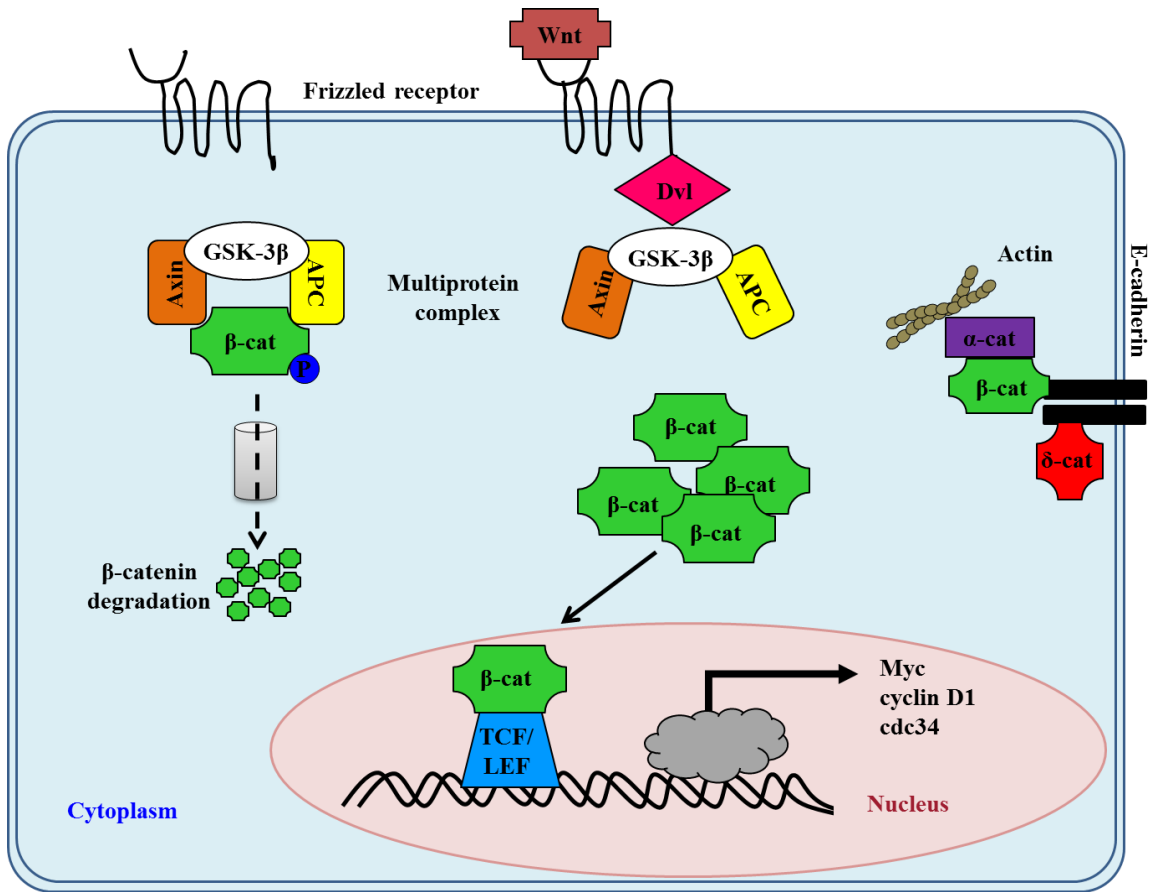


**Figure 1.5 Schematic representation of the canonical Wnt/ $\beta$ -catenin signaling pathway.**

$\beta$ -Catenin is a multifunctional protein involved in two independent processes: cell to cell adhesion (associated with E-cadherin) and signaling transduction. In the presence of the Wnt ligand, it will inhibit the activity of the multiprotein complex, which targets  $\beta$ -catenin by phosphorylation for degradation by the proteasome. Stabilized  $\beta$ -catenin thus accumulates in cytoplasm and is then translocated to the nucleus where it associates with members of the T-cell factor (TCF) and lymphoid enhance factor (LEF) family of transcriptional factors, resulting in activation of target genes (i.e., Myc, cyclin D1, and cdc 34). In contrast, when the Wnt ligand is absent,  $\beta$ -catenin will be phosphorylated by multiprotein complex and degraded by the proteasome, reducing the level of cytosolic  $\beta$ -catenin.

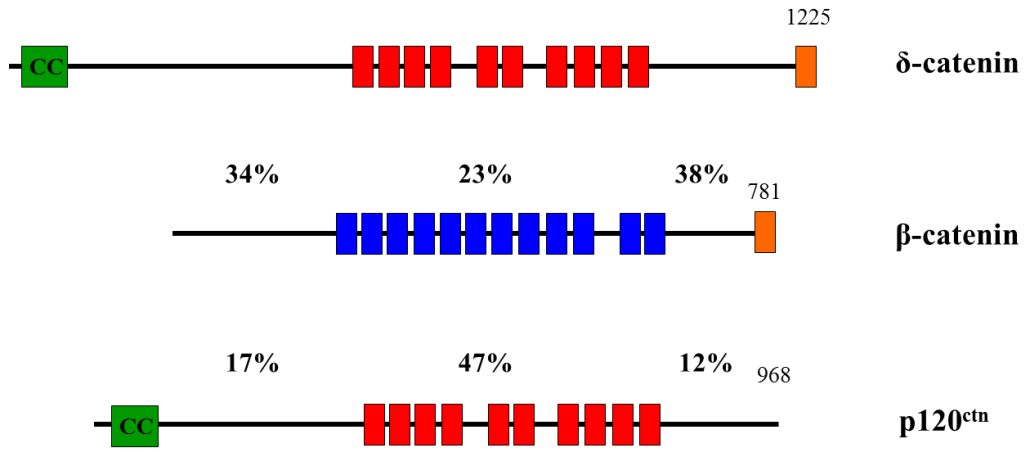


**Figure 1.6 Comparisons of sequence analysis between  $\delta$ -catenin,  $\beta$ -catenin, and p120<sup>ctn</sup>.**

Percentages represent identity compared with human  $\delta$ -catenin. The blue and red boxes indicate armadillo repeats, CC in green box indicates a predicted coiled-coil domain and the orange box refers to a PDZ-binding domain. Identity (%) is listed above each Arm repeat and the flanking regions (amino- and carboxyl-termini).

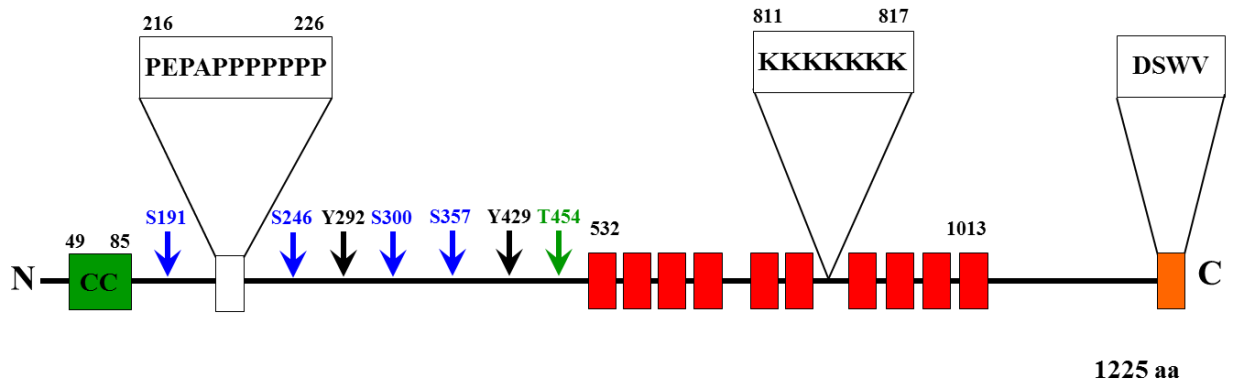


**Figure 1.7 Linear structural representation of full-length human  $\delta$ -catenin.** Amino acids 49-85 have a high probability of forming a coiled-coil  $\alpha$ -helical structure (green box). Amino acids 216-226 contain a proline rich motif. Red boxes represent 10 armadillo repeats extending from residue 532 to residue 1013. Amino acids 811-817 illustrate a lysine rich motif which is a potential nuclear localization signal (NLS) sequence. PDZ-binding motif of sequence DSWV is present at the extreme carboxyl-terminus of  $\delta$ -catenin (orange box). Cdk5-mediated phosphorylation is identified at four sites including serine 191, serine 300, serine 357, and serine 426 (S191, S300, S357, and S426). Black arrows indicate two Abl tyrosine phosphorylation consensus sites (Y292 and Y492). Finally, Akt1 shows specific phosphorylation of  $\delta$ -catenin at residue threonine 454 (T454).

**Table 1.1  $\delta$ -Catenin binding partners and outcomes of their interactions.**

<b>Protein</b>	<b>Outcomes of functional interactions with <math>\delta</math>-catenin</b>	<b>References</b>
Presinilin-1	Synaptic plasticity and dendritic outgrowth	(Tanahashi and Tabira, 1999; Zhou et al., 1997)
S-SCAM	Organization of synaptic junction components	(Ide et al., 1999)
Abl	Modulation of actin-based neuronal morphogenesis	(Lu et al., 2002; Lu et al., 1999)
Papin	Establishment of neuronal epithelial cell polarity	(Deguchi et al., 2000)
Erbin	Maintaining integrity of epithelial cell monolayer	(Jaulin-Bastard et al., 2002; Laura et al., 2002)
Densin-180	Organization of synaptic cell-cell junction	(Izawa et al., 2002)
mGLUR1 $\alpha$	Neuronal dendritic morphogenesis and synaptic maturation	(Jones et al., 2002)
NR2A	Neuronal dendritic morphogenesis and synaptic maturation	(Jones et al., 2002)
PSD-95	Synaptic signaling pathway during neuronal development	(Deguchi et al., 2000; Jones et al., 2002)

<b>Protein</b>	<b>Outcomes of functional interactions with <math>\delta</math>-catenin</b>	<b>References</b>
E-cadherin	<ul style="list-style-type: none"> <li>- Formation of adhesion complexes</li> <li>- Regulation of cadherin stability</li> </ul>	(Hartsock and Nelson, 2008; Kim et al., 2012; Lu et al., 1999)
Cortactin	Neurite elongation and branching effects	(Abu-Elneel et al., 2008; Martinez et al., 2003)
Kaiso	Activation of rapsyn promoter	(Dai et al., 2011; Rodova et al., 2004)
SPHK1	Enhancement of cell migration	(Fujita et al., 2004)
14-3-3 $\epsilon/\zeta$	Regulation of dendrogenesis	(He et al., 2013a; Mackie and Aitken, 2005)
Pax 6	Regulation of synapse connection in CNS	(Duparc et al., 2006; Zhang et al., 2010b)
ABP/GRIP	Anchoring synaptic adherens junction	(Ochiishi et al., 2008; Silverman et al., 2007)
Cdk5/p53	Formation of dendrites and synaptic activity	(Munoz et al., 2007; Poore et al., 2010)

<b>Protein</b>	<b>Outcomes of functional interactions with <math>\delta</math>-catenin</b>	<b>References</b>
Pin 1	Formation of dendrites	(Munoz et al., 2007)
E2F1	Transcriptional regulation	(Kim et al., 2008c)
p190RhoGEF	Downregulation of Rho A activity	(Kim et al., 2008a; Kim et al., 2008b)
Hes1	Transcriptional regulation	(Lu et al., 2010)

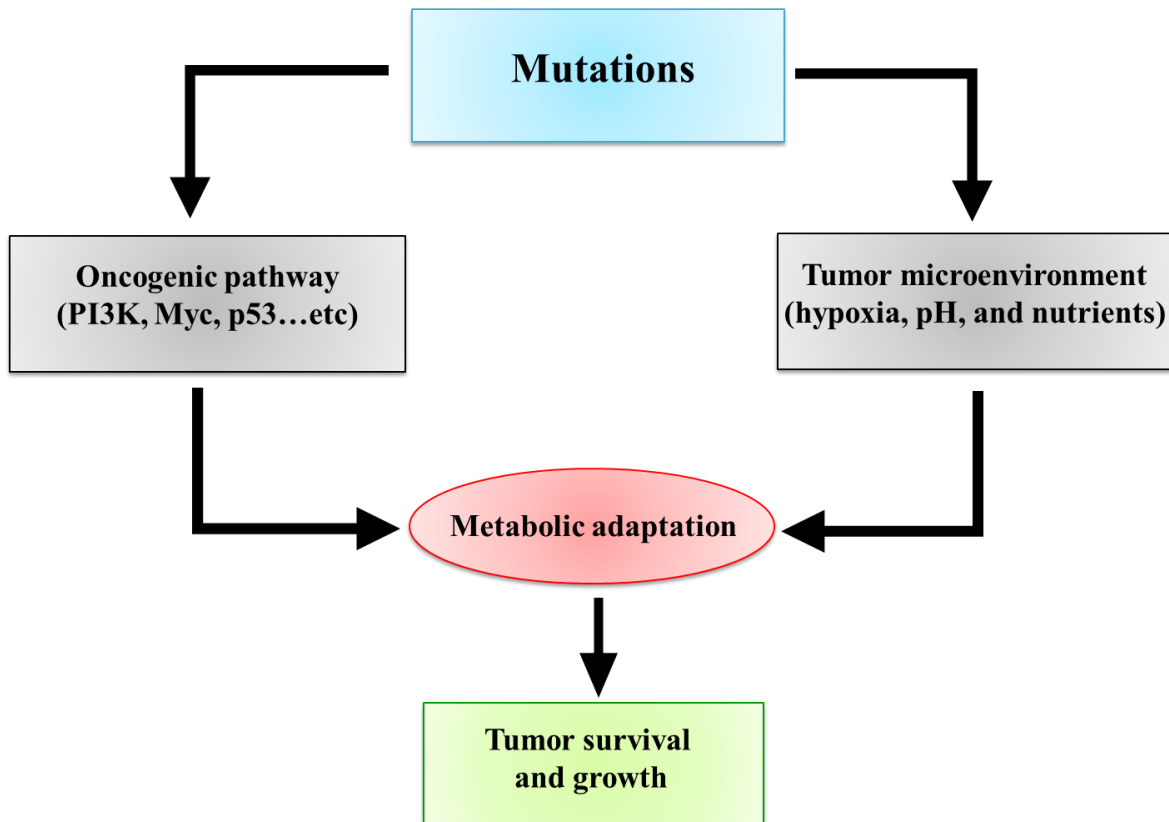


**Figure 1.8 Schematic illustration represents the driving-force of abnormal metabolic phenotype of tumor cells.** The metabolic adaption of tumor cells is regulated by oncogenic signaling pathways (i.e., the loss of tumor suppressor, p53, and the activation of PI3K and/or Myc oncoproteins) and the tumor microenvironment (i.e., hypoxia, low pH and/or nutrient deprivation), as consequences of intrinsic genetic mutations. The altered signalings result in cellular metabolism reengineering to match the requirements of rapidly dividing tumor cells, thereby enhancing their survival and growth.

## CHAPTER II: $\delta$ -CATENIN, A WNT/ $\beta$ -CATENIN MODULATOR, REVEALS INDUCIBLE MUTAGENESIS PROMOTING CANCER CELL SURVIVAL ADAPTATION AND METABOLIC REPROGRAMMING

This chapter is modified and reprinted from *Oncogene* advance online publication 14 April 2014; doi: 10.1038/onc.2014.89, see Appendix B.

### A. Summary

Mutations of the Wnt/ $\beta$ -catenin signaling pathway play essential roles in development and cancer. Although  $\beta$ -catenin and adenomatous polyposis coli (APC) gene mutations are well established and are known to drive tumorigenesis, discoveries of mutations in other components of the pathway have lagged, which hinders the understanding of cancer mechanisms. Here we report that  $\delta$ -catenin (gene designation: *CTNND2*), a primarily neural member of the  $\beta$ -catenin superfamily which promotes canonical Wnt/ $\beta$ -catenin/LEF-1-mediated transcription, displays exonic mutations in human prostate cancer and promotes cancer cell survival adaptation and metabolic reprogramming. When overexpressed in cells derived from prostate tumor xenografts,  *$\delta$ -catenin* gene invariably gives rise to mutations leading to sequence disruptions predicting functional alterations. Ectopic  *$\delta$ -catenin* gene integrating into host chromosomes is locus non-selective. The mutant cells empower survival advantage upon overgrowth and glucose deprivation. Reprogramming energy utilization accompanies the down-regulation of glucose transporter-1 (Glut-1) and Poly (ADP-ribose) polymerase (PARP) cleavage while preserving tumor type 2 pyruvate kinase (PKM<sub>2</sub>) expression.  *$\delta$ -Catenin* mutations increase  $\beta$ -catenin translocation to the nucleus and HIF-1 $\alpha$  expression. Therefore, introducing  *$\delta$ -catenin* mutations

is an important milestone in prostate cancer metabolic adaptation by modulating  $\beta$ -catenin and HIF-1 $\alpha$  signaling under glucose shortage to amplify its tumor promoting potential.

## **B. Introduction**

Mutations, such as that of the  *$\beta$ -catenin* and *adenomatous polyposis coli (APC)* genes of the Wnt/wingless signaling pathway, play pivotal roles in human diseases, including cancer (Vogelstein and Kinzler, 2004). Mutations contribute to genetic instability, a major underlying hallmark of cancer, which propels human tumor progression (Hanahan and Weinberg, 2011). Such mutations in oncogene  *$\beta$ -catenin* and tumor suppressor *APC* endow cancer cells with the ability to outgrow or outlive their neighboring cells not affected by mutations (Vogelstein and Kinzler, 2004). However, the understanding of other genes in the Wnt/wingless pathway is less clear. Many genes and their proteins, upon modifications, can elicit opposing growth-promoting and suppressive functions at different cancer stages. Yet, little is known as to how these processes are controlled at the genetic level.

$\delta$ -Catenin/NPRAP/Neurojungin (gene designation: *CTNND2*) is primarily a neuronal protein expressed in brain (Lu et al., 1999; Paffenholz and Franke, 1997; Zhou et al., 1997). However, this initially described neural specific member of the  $\beta$ -catenin/armadillo superfamily is commonly overexpressed in cancers of peripheral tissues, including prostate, esophageal, breast, lung and ovarian cancers (Burger et al., 2002; Lu et al., 2005; Zhang et al., 2010c; Zheng et al., 2004). While the mechanisms of  $\delta$ -catenin regulation in neurologic disorders and cancer are beginning to emerge, studies show that  $\delta$ -catenin promotes canonical Wnt/ $\beta$ -catenin/LEF-1-mediated transcription (Kim et al., 2012). The  *$\delta$ -catenin* gene locus (5p15.2) is highly susceptible for generating single nucleotide polymorphism (SNP). Compelling recent evidence

has linked *CTNND2* SNP or mutations to cancer, myopia, cortical cataract and Alzheimer's disease (Jun et al., 2012; Lu et al., 2011). Chromothripsis and focal copy number alterations in 5p12-5p15 also determine poor outcomes in malignant melanoma (Hirsch et al., 2013). In cancer cells,  $\delta$ -catenin can exert both pro- and anti-growth effects, and is correlated with poor patient survival (Westbrook et al., 2005; Zeng et al., 2009; Zhang et al., 2010c). Although the mechanisms by which these paradoxical functions are controlled genetically, and how they promote cancer pathogenesis have not been well established,  $\delta$ -catenin is a potential cancer biomarker and could be an important target for therapeutic interventions.

Here we take the advantage of a serendipitous discovery of induced *CTNND2* mutations in prostate cancer xenografts, which lead to sequence disruptions predicting functional alterations. We further reveal a broad spectrum of exonic mutations in  $\delta$ -catenin associated with human prostatic adenocarcinoma. We found that the integration of ectopic  $\delta$ -catenin gene into the host chromosomes is not locus selective. The mutant cells empower survival advantage upon overgrowth and glucose deprivation. We found that reprogramming energy utilization accompanies the down-regulation of glucose transporter-1 (Glut-1) and PARP cleavage, preserving PKM<sub>2</sub>,  $\beta$ -catenin translocation to the nucleus and increases in HIF-1 $\alpha$  expression. We conclude that the introduction of *CTNND2* gene variation is an important milestone in prostate cancer metabolic adaptation with the potential of being a target element for prostate cancer treatment.

## **C. Experimental procedures**

### *C1. Antibodies and reagents*

Mouse anti-E-cadherin, anti-p120<sup>ctn</sup>, and anti- $\delta$ -catenin clone 30 (to amino acids 85-194) were from BD Biosciences (Palo Alto, CA). Monoclonal anti-GAPDH was from EMD Science (Darmstadt, Germany). Rabbit, guinea pig, and mouse antibodies against different epitopes of mouse or human  $\delta$ -catenin (epitopes on mouse 85-194, 292-309, 691-708, 1017-1035; human 434-530, 828-1022) were described previously (Burger et al., 2002; Zhou et al., 1997). Rabbit anti-PARP and anti-PKM<sub>2</sub> were from Cell Signaling (Danvers, MA). Rabbit anti-HIF-1 $\alpha$  and anti-Bcl-2 were from Santa Cruz Biotechnology (Santa Cruz, CA) whereas rabbit anti- $\beta$ -catenin was from Sigma (St. Louis, MO). Rabbit anti-Glut-1 and mouse anti-mitochondrial NADPH dehydrogenase/complex cocktail were from Abcam (Cambridge, MA). All other chemicals were procured from Sigma (St. Louis, MO) unless otherwise indicated.

## C2. Cell culture, mutagenesis, and transfection

Human prostate tumor xenograft CWR22Rv-1 or PC-3 cells were stably transfected with full-length  $\delta$ -catenin (named as Rv/ $\delta$ ) or GFP vector alone (named as Rv/C) using FuGENE 6 (Roche Scientific, Gaithersburg, MD). For selection of pEGFP- $\delta$ -catenin transfected cells, cells were first selected in G418 containing medium. Then, pEGFP- $\delta$ -catenin transfected cells were further selected by GFP-based cell sorting using a FACS Vantage (BD Biosciences, San Jose, CA). The amino-terminal 280 amino acid deleted (Rv/ $\Delta$ N) or carboxyl-terminal 207 amino acid deleted (Rv/ $\Delta$ C)  $\delta$ -catenin cDNA with pEGFP fusion were transfected similarly. The stable cell lines were maintained in RPMI1640 medium containing 25 mM glucose and supplemented with 10% FBS and 0.25% Gentamicin (G418) (Gibco, Grand Island, NY). To spontaneously generate a truncation variant, cell cultures were plated in high glucose medium with 10% FBS followed by repeated interruption of medium replenishment. Cells subjected to glucose deprivation were

cultured in RPMI1640 medium with 0.25 mM, or no glucose, and were then supplemented with 10% dialyzed FBS. All cells were incubated at 37°C in 5% CO<sub>2</sub> environment.

To generate the truncated  $\delta$ -catenin with targeted mutation, we performed *in vitro* mutagenesis with the following strategy. We took part of the  $\delta$ -catenin sequence from the original *pEGFP- $\delta$ -catenin* vector and made the mutation to “TGGGCTGAGGAATGTGGCAGGC” from “TGGGCTGAGGATGTGGCAGGC” using primer sets as forward primer “AAGGGCTGGGCTGAGGAATGTGGCAGGCATGG” and reverse primer “CCATGCCTGCCACATTCTCAGCCCAGCCCTT” by PCR. This mutation predicts a stop codon after 138 nucleotide sequences in the mutant  $\delta$ -catenin. Mutated  $\delta$ -catenin sequence was verified by sequencing.

### C3. Genomic DNA extraction from tissue and PCR amplification of $\delta$ -catenin gene

The archival paraffin blocks of radical prostatectomy (RP) cases were performed at the Brody School of Medicine. The clinical pathology analysis regarding Gleason score, tumor stage, and status of surgical margins were assessed as described (Lu et al., 2005). All 16 prostate cancer and clinically disease-free tissue samples were transferred to the laboratory according to the Institutional Research Board approved protocol #06-0300. Additionally, two cases of commercial DNA from prostate cancer patients were obtained from Promega (Madison, WI).

Genomic DNAs were extracted from fresh tissue using DNeasy Tissue Kit (Qiagen Science, Maryland) or from paraffin embedded primary prostatic adenocarcinoma samples and non-cancer prostate tissues. PCR analysis was performed to amplify  $\delta$ -catenin exon sequences using genomic DNA as templates from cells of prostate cancer tissue specimens. The PCR primers and reaction conditions used for detection of  $\delta$ -catenin DNA sequences were listed in Table 2.1.

**Table 2.1 Specific primer sets for human *δ-catenin***

<b>Primers for exon</b>	<b>Sequence of primers</b>	<b>Tm (°C)</b>	<b>Size (bp)</b>
Exon1	Forward: AAAGCGGAAGATGCTGCAGTTGG Reverse : TTGGTAACCGCTCCAAGAAAG GCA	60	378
Exon2	Forward: TGTCTTGGTCTTTCTCAGCAGC Reverse: TTTCAAGGAAGGCTGCCCAA	57	462
Exon3	Forward: ATTCAAAGTTGCATGGCCAGTGG G Reverse: GACTGAAGTTCCAATTCCACCACCG	60	406
Exon4	Forward: TGAGTCTAACAGGTTGGGCTTTGT Reverse: GGTCAGCAATTCATGTACCCTTG	58	533
Exon5	Forward: GGGTACATGAAATTGCTGACCTTGGC Reverse: AATGTGGGAAGGGAACAGATGGGA	60	468
Exon6	Forward: AGCATGGATGGCTGGAATCATGTG Reverse: CTCATTCACAGCACCAAAGGGCA	60	448
Exon7	Forward: CTGTGCCAGTGTCAGGACAAGAAA Reverse: TCCTGCAACTACTACAACCTGGCA	60	875
Exon8	Forward: ATGCCGACAGGCTGATTAGGTTGA Reverse: GTGGACACAGACACACACCTTTCA	60	466
Exon9	Forward: GGTTAACCATTTCTGTGAGCAGGTCC Reverse: GGGATCCATTGCAAGCACACACAT	60	486
Exon10	Forward: CTCAAGGGAATCTCTTCCAATCCC	58	537

	Reverse: ACTATTGGTCCTCTGTTCCCTCGGT		
Exon11	Forward: TGCCTTAATTCAGTTTGGTGCGA	57	451
	Reverse: GACCGCCTATGTTATTAGAACACCAC		
Exon12	Forward: TCATCCTTCCTGCCAGTTCCGTTA	59	421
	Reverse: ACTCCGTTGCCACATCAACATTCA		
Exon13	Forward: TGACTTACCCA ACTCTGGGATGTG	59	575
	Reverse: TACTCAACTGGAACACCTGTGG		
Exon14	Forward: ATGGAGAAAGAGGCCTTCCAGGT	59	486
	Reverse: TTCCTATCCTGGCTCAACTGCGA		
Exon15	Forward: TGATCCCTGGACTGCTGATGCAAT	59	537
	Reverse: AGTGATCTTCAAGGACTCCTGAGC		
Exon16	Forward: TCCTGTAAGCAGCCGCTGAAA	57	468
	Reverse: GCAAGGATTAGAAATGTCAACGAGC		
Exon17	Forward: TGGATGCACTGCCATGAGGAATGA	60	489
	Reverse: CGTCATCAGGAGTTGAAAGGCACA		
Exon18	Forward: TTACGGTTGCTGTCTTAGGTGGGT	60	484
	Reverse: ACAGGTCTGTCCAGTCCAGAAAGT		
Exon19	Forward: CACATTTGGCTCTGTTACCTCCA	60	454
	Reverse: AGAGTGGCCACCACAGTACAAAGA		
Exon20	Forward: TCTTTATGTAGCAAGTGCCCCAGC	148	59
	Reverse: CTCACCTGTCATGGCATCTTTCC		
Exon21	Forward: CAAATAACA ACTATTCCTTATT	50	165
	Reverse: AACGTGTTGCATTTACTTAC		

Exon22 Forward: TCCCGTTTAGGTTTCAGCACAG  
Reverse: CTGCTCCTCACACCCAGGAGTC

---

59

278

#### C4. PCR products sequence analysis

The purified PCR products using QIAquick PCR Purification Kit (Qiagen Science, Maryland) were sent for sequencing. The DNA sequences of amplified PCR fragments obtained from prostate cancer tissues were compared to the human *δ-catenin* DNA sequence as reference published in the NCBI database using BLAST Program. To conduct mutation cluster region (MCR) analysis, mutations deposited in the Sanger cancer sequencing database were combined with the ones in this study. Nucleotide position of the mutations was plotted against the exons in *δ-catenin*.

#### C5. Genomic DNA extraction from cultured cell line and PCR amplification of mouse *δ-catenin* cDNA sequence

PCR analysis was performed to amplify *δ-catenin* exon sequence using genomic DNA as templates isolated from Rv/δ and Rv/C cell lines. The PCR primers and reaction conditions used for detection of mouse *δ-catenin* cDNA sequences were listed in Table 2.2. Purified PCR products were sequenced and compared to mouse *δ-catenin* cDNA sequence as reference published in the NCBI database using BLAST Program.

**Table 2.2 Specific primer sets for mouse  $\delta$ -catenin**

<b>Primers for exon</b>	<b>Sequence of primers</b>	<b>Tm (°C)</b>	<b>Size (bp)</b>
Exon1 to 5	Forward: ATCACATGGTCCTGCTGGAGTT Reverse : ATTGAGCTGAAGTGC ACTCTGGGA	59	557
Exon6 to 7	Forward: AGGCATTCTGGACCCACAGGATTA Reverse: AGACACGGTCTTCATAGATGGG	58	875
Exon8 to 9	Forward: CGTCTGAGCAGTACAGCAAGCATT Reverse: AGCATTGGACTGGACTGAAGGGAA	59	608
Exon10 to 12	Forward: TGCAGTATTGTGCCTCCGTTGACT Reverse: ACTGGATCACGTACAGCAAGGCAT	60	729
Exon13 to 17	Forward: TACAGCTGCATTCATCACAGGTGC Reverse: CGCATGGCATACTTGCCAATGAGT	59	769
Exon18 to 20	Forward: TGTGGAGCTCCTCCGAATAGACAA Reverse: TTGAGGCTGATCATTCCCGAGGT	59	561
Exon21 to 23	Forward: AGCCTCATCTTCAACCATCG Reverse: CAAATGTGGTATGGCTGATTATG	59	606

**C6. Immunofluorescent light microscopy**

Cultured cells were plated on the coverslips and fixed in warm 4% paraformaldehyde. Following permeabilization in 0.2% Triton X-100, the cells were stained using mouse monoclonal anti-p120<sup>ctn</sup>. The cells were then incubated with the goat anti-mouse Cy3 conjugated

secondary antibodies. The nuclei of the cells were stained with Hoechst 33258. The cover slips were mounted on slides using Anti-Fade medium (Invitrogen, Carlsbad, CA) and photographed under the Zeiss Axiovert inverted fluorescent microscope (Carl Zeiss, Thornwood, NY).

#### C7. Western blot with ECL detection

Cells for protein analysis were lysed in RIPA buffer (1% Triton x-100, 0.5% Deoxycholic Acid, 0.2% SDS, 150 mM sodium chloride, 2 mM EDTA) with complete protease inhibitor cocktail tablet (Roche, Germany) and pepstatin A. After removing cell debris by centrifugation, protein concentration was determined using the BCA method. The proteins separated by SDS-PAGE were transferred to the nitrocellulose membrane (Optitran, Germany) for Western blot analyses. After incubation in appropriate primary and secondary antibodies, the membranes were developed with ECL detection reagents. Densitometry using Quantity One (Bio-Rad, Hercules, CA) was carried out to quantitatively measure protein intensity on the Western blots. Statistical analysis was performed to obtain means and standard errors with *p*-values.

#### C8. Chromosome spread preparation

Metaphase chromosomes were prepared following the method of Deng et al. with minor modification (Deng et al., 2003). Briefly, the cells were treated with nocodazole (0.01%) at 37°C for 3 h. After being treated with a hypotonic solution (0.8% Sodium Citrate), the cells were prefixed in freshly prepared Carnoy's fixative (methanol: glacial acetic acid = 3:1 v/v) for 10 min. The cells were collected by centrifugation and washed with Carnoy's fixative three times.

After the final centrifugation, the supernatant was removed completely and the cell pellet was resuspended in 0.3 ml of Carnoy's fixative, and optimal cell spreading was accomplished.

#### C9. Fluorescence in situ hybridization (FISH)

To determine whether mouse  $\delta$ -catenin cDNA integrates into multiple chromosomes after transfection and stabilization into cultured CWR22Rv-1 cells, biotin-labeled probe were designed for FISH analysis. The probe for oligonucleotide sequences was as follows and labeled with biotin at 5-terminal: TCGGCATGGACGAGCTGTACAAGTCCGGACTCAGATCTAT GTTCGCCAGGAAGCAGTCGG.

FISH was carried out according to Huang et al. with some modifications (Huang et al., 2007). Briefly, the chromosome spreads were digested at 37°C with 0.01% pre-warmed pepsin in 10 mM HCl for 10 min. After being prefixed with 37% formaldehyde for 5 min at room temperature, the chromosome spreads were denatured in a mixture containing 75% formamide and 2 × SSC at 75°C for 15 min, then dehydrated with a chilled ethanol series, 70%, 90%, 100%, for 3 min each, and air-dried. The hybridization mixture (10 ng/μl probes, 10% dextran sulfate, and 50% deionized formamide in 2x SSC) was denatured at 100°C for 15 min and chilled immediately by being put on ice for at least 5 min. Denatured probe was applied onto the slide and DNA-DNA *in situ* hybridization was carried out in a humidity chamber at 37°C overnight. Following hybridization, the slides were washed in 2x SSC at 37°C for 10 min, 0.2x SSC at 53°C for 5 min and, finally, briefly equilibrated with 4x SSC/Tween 20 at room temperature. The slides were then blocked with 3% BSA in 4x SSC/Tween 20 solution at 37°C for 30 min. After washed with 4x SSC/Tween 20 at 45°C for 5 min, the slides were incubated with anti-avidin-Cy3 (1:500 dilution in 4x SSC, 0.1% Tween 20, 1% BSA) at 37°C for 30 min. Finally,

chromosomes were counterstained with Hoechst and mounted with anti-fade medium before imaging acquisition and analysis under a Zeiss Axiovert fluorescent light microscope (Carl Zeiss, Thornwood, NY) equipped with the MatMorph software.

#### C10. Cell growth with high glucose or with glucose deprivation

Cells under the normal growth condition of high glucose and FBS for seven days were harvested after trypsinization and mixed with trypan blue at a 1:1 dilution. They were counted using an automated cell counter (Invitrogen, Countness<sup>TM</sup>). All experiments were performed in triplicate. Data are expressed as mean  $\pm$  SEM. To determine growth after cells piled up, cells were plated in the FBS containing medium for two days and were replenished with fresh FBS, allowing them to grow to near confluency. Then, the cell numbers were counted following an additional five days without fresh FBS replenishment.

Some cell cultures grown under high glucose (25 mM) or low glucose (0.25 mM) with dialyzed FBS were divided into two groups: healthy adherent cells and detached dying cells. The ratio of detached to adherent cells was designated as the death index.

To determine cell death by flow cytometry, Rv/C, Rv/ $\delta$ , Rv/ $\Delta$ N, and Rv/ $\Delta$ C cells were grown to 60% confluency, trypsinized, and centrifuged at 1000 rpm to pellet the cells. The supernatant was carefully removed and the cells were re-suspended in 0.7 mL cold 100% ethanol and 0.3 mL cold PBS. The cells were stained with propidium iodide before they were taken for flow cytometry analysis. The propidium iodide staining solution was made with 470  $\mu$ L PBS with 5  $\mu$ L RNase A and 25  $\mu$ L stain propidium iodide (1 mg/mL in de-ionized water). The cells were incubated in propidium iodide stain for 1 h. The cell counts were obtained using the

software *Cell Quest*, with the parameters set to include apoptosis as sub-G1 populations. The results were analyzed by taking the mean and standard error results.

### C11. Metabolic measurement

Two days before the experimental analysis, Rv/C, Rv/ $\delta$ , and Rv/M1 cells were plate (20,000 cells/well) onto custom XF24 microplate (Searhorse Bioscience, North Billerica, MA). Some cells were cultured in the presence of normal glucose (25 mM) and 10% FBS, while other cells were cultured in low glucose (0.25 mM) with dialyzed FBS. Cells were rinsed three times in unbuffered Dulbecco's modified essential medium (DMEM), and incubated for 1 h at 37°C without CO<sub>2</sub> in 600  $\mu$ L of unbuffered DMEM (pH 7.4) supplemented with 10mM glucose, 1mM sodium pyruvate. The cell glycolysis (ECAR) and mitochondrial oxidative phosphorylation (OXPHOS) (OCR) were measured in real-time using a Seahorse Bioscience XF24 Extracellular Flux Analyzer (Billerica, MA). Following the basal rates of OCR and ECAR measurements, a series of injections of three compounds that affect bioenergetics was introduced which included: 100  $\mu$ M 2, 4 dinitrophenol (2,4 DNP), 100 mM 2-deoxyglucose (2-DG), and 1 uM rotenone. Each cell type was plated and analyzed by quintuplicate while outliers were removed so the most consistent triplicate data were integrated.

### C12. Preparation of nuclear and cytoplasmic protein fractions

In order to prepare the cytoplasmic and nuclear fractions, cultured Rv/C, Rv/ $\delta$ , and Rv/M cells were resuspended in buffer A containing 15 mM HEPES, pH 7.4, 80 mM KCl, 15 mM NaCl, 5 mM EDTA, 1 mM phenylmethylsulfonyl fluoride, and 25 mM sucrose with protease and phosphatase inhibitor cocktails. The cells were lysed in the buffer, homogenized in a syringe

with 22 gauge needles, and centrifuged at 1,000 rpm for 10 min at 4°C. The supernatants were again centrifuged at 21,000 rpm (Beckman coulter Optima<sup>tm</sup> Max-E ultracentrifuge, Brea, CA) for 90 min at 4°C. The supernatants were used as the cytoplasmic fractions, and the pellets were used as the nuclear fractions.

## **D. Results**

### *D1. Ectopically expressed $\delta$ -catenin is invariably mutated in prostate cancer cells*

We overexpressed  $\delta$ -catenin into CWR22-Rv1 cells derived from human primary prostatic tumor xenografts and PC-3 cells of prostate cancer bone metastasis. Stable cell lines were successfully established. But to our surprise, the full-length  $\delta$ -catenin gradually and invariably gave way to faster migrating variants, which eventually stabilized at ~ 100 kDa on SDS-PAGE when the cells were cultured with repeated interruption of medium replenishments (Fig. 2.1A). We initially regarded this variant as being derived either from a truncated cDNA contamination or proteolysis due to unfavorable culture conditions. However, mapping with antibodies against epitopes covering the entire protein length ruled out cDNA contamination as the cause because it would have represented a nonexistent cDNA. We then applied a panel of protease inhibitors to determine whether the presumptive proteolysis can be reduced or prevented. E64D, E64D plus leupeptin (which inhibits most peptidases), or A-acetyl-cysteine (NAC) as anti-autophagy/oxidant agent (Yuan et al., 2009) did not inhibit this variant (Fig. 2.1B). E-cadherin and p120<sup>ctn</sup>, two adherens junction proteins that are co-localized with  $\delta$ -catenin and are known to undergo proteolysis (Davis et al., 2003; Rios-Doria et al., 2003), were quite stable under the same culture conditions (Fig. 2.1C). The phenomenon that fast migrating protein bands became dominant over time was also observed in PC-3 cells when full-

length  $\delta$ -catenin was ectopically overexpressed (Fig. 2.1D). Furthermore, once cell cultures with the variant were established, the truncated protein could be observed from cells lysed soon after re-plating. Therefore, protein degradation due to culture aging cannot be the major mechanism of generating this variant.

A closer examination of  $\delta$ -catenin cDNA isolated from the stable cell lines that express the mixed full-length and truncated  $\delta$ -catenin bands showed sequence variations. This surprising result prompted the hypothesis that the  $\delta$ -catenin gene may be genetically targeted by cancer cells. We then sequenced the entire  $\delta$ -catenin cDNA stably expressed in CWR22-Rv1 cells. We discovered that the cells expressing mainly the truncated  $\delta$ -catenin variant displayed frame-shifting mutations that lead to premature termination (Fig. 2.1E). Remarkably, the predicted mutant protein variants derived from some of these premature terminations (e.g., exon 16 in Fig. 2.1E) fell in the close range of the size of the fast migrating protein band on SDS-gels. To demonstrate that the mutations in  $\delta$ -catenin can indeed generate the fast migrating protein band, we performed a mutagenesis experiment. We generated the identical mutation as the naturally occurring frame-shifting mutation described in Figure 2.1E, and then transiently transfected it into CWR22Rv1 and PC-3 cells. Western blot analysis confirmed that the fast migrating protein band was at the same size of the predicted molecular weight for the truncated protein as the mutation would cause (Fig. 2.2). These findings highlighted the potential of a malignant tumor environment in inducing genetic mutations in an overexpressed gene.

D2. There are hot-spot mutation cluster regions in CTNND2 exons in human primary prostatic adenocarcinomas

The above data prompted the question of whether the mutations are the consequences of  $\delta$ -catenin overexpression in cultures *in vitro* or reflect an event that also occurs in human prostate cancer *in vivo* (Burger et al., 2002; Lu et al., 2005) where  $\delta$ -catenin expression is increased. Therefore, we sequenced and analyzed the entire coding region of  $\delta$ -catenin gene (exon 1-22) isolated from human prostatic adenocarcinomas. Most functional mutations occurred after exon 9 (Fig. 2.3A). Some mutations that are either mis-sense or frame-shifting occurred after exon 13 (Fig. 2.3A and Fig. 2.3B-F, bottom panels). So far, gene variations in the  $\delta$ -catenin coding region have been identified in 24 of 40 pathologically confirmed prostatic adenocarcinomas (Fig. 2.3 and Fig. 2.4). Little or no mis-sense or frame-shifting mutations were found in four exonic DNAs from clinically disease-free normal specimens (Fig. 2.3B-F, top panels). We also did not observe significant mutations at the amino-terminus corresponding to exons 1-9 (Fig. 2.3A). These data strongly suggested that human  $\delta$ -catenin gene contains hot-spot mutation cluster regions (MCRs) in prostate cancer.

D3. CTNND2 mutations are not locus-selective

We then cloned CWR22-Rv1 cells that expressed only the truncated  $\delta$ -catenin variant (Fig. 2.5A). As expected, full-length  $\delta$ -catenin was distributed at the cell-cell junction (Fig. 2.5B, GFP: arrows, Rv/ $\delta$ ) (Kim et al., 2012; Lu et al., 1999). However, the truncated  $\delta$ -catenin was exclusively cytoplasmic (Fig. 2.5B, GFP: arrowhead, Rv/M1) and did not co-localize with the cell-cell junction protein p120<sup>ctn</sup> (Fig. 2.5B, p120<sup>ctn</sup>: arrows) (Lu et al., 1999). We also examined CWR22-Rv1 cells stably transfected with cDNAs with amino-terminal 280 amino acid truncated

( $\Delta$ N) or carboxyl-terminal 207 amino acid truncated ( $\Delta$ C)  $\delta$ -catenin (Fig. 2.5C). Although the truncation was further toward the carboxyl-terminus,  $\Delta$ C also showed cytoplasmic localization as Rv/M1 (Fig. 2.5B and C, compare Rv/M1 and  $\Delta$ C).

It is widely known that ectopically transferred genes do not insert into a specific chromosome in host cells (Baum et al., 2004). FISH analysis showed that a biotin-tagged DNA probe specific to  *$\delta$ -catenin* DNA sequence labeled multiple host chromosomes in  *$\delta$ -catenin* transfected cells (Fig. 2.5D, Rv/ $\delta$ ) but not in vector transfected control cells (Fig. 2.5D, Rv/C). These observations suggest that the generation of  *$\delta$ -catenin* mutations was not relying upon its *bona fide* chromosomal locus of 5p15.2. Cancer cells must have developed the capacity to target an overexpressed  *$\delta$ -catenin* gene by altering its DNA sequences genetically (Yun et al., 2009).

We found that while Rv/ $\delta$  cells grew faster as previously reported (Zeng et al., 2009), Rv/M1 cells grew slower than either Rv/C or Rv/ $\delta$  cells. Likewise, Rv/ $\Delta$ C cells showed a similar cell death rate to Rv/C, while apoptosis of Rv/ $\delta$  cells was reduced (Fig. 2.6A). These results suggest that carboxyl-terminal deletion of  $\delta$ -catenin did not confer growth advantage under the normal culture condition in which the supplies of glucose and serum factors were abundant. However, when cultures grew until they reached beyond full confluency, Rv/M1 cells displayed increased cell numbers (Fig. 2.6B).

#### D4. $\delta$ -Catenin mutations lead to survival adaptation under glucose deprivation and reprogram energy utilization

Recent studies highlighted the ability of cancer cells to adapt to glucose-deprived conditions by introducing mutations, e.g., in Ras expressing tumor cells (Yun et al., 2009). When grown in culture with high glucose, Rv/M1 and Rv/C cells had similar death indexes whereas

that of Rv/ $\delta$  cells was reduced (Fig. 2.7A, High glucose). However, under glucose deprivation, the death index of Rv/M1 cells reduced precipitously whereas that of Rv/C cells increased dramatically (Fig. 2.7A, Low glucose). Rv/M1 cells were visibly more resilient to glucose starvation than Rv/C cells (Fig. 2.7B). According to Warburg hypothesis, cancer cells require much less energy to survive than they do for growth under densely packed conditions (Vander Heiden et al., 2009; Warburg, 1956).  $\delta$ -Catenin mutations clearly empowered prostate cancer cells with an increase in such capabilities of survival under glucose deprivation.

Our previous study showed that Rv/ $\delta$  cells increased expression of hexokinase II, a key enzyme for phosphorylation of glucose in entering glycolysis, which is increased in prostate cancer (Mathupala et al., 2006; Zeng et al., 2009). To determine how  $\delta$ -catenin mutations may reprogram energy metabolism to promote survival under nutrient deprived conditions, we examined the ability of transfected cells to utilize energy. Under normal growth conditions, Rv/ $\delta$  and Rv/M1 cells showed an increased ratio of oxygen consumption rate (OCR) over a glycolysis-mediated extracellular acidification rate (ECAR) when compared to Rv/C cells (Fig. 2.8A, High glucose). However, under glucose deprivation, Rv/M1 cells displayed higher OCR/ECAR than that of either Rv/C or Rv/ $\delta$  cells (Fig. 2.8A, Low glucose).

After the cultures were maintained with low glucose for a week, Rv/C cells suffered massive cell death (Fig. 2.7B, Low glucose-Rv/C). Correspondingly, the OCR of Rv/C cells did not respond to 2, 4 DNP (Fig. 2.8B), indicating their reliance on glucose for mitochondrial respiration (Wu et al., 2007). Rv/ $\delta$  cell death was moderate, while Rv/M1 cell death was minimal (Fig. 2.8B, Low glucose-Rv/ $\delta$  and Rv/M1). Under this condition, Rv/ $\delta$  and Rv/M1 responded to 2, 4 DNP and displayed an OCR uptrend (Fig. 2.8B), which resembled that of Rv/C, Rv/ $\delta$  and Rv/M1 cells under normal culture condition (Fig. 2.8C). Therefore, Rv/ $\delta$  and Rv/M1 cells

preserved mitochondrial respiration capability and they can unleash its utilization under glucose starvation. Continuing with 2-DG treatment, which inhibits glycolysis (Wu et al., 2007), Rv/C and Rv/ $\delta$  cells increased their relative OCR levels, but Rv/M1 cells showed a sharp reduction in OCR. Corresponding to the very low cell death observed under the low glucose condition, the deficient OCR response of Rv/M1 following 2-DG treatment suggests the potential adaptation mechanisms by which  $\delta$ -catenin mutations promote cell survival (Fig. 2.7B). All cells responded to rotenone, which inhibits mitochondrial NADH dehydrogenase/complex I and, consequentially, blocks mitochondrial respiration.

While the tumor-selective pyruvate kinase, tumor type 2 (PKM<sub>2</sub>) was reduced in Rv/C cells upon glucose deprivation for one week, PKM<sub>2</sub> expression remained strong in Rv/ $\delta$  and Rv/M1 cells (Fig. 2.9A and Fig. 2.9C). The expression of mitochondrial complexes was not significantly changed in Rv/M1 compared to Rv/C and Rv/ $\delta$  cells (Fig. 2.9A). However, compared to Rv/C and Rv/ $\delta$ , Rv/M1 cells showed reduced expression of cleaved PARP, a critical enzyme in the DNA repair defect-initiated apoptosis (Fig. 2.9B and Fig. 2.8D). Bcl-2 expression was increased in Rv/ $\delta$  and Rv/M1 cells when compared to Rv/C cells with or without glucose deprivation (Fig. 2.9B and Fig. 2.9C). Glucose transporter-1 (Glut-1) showed a distinct shift of protein migration pattern of Glut-1H and Glut-1L variants from high glucose to low glucose culturing conditions (Fig. 2.9B). Both variants showed a reduced expression under glucose deprivation in Rv/M1 cells (Fig. 2.9B).

To determine whether the changes in cell growth and survival properties involved Wnt/ $\beta$ -catenin signaling, we found that with high glucose in the medium,  $\beta$ -catenin expression and translocation to the nucleus was increased in Rv/ $\delta$  and Rv/M1 in comparison to that of Rv/C (Fig. 2.10A and Fig. 2.10C). But there were no meaningful differences in HIF-1 $\alpha$  expression

among Rv/C, Rv/ $\delta$ , and Rv/M1 cells (Fig. 2.10A and Fig. 2.10D, Glucose). However, there was a remarkable increase in both  $\beta$ -catenin and HIF-1 $\alpha$  expression and translocation to the nucleus in Rv/M1 compared to Rv/C cells during glucose deprivation (Fig. 2.10B, Fig. 2.10C, and Fig. 2.10D, No Glucose). These results are consistent with our previous studies (Zeng et al., 2009), and further support that the carboxyl-terminus of  $\delta$ -catenin is important for prostate cancer expansion under the normal growth condition. Eliminating these sequences reassigned energy utilization for survival over proliferation-required biomass production under nutrition deprivation (Vander Heiden et al., 2009).

## **E. Discussion**

Our studies identified that  *$\delta$ -catenin* (*CTNND2*) gene displays somatic mutations that are highly inducible when overexpressed, likely representing and predicting an important milestone in prostate cancer cell survival and metabolic adaptation during densely-packed tumorigenesis.

The molecular mechanism of inducible mutagenesis of  *$\delta$ -catenin* in prostate cancer is not clear at present. Our studies showed that the generation of truncated  $\delta$ -catenin protein species is not due to protein degradation. We also showed that the ectopic  *$\delta$ -catenin* gene integrating into host chromosomes is not locally adherent to its native gene locus at Chr5p15.2. It is possible that an increased expression of  $\delta$ -catenin ignited a feedback reaction onto replicating chromosomes where ectopic  *$\delta$ -catenin* cDNA was inserted and a low fidelity replication due to destabilized genome in  $\delta$ -catenin transfected cells allowed un-conserved base pairing to proceed. These random hits towards the 3'-region of ectopic  *$\delta$ -catenin* sequences were then followed by functional selection to favor carboxyl-terminal truncation mutant cells while eliminating full-length  $\delta$ -catenin expressing cells from the prostate cancer cell populations.

Examination of the Sanger cancer gene mutation database found similar trends of sequence variation in the  $\delta$ -catenin coding region in other cancer types (<http://cancer.sanger.ac.uk/cosmic/>). For example, hot-spot MCRs are located at exons 10-14 and 17-22 in cancers including lung, prostate, pancreas, skin, intestine and upper gastrointestinal tract cancers, as well as leukemia (Fig. 2.11A and Fig. 2.11C). The F1172F (c.3516C>T) mutation in exon 22 in human skin cancer, while it is a same-sense mutation, is identical to that in prostate cancer. A number of mutations predicted a significant impact, as they either lead to premature termination or potential alteration of protein functions (Fig. 2.11B). Searching for commonly mutated genes in cancer exerts significant impact on effective cancer diagnosis and therapeutic design (Ding et al., 2008; Papadopoulos et al., 2006). Our findings clearly support  $\delta$ -catenin as one such somatically mutated gene in prostate cancer.

$\delta$ -Catenin is at the cross points of several signaling pathways that play critical roles in development and cancer.  $\delta$ -Catenin interacts with classical cadherins at their juxtamembrane domain, an association motif shared with that for p120<sup>ctn</sup> which is another protein of the p120<sup>ctn</sup> subfamily (p120<sup>ctn</sup>: *CTNND1*) of  $\beta$ -catenin/armadillo superfamily (Kim et al., 2012; Lu, 2010; Lu et al., 1999). This interaction is critical for regulating E-cadherin stability and in the brain it involves the regulation by presenilin (PS) of Alzheimer's disease (Kim et al., 2006; Kouchi et al., 2009). While the roles of  $\beta$ -catenin and its mutations in development and cancer by effecting Wnt/wingless signaling are well established, recent evidence placed  $\delta$ -catenin in the same pathway. Indeed,  $\delta$ -catenin promotes E-cadherin processing and activates  $\beta$ -catenin-mediated signaling in human prostate cancer (Kim et al., 2012).  $\delta$ -Catenin was shown as a new member of the glycogen synthase kinase-3 (GSK-3) signaling complex that promotes  $\beta$ -catenin turnover (Bareiss et al., 2010). GSK-3 phosphorylates  $\delta$ -catenin and negatively regulates its own stability

via ubiquitination/proteasome-mediated proteolysis (Oh et al., 2009). Besides the interaction of  $\delta$ -catenin and p120<sup>ctn</sup> with the canonical Wnt-GSK3- $\beta$ -catenin-LEF1 signaling pathway, non-canonical Wnt signals are modulated by the Kaiso transcriptional repressor, which is also a downstream target of  $\delta$ -catenin and p120<sup>ctn</sup> (Dai et al., 2011; Kim et al., 2004; Rodova et al., 2004). Therefore,  $\delta$ -catenin is intimately involved in Wnt signaling and promotes cancer cell growth and shows poor cancer survival when it is overexpressed.

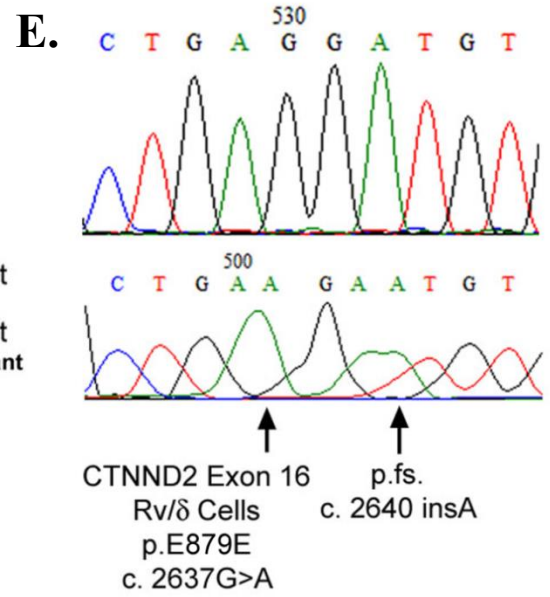
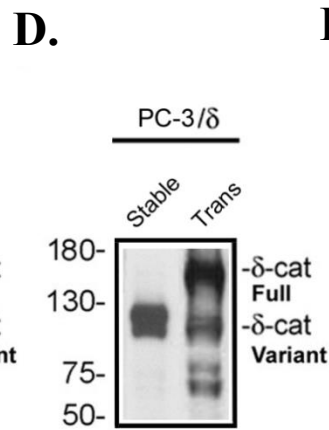
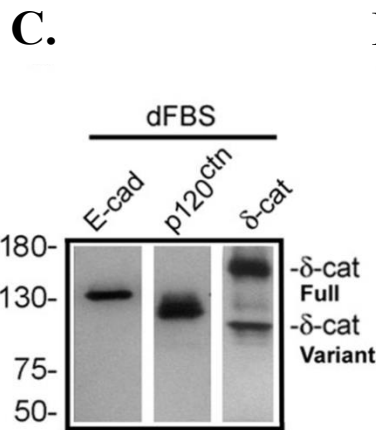
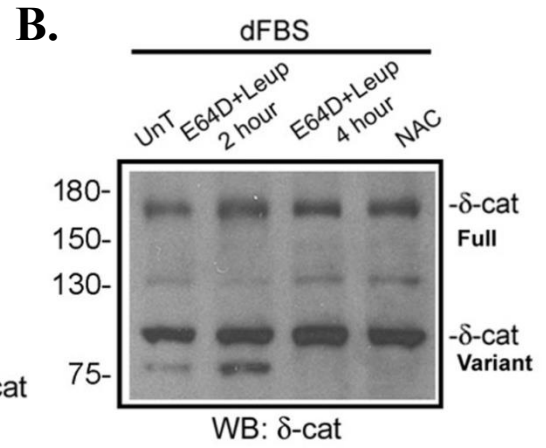
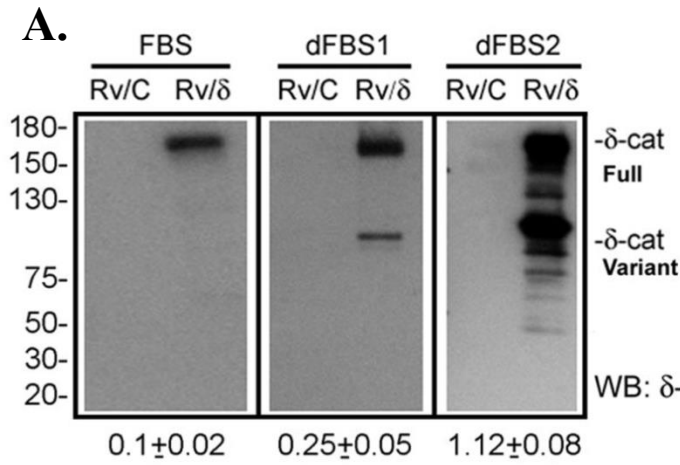
When released from cadherins,  $\delta$ -catenin clearly interacts functionally with actin regulatory network proteins, notably with Rho family small GTPases. Overexpression of  $\delta$ -catenin induces branched cellular processes, which is reminiscent of RhoA inhibition (Kim et al., 2002).  $\delta$ -Catenin overexpression decreased the binding between p190RhoGEF and RhoA, and significantly lowered the levels of GTP-RhoA (Kim et al., 2008a; Kim et al., 2008b).

$\delta$ -Catenin mutant cells (Rv/M1) survived better than Rv/C cells under glucose deprivation but the expression of well-established mitochondrial complexes was not significantly changed. These data indicated that the changes in mitochondrial respiration due to an altered expression pattern of these complexes are less likely the mechanism of enhanced survival of RvM1 cells. Seahorse XF24 metabolic analysis showed that Rv/M1 cells are sensitive to the treatment of 2-DG, an inhibitor of glycolysis. Although we do not yet understand the molecular mechanism how truncated  $\delta$ -catenin leads to metabolic reprogramming, it is possible that carboxyl-terminal truncation reduced the ability of  $\delta$ -catenin to inhibit GTPase RhoA (Kim et al., 2008a) and allow cytokinesis to proceed. The removal of cytokinesis inhibition could result in reprogramming energy utilization in cell cycle progression and prevent cytokinesis checkpoint-initiated apoptosis.

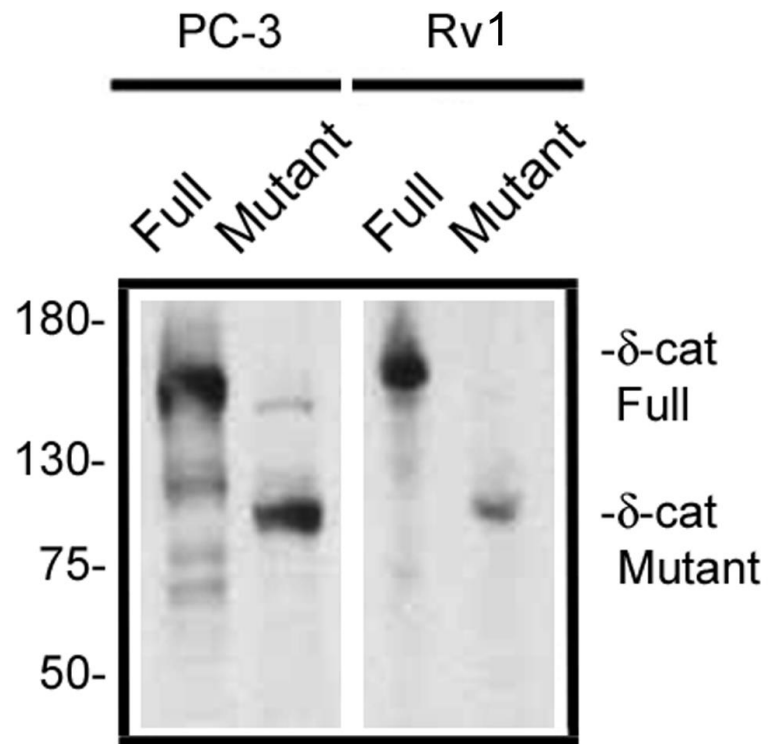
We propose that in normal cells, full-length  $\delta$ -catenin displays tumor suppressive function. This means that overexpressing  $\delta$ -catenin ectopically in a normal cell type would reduce cell proliferation, which is supported by our studies as well as others (Lu et al., 1999; Westbrook et al., 2005). We further speculate that, in malignant tumors, as the cancer cells deregulate many genes' expression during transformation, some genes, when their expressions are high, can be harmful for cancer cell growth. This is well supported in the literature that many genes show both oncogenic and tumor-suppressive functions (Zhang et al., 2010a). We hypothesize that while the amino-terminus of  $\delta$ -catenin promotes prostate cancer cell growth (Zeng et al., 2009), the carboxyl-terminus of  $\delta$ -catenin interacts with the small GTPase RhoA to hinder cytokinesis as seen in p0071 which shares extensive homology at the carboxyl-terminus to that of  $\delta$ -catenin (Wolf et al., 2006). When the promoter of  *$\delta$ -catenin* is activated in prostate cancer (Burger et al., 2002), the cancer cells can balance the rate of cell cycle progression by partially inactivating the overexpressed  $\delta$ -catenin carboxyl-terminus.

Recent studies of Rho GTPase links to mitochondrial enzyme glutaminase (GLS1) suggested that signaling via the Rho GTPases, together with NF- $\kappa$ B, can elevate mitochondrial glutaminase activity in cancer cells, thereby helping cancer cells meet their altered metabolic demands (Wilson et al., 2013). There is also evidence that TSC2 inhibits cell growth by acting as a GTPase-activating protein toward Rheb, thereby inhibiting mTOR. TSC2 integrates Wnt and energy signals via a coordinated phosphorylation by AMPK and GSK3 to regulate cell growth (Inoki et al., 2006). Despite the understanding of  $\delta$ -catenin functions in Rho GTPase and Wnt/ $\beta$ -catenin signaling, the current study is the first to provide significant evidence of exonic mutations in the  *$\delta$ -catenin* coding region and demonstrate their consequences in cancer metabolic adaptations in tumor progression.

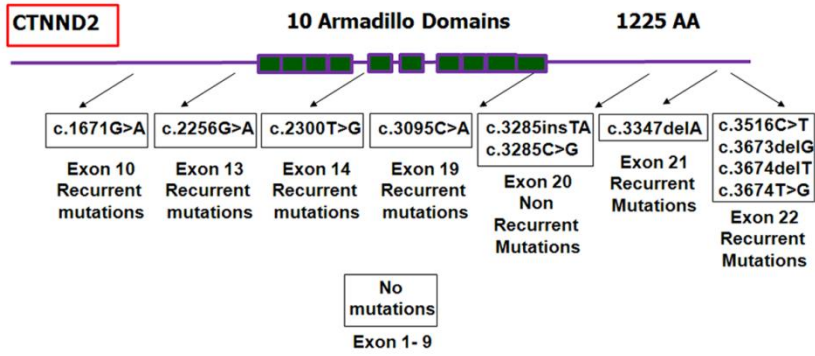
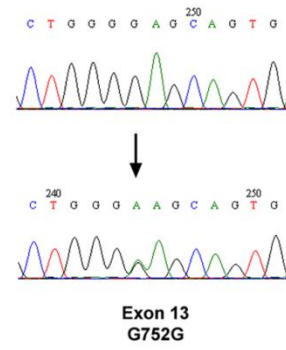
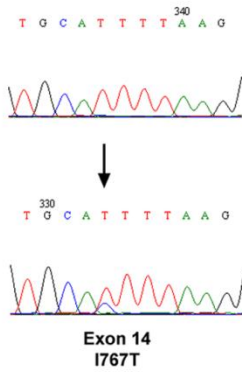
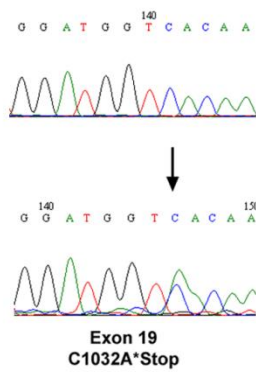
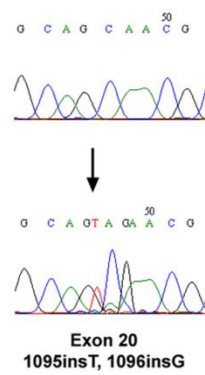
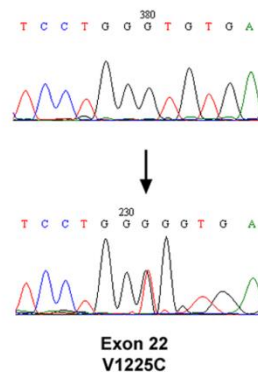
These studies thus raise questions for cancer mechanisms and drug targeting strategies. Cancer cells can apparently alter genetic composition and subsequent functions of foreign DNAs, potentially evading ectopic expression-based gene therapy. Additionally, targeting cancer metabolism may benefit by incorporating enforcers that inhibit genes promoting adaptation under metabolic stress. Finally, chromosomal machinery responsible for mutagenesis is likely not locally adhering to a specific gene locus and is deregulated in cancer homing for introduction of cancer driving and adapting mutations. We have now succeeded in generating an innovative cell which can potentially elucidate such mechanisms that can hold a key to reduce genomic rearrangements and make targeting cancer more effective.



**Figure 2.1 Mutations and formation of  $\delta$ -catenin variants.** (A). Ectopically expressed full-length  $\delta$ -catenin gradually changes to truncated variants in human prostate cancer xenograft CWR22Rv-1 in culture. FBS: fetal bovine serum with high glucose; dFBS1 and dFBS2: the first and second rounds of treatment with FBS and glucose deprivation. Rv/C: control cells; Rv/ $\delta$ : cells expressing full-length  $\delta$ -catenin. Numbers underneath the gels: ratio of truncated variant to full-length  $\delta$ -catenin in Rv/ $\delta$  cells. (B). Protease inhibition did not prevent the formation of  $\delta$ -catenin variant. Rv/ $\delta$  cells from dFBS2 culture were either untreated (UnT), treated with E64D+leupeptin for 2 or 4 hours, or treated with NAC for 4 hours. (C). Rv/ $\delta$  cells from dFBS2 culture displaying fast migrating  $\delta$ -catenin variant but not E-cadherin or p120-catenin proteolysis. (D). Ectopically expressed full-length  $\delta$ -catenin in transient (Trans) transfected human prostate cancer bone metastasis PC-3 cells (PC-3/ $\delta$ ) gave rise to truncated variants that migrated faster on SDS-gel after the  $\delta$ -catenin overexpressing cells became stable cell lines (Stable) in culture. (E). Example of  *$\delta$ -catenin* mutations in Rv/ $\delta$  cells from dFBS2 culture. The lower panel indicates mutation and the upper panel indicates the normal control sequence. Molecular weights are on the left.



**Figure 2.2 Targeted mutation of  $\delta$ -catenin cDNA generated the truncated protein with predicted size on SDS-gel.** *In vitro* mutagenesis was performed to generate the frame-shifting mutation in  $\delta$ -catenin cDNA as described in Figure 2.1E. The mutant  $\delta$ -catenin cDNA was then transfected transiently into CWR22Rv1 and PC-3 cells. Western blots showed that compared to the full-length  $\delta$ -catenin, the mutant  $\delta$ -catenin cDNA transfection resulted in a truncated protein band at the expected size of ~100 kDa. The Molecular weights are shown on the left.

**A.****B.****C.****D.****E.****F.**

**Figure 2.3 Mutation cluster regions (MCRs) of  $\delta$ -catenin coding sequences in human prostate cancer.** (A). Schematic illustration of MCRs in  $\delta$ -catenin coding region. The entire coding region of  $\delta$ -catenin gene was sequenced. Recurrent and non-recurrent mutations were identified. Shown here are mutations in exons 10, 13, 14, 19, 21, and 22 (recurrent) as well as 20 (non recurrent). No mutations were observed from exons 1 to 9. (B-F). Sequence chromatograms showing examples of somatic  $\delta$ -catenin exon mutations. Some mutations lead to the disruption of protein sequences. Note: The lower panels indicate the tumor and the upper panels indicate the matched normal control.

Case	Exon 10	Exon 13	Exon 14	Exon 19	Exon 20	Exon 21	Exon 22
1				c.3095C>A; Stop		c.3347delA; FS	c.3517C>T; Same Sense; c3675T>G; missense
2	c1671G>A; Same sense	c.2256G>A; Same Sense		c.3095C>A; Stop		c.3347delA; FS	c3675T>G; missense
3	c1671G>A; Same sense			c.3095C>A; Stop		c.3347delA; FS	c3675T>G; missense
4	c1671G>A; Same sense				c.3285insT; c. 3286insG; FS	c.3347delA; FS	c3675T>G; missense
5							c3675T>G; missense
6							c3675T>G; missense
7							c3675T>G; missense
8							c3675T>G; missense
9							c3675T>G; missense
10							c3675T>G; missense
11							c3675T>G; missense
12							c.3517C>T; Same sense; c3675T>G; missense
13							c3675T>G; missense
14							c.3517C>T; Same sense; c3675T>G; missense
15							c.3517C>T; Same sense; c3675T>G; missense
16							c.3517C>T; Same Sense
17							c3675T>G; missense
18							c.3517C>T; Same Sense
19							c.3517C>T; Same Sense
20		c.2256G>A; Same Sense	c.2300T>C; Missense			c.3347delA; FS	
21						c.3347delA; FS	
22		c.2256G>A; Same Sense	c.2300T>C; Missense				
23		c.2256G>A; Same Sense					
24							c3674delT

**Figure 2.4 Summary of mutation cluster regions (MCRs) of  $\delta$ -catenin coding regions in human prostate adenocarcinoma tissues.** This schematic represents gene variations in  $\delta$ -catenin coding regions identified in 24 of 40 pathologically confirmed human prostate adenocarcinomas. The mutation cluster region (MCR) analysis was conducted by combined mutations deposited in the Sanger cancer sequencing database with the ones in this study (<http://cancer.sanger.ac.uk/cosmic/>).

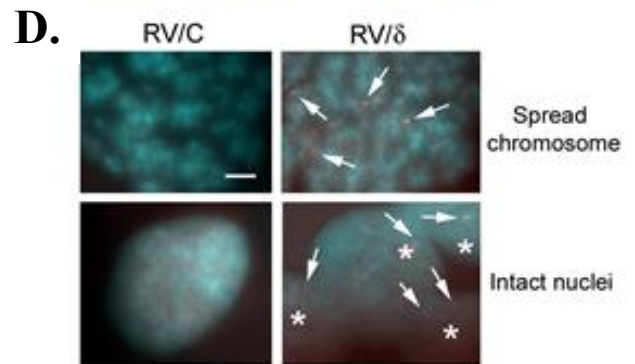
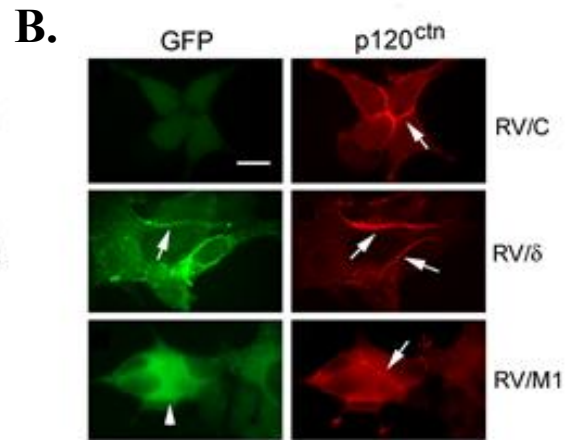
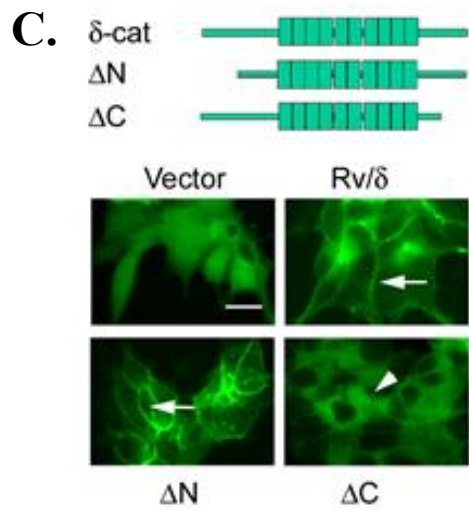
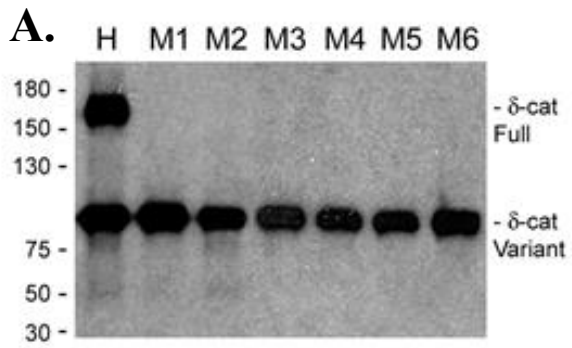
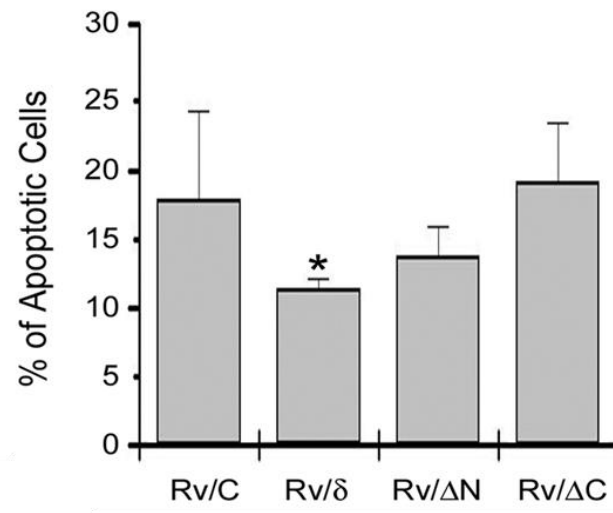


**Figure 2.5 Cancer cells are capable of altering ectopic  $\delta$ -catenin gene sequence and function.** (A). Establishment of  $\delta$ -catenin truncation variant clones. CWR22Rv-1 cells displaying both full-length and truncation variants (H) were subcloned. Shown here are six examples of clones expressing only the truncation variant (M1 to M6). (B). Distribution of GFP-tagged full-length  $\delta$ -catenin and its induced truncation variant in comparison to a closely related protein p120<sup>ctn</sup>. Arrows: cell-cell junction; Arrowheads: truncated  $\delta$ -catenin distribution. Bar: 10  $\mu$ m. (C). Distribution of full-length  $\delta$ -catenin and its amino- or carboxyl-terminal truncation mutants. Upper panel:  $\delta$ -catenin cDNA construct illustration. Arrows: cell-cell junction; Arrowheads: cytoplasm. Bar: 10  $\mu$ m. (D). FISH probe specific to mouse  $\delta$ -catenin cDNA detected multiple hybridization signal (Arrows) in Rv/ $\delta$  but not in Rv/C cell chromosomal spreads. Blue: Hoechst; Red: FISH probe for  $\delta$ -catenin; Asterisks: intact Rv/ $\delta$  cells. Bar: 0.5  $\mu$ m.

**A.**



**B.**

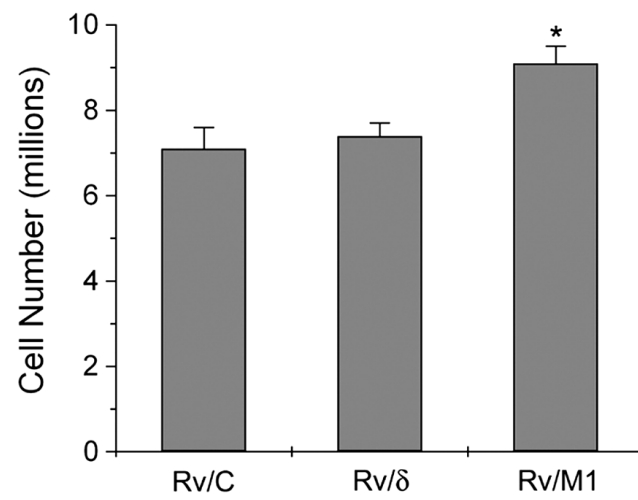
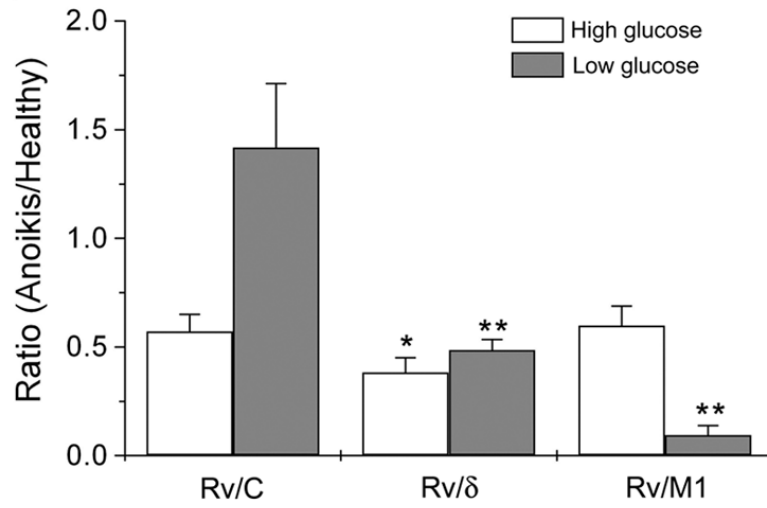


**Figure 2.6  $\delta$ -Catenin truncation variant promotes overgrowth *in vitro*.** (A). Percentage of CWR22Rv-1 cell death. Rv/C: Vector transfected cells; Rv/ $\delta$ : cells transfected with full-length  $\delta$ -catenin; Rv/ $\Delta$ N: cells transfected with amino-terminal 280 amino acid truncated  $\delta$ -catenin; Rv/ $\Delta$ C: cells transfected with carboxyl-terminal 207 amino acid truncated  $\delta$ -catenin. \*:  $p < 0.05$ .

(B).  $\delta$ -Catenin truncation variant promotes overgrowth. The numbers of Rv/C, Rv/ $\delta$ , and Rv/M1 cells were counted without fresh FBS replenishment after full confluence of cultures. \*:  $p < 0.05$ .

**A.**



**B.**

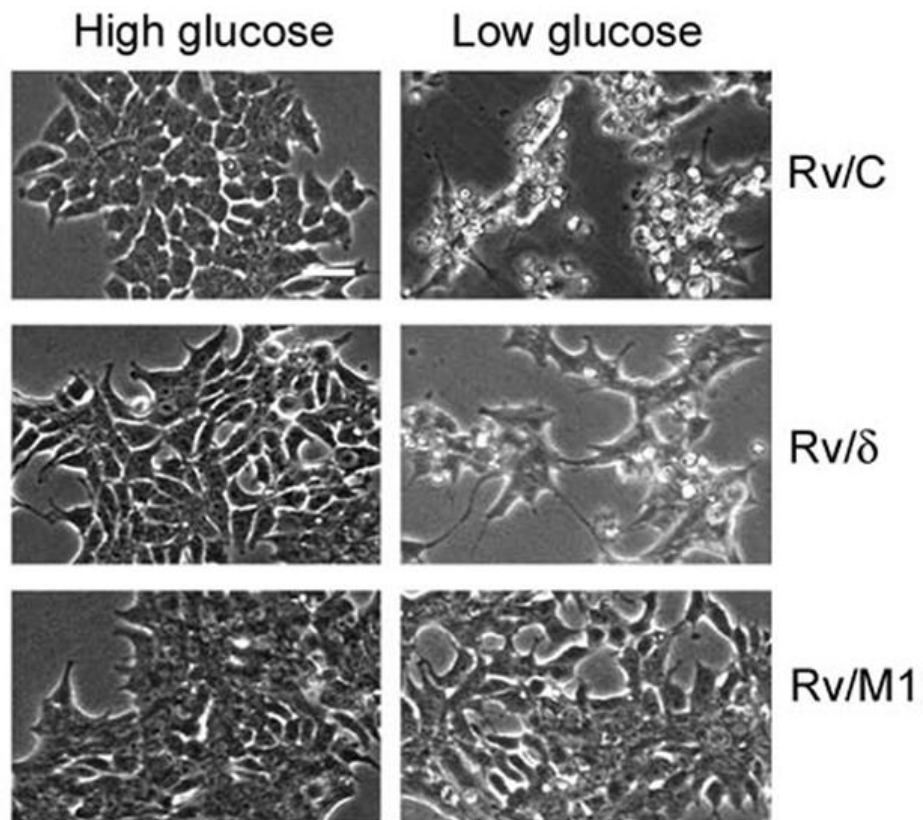
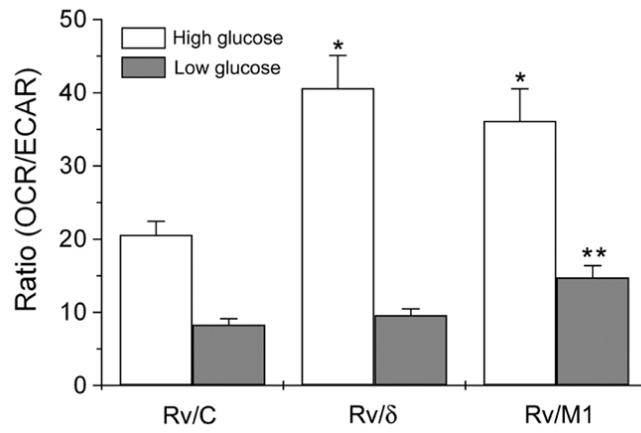
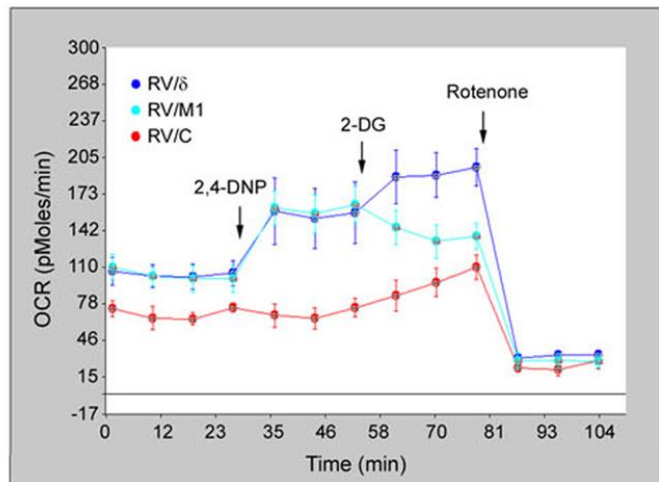


**Figure 2.7  $\delta$ -Catenin mutations promote metabolic reprogramming to increase cancer cell survival and adaptation under glucose deprivation. (A).** Rv/M1 cells show survival advantage under low glucose but not normal growth condition with high glucose. The dying, floating cells versus the healthy, adherent cells were counted separately and their ratio was obtained as death index. \*:  $p < 0.05$  (High glucose); \*\*:  $p < 0.05$  (Low glucose). **(B).** Phase images of cells that grew for seven days under either high glucose or low glucose conditions. Rv/M1 cells showed increased survival under glucose deprivation. Bar: 50  $\mu\text{m}$ .

**A.**



**B.**



**C.**

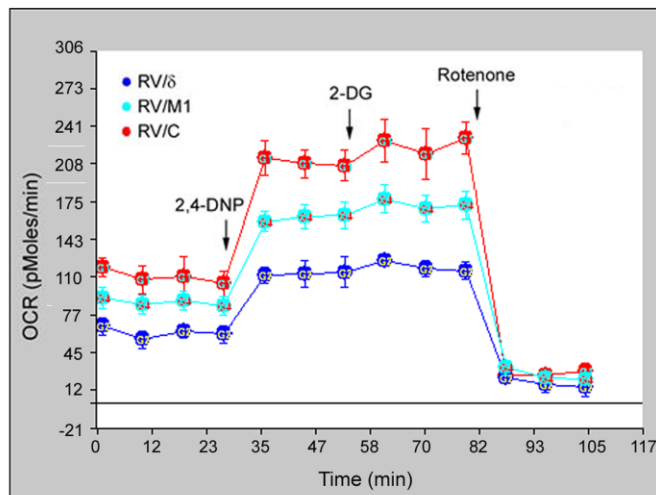
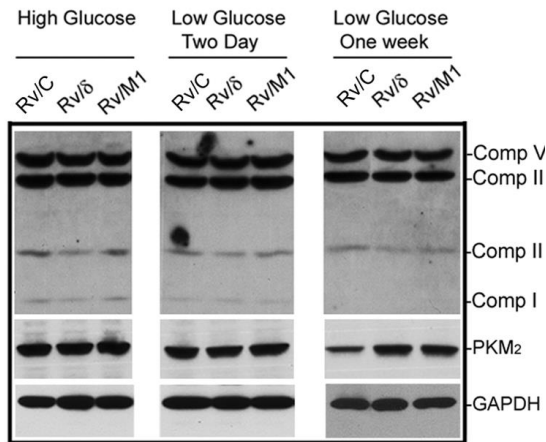


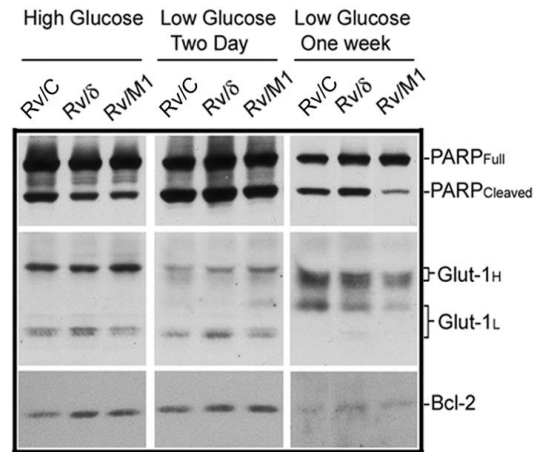
**Figure 2.8  $\delta$ -Catenin mutations promote metabolic adaptation under glucose deprivation.**

(A). Rv/ $\delta$  and Rv/M1 cells showed increased OCR/ECAR when compared to Rv/C under the normal growth condition with high glucose. Rv/M1 cells maintained higher OCR/ECAR, whereas Rv/C and Rv/ $\delta$  cells showed much lower OCR/ECAR during glucose deprivation. \*:  $p < 0.05$  (High glucose); \*\*:  $p < 0.05$  (Low glucose). (B). Rv/ $\delta$  and Rv/M1 cells preserved mitochondrial respiration functions and unleashed its utilization under glucose starvation. Seahorse XF24 analyzer acquisition showed an example of real-time OCR responses to the 2, 4 DNP, 2-DG, and rotenone treatments. (C). OCR over time in CWR22Rv-1 cells expressing  $\delta$ -catenin wild type (Rv/ $\delta$ ) or  $\delta$ -catenin mutations (Rv/M1) under normal condition. Seahorse XF24 analyzer acquisition showing real-time OCR responses to the 2,4 DNP, 2-DG, and rotenone treatments.

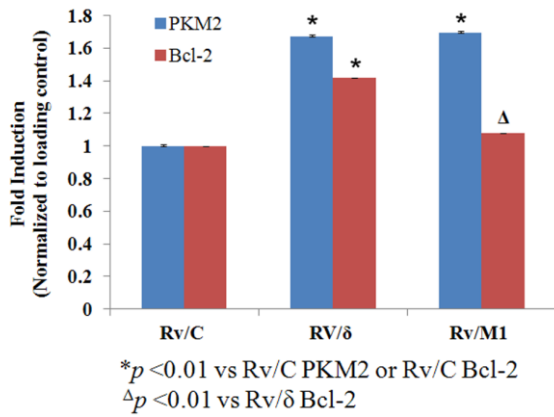
**A.**



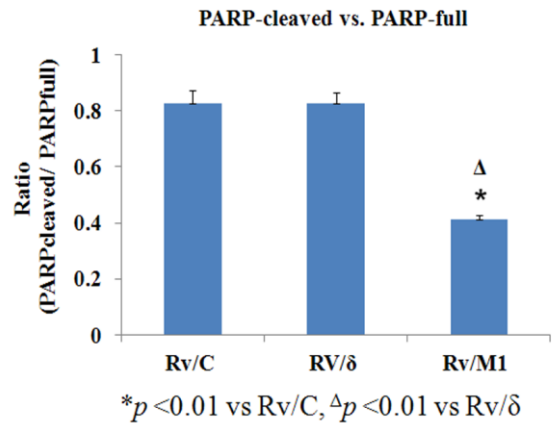
**B.**



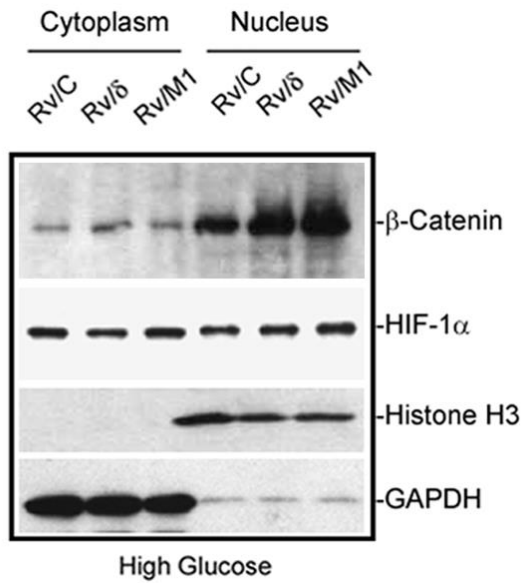
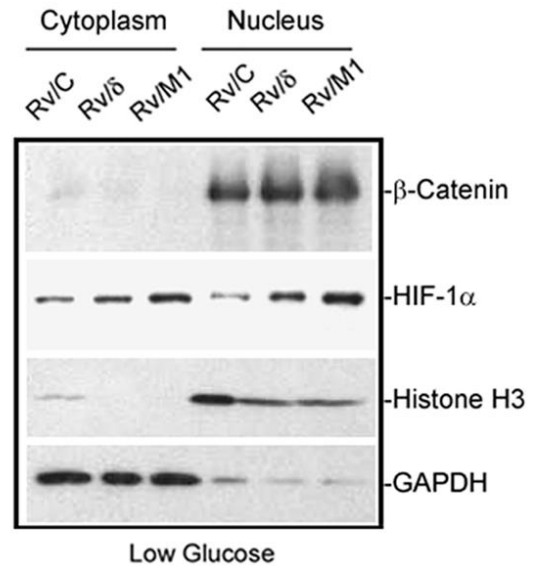
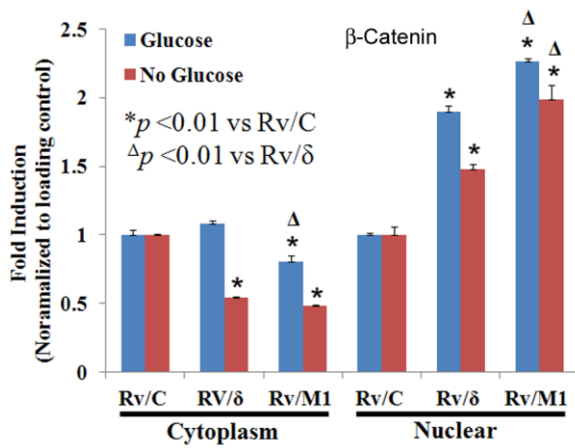
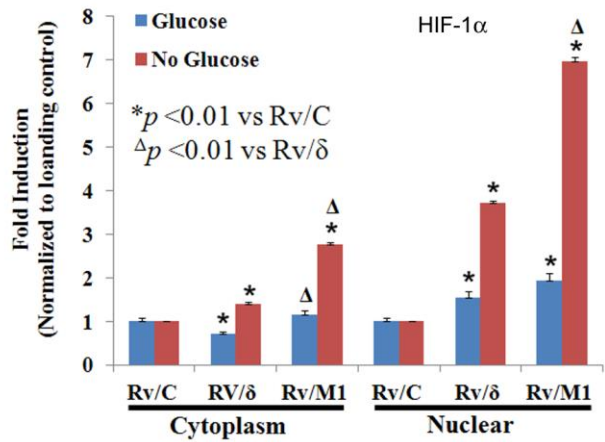
**C.**



**D.**

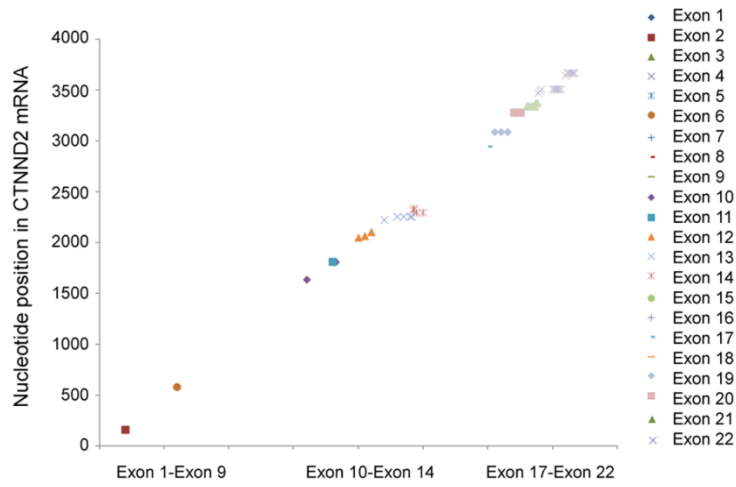


**Figure 2.9  $\delta$ -Catenin mutations lead to survival adaptation under glucose deprivation. (A).** Rv/ $\delta$  and Rv/M1 cells preserved PKM<sub>2</sub> expression but did not alter mitochondrial respiratory complex proteins under glucose deprivation. GAPDH was used as loading control. **(B).** Rv/M1 cells suppressed PARP cleavage and altered Glut-1 expression under glucose deprivation. Both Rv/ $\delta$  and Rv/M1 cells showed increased Bcl-2 expression than that of Rv/C cells with or without glucose deprivation. **(C).** and **(D).** Quantification of Western blots on PKM<sub>2</sub>, Bcl-2, PARP-cleaved, PARP-full-length, corresponding to Western blots shown in **(A)** and **(B)**. All data were from at least two independent experiments.

**A.****B.****C.****D.**

**Figure 2.10  $\delta$ -Catenin mutations alter protein expression and distribution in the Wnt/ $\beta$ -catenin and hypoxia pathways. (A).** There were only moderate changes in HIF-1 $\alpha$  expression but significant changes in  $\beta$ -catenin expression and nuclear translocation among Rv/C, Rv/ $\delta$  and Rv/M1 cells when grown in normal medium with high glucose. **(B).** There were significant increases in  $\beta$ -catenin and HIF-1 $\alpha$  expression and nuclear translocation in Rv/M1 cells when compared to Rv/C cells under glucose deprivation. **(C).** and **(D).** Quantification of Western blots on  $\beta$ -catenin, and HIF-1 $\alpha$  corresponding to Western blots shown in **(A)** and **(B)**. All data were from at least two independent experiments.

**A.**



**B.**

Impacts of functional mutations

Exomic Mutations	Outcomes
T779M	Initiation codon
M605I	Remove alternative initiation potential
Y1128fs*6	Premature termination
P1218L	Break proline-directed kinase consensus PASP
C1032A*	Premature termination
1095insT, 1096insG	Premature termination
V1225C	Remove PDZ binding domain

**C.**

Somatic Mutations in Cancer (Sanger)

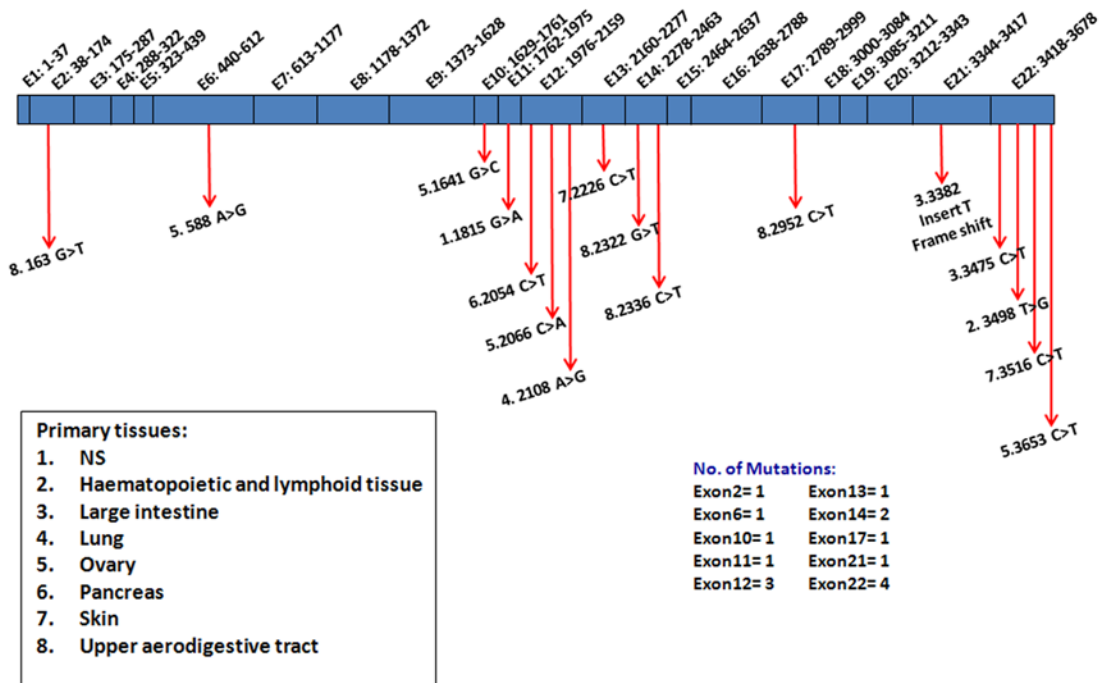


**Figure 2.11 MCR of *δcatenin* showing functional impacts.** (A). Summary of MCR of *δcatenin* coding region in different cancer types. Note: *δcatenin* mutations were clustered around exons 10-14 and exons 17-22. There are few mutations in the exon 1-9. The data reflect MCR from eight different cancer types. (B). *δ-Catenin* exonic mutations in cancer predictive of functional impacts. Seven exonic mutations are listed here as examples to show the potential to alter protein functions, including premature termination. (C). Schematic illustration of somatic mutations extracted from the Sanger cancer mutation database. Note: this database is evolving, so the data reflect the mutations as of the submission date (<http://cancer.sanger.ac.uk/cosmic/>).

## **F. Acknowledgements**

We would like to acknowledge Dr. Jiao Zhang, who assisted in generating Figures 2.1, 2.6, 2.7, and 2.8. Dr. Jain-Ping Lu assisted in mutagenesis experiment. The metabolic measurement was performed by Dr. Donghai Zheng in Figures 2.9B and 2.9C. Christi Boykin assisted in generating Western blot analysis in Figures 2.10A and 2.10B.

# CHAPTER III: MUTATIONS OF $\delta$ -CATENIN CONTRIBUTE TO MOUSE PROSTATE TUMORIGENESIS THROUGH ENHANCED $\beta$ -CATENIN-MEDIATED ONCOGENIC SIGNALS LEADING TO INCREASED CELL PROLIFERATION AND SURVIVAL THEREBY PROMOTING PROSTATE TUMOR GROWTH

## A. Summary

Prostate cancer (PCa) is the most common non-cutaneous malignant neoplasm in men in Western countries. In humans, PCa progresses from precursor lesions, termed prostatic intraepithelial neoplasia (PIN), to overt carcinoma confined to the prostate, and finally to metastatic disease that often results in lethality. Previous studies in our laboratory have shown that  $\delta$ -catenin/NPRAP/Neurojungin (gene designation: *CTNND2*), a primarily neural-enriched protein in the brain of healthy individuals, is overexpressed corresponding to human PCa progression. In this study, we utilized a novel mouse transgenic model of PCa with overexpression of human *Myc* oncogene driven by derivative rat-probasin promoter ( $ARR_2PB$ ) as the initiating event. These *Myc* transgenic mice were further crossbred with either the  $\delta$ -catenin transgene using the same promoter (designated as *Myc/ $\delta$ -cat*) or  $\delta$ -catenin mutant mice, whose exon 9 of the  $\delta$ -catenin gene was disrupted (designated as *Myc/ $\delta$* ). We observed that morphological alterations characteristic of mPIN developed in luminal epithelial cells of *Myc/ $\delta$ -cat* double transgenic mice at 6 months old. Surprisingly, homozygous deletion of the  $\delta$ -catenin gene in *Myc* mutant (*Myc/ $\delta^{-/-}$* ) mice displayed mPIN as early as 6 weeks of age and continued to develop prostatic adenocarcinoma by 6 months, suggesting that  $\delta$ -catenin

homozygous mutation induced much more severe pathological lesions. We also discovered that *Myc/δ<sup>-/-</sup>* increased in both number of proliferating cells and cells undergoing apoptosis compared with that of wild type animals. Moreover, increased expression of β-catenin, Myc, GSK-3β is correlated with the decreased expression of phosphorylated β-catenin in *Myc/δ<sup>-/-</sup>*. Additionally, *Myc/δ<sup>-/-</sup>* mice showed remarkable upregulation of HIF-1α and Glut-1, suggesting reengineered glycolytic pathway upon the formation of solid prostate tumors in *Myc/δ<sup>-/-</sup>* mice. Collectively, our findings suggest that mutations of δ-catenin contribute to mouse prostate tumorigenesis through enhanced β-catenin-mediated oncogenic signals leading to increased cell proliferation and survival, thereby promoting prostate tumor growth.

## **B. Introduction**

The human *δ-catenin* gene (*CTNND2*) spans 933 Kb with 22 coding exons and resides within a 17.45 centimorgan region on chromosome 5p15 (Li et al., 2011; Lu et al., 1999). As described earlier, δ-catenin is a member of the p120<sup>ctn</sup> subfamily of armadillo/β-catenin proteins, which are defined as proteins with 10 armadillo (ARM) repeats in characteristic spacing and often with quite diverse amino- and carboxyl-terminal sequences that flank the ARM repeats (Paffenholz and Franke, 1997; Lu et al., 1999). Cloning and sequencing of human *δ-catenin* cDNA sequence reveal that exons 1-9 correspond to the amino-terminus, exons 10-18 correlate with the ARM domains, and exons 19-22 associate with the carboxyl-terminus. Of note, the exon boundaries do not strictly correspond to the repeating armadillo motifs (Medina et al., 2000).

There are several lines of evidence supporting the important regulatory roles of the sequences outside the ARM domains of δ-catenin. Lu et al (1999) revealed that the ARM domains were required for localizing δ-catenin to cell-cell junctions and interact with cadherin in

epithelial cells (Lu et al., 1999). Additional studies reported that ectopic expression of full-length  $\delta$ -catenin in NIH3T3 fibroblast cells induced dendrite-like branching with process extensions, indicating its functional role in cytoskeleton remodeling. However, the carboxyl-terminal truncation mutant of  $\delta$ -catenin inhibited its branch-inducing effect (Kim et al., 2002). In support of these results, previous studies from our laboratory showed that  $\delta$ -catenin with the deletion of either amino-terminal 280 amino acids or carboxyl-terminal 207 amino acids abolished the  $\delta$ -catenin mediated-PCa cell colony formation in soft agar and tumor xenograft growth in nude mice (Lu et al., 2005). These results imply that full-length  $\delta$ -catenin is crucial in achieving its tumor promoting effect. Additionally, we demonstrated in chapter II that human PCa cells overexpressing  $\delta$ -catenin induced exonic mutations of ectopic  *$\delta$ -catenin* gene, resulting in increased cell survival and metabolic reprogramming. A closer examination of human primary prostatic adenocarcinoma revealed significant mutations towards the Arm domains and carboxyl-terminus corresponding to exons 10-22 of  *$\delta$ -catenin* gene (Nopparat et al., 2014). Taken together, these data highlight the importance of the amino- and carboxyl-termini and their diverse biological functions. However, little is known about how changes in each domain of  $\delta$ -catenin could contribute to PCa progression.

Given that cell culture models cannot reveal the complex cellular interactions within the tumor microenvironment, we sought to further investigate the function of  $\delta$ -catenin *in vivo*. In this study, we intend to address the effects of  $\delta$ -catenin overexpression and mutations in a novel mouse transgenic model of PCa using the human *Myc* oncogene as the initiating event (Ellwood-Yen et al., 2003). We have successfully generated two mouse models, which are *Myc*/ $\delta$ -cat double transgenic and *Myc*/ $\delta$ -catenin mutant mice. For the *Myc*/ $\delta$ -cat double transgenic mice, they were generated by introducing *Myc* and  *$\delta$ -catenin* transgenes in prostate-specific manner by

the derivative of probasin promoter (ARR<sub>2</sub>PB). Myc/ $\delta$ -catenin mutant mice, on the other hand, were generated by cross-bred of Myc transgenic mice with  $\delta$ -catenin mutant ( $\delta$ -cat<sup>+/-</sup>) mice, which carry the targeted deletion at exon 9 of  $\delta$ -catenin gene. Exon 9 lies upstream of Arm domains; therefore, this disruption prevents transcription of the Arm domains, which are required for  $\delta$ -catenin localization to cell-cell junction, and the carboxyl-terminal region of the  $\delta$ -catenin gene (Israely et al., 2004). Furthermore, Tanahashi and Tabira (1999) isolated and characterized the full-length cDNA of human  $\delta$ -catenin and found that human  $\delta$ -catenin revealed strong sequence homology (97.1%) with mouse  $\delta$ -catenin. The amino acid sequences in the coiled-coil helical motif (100%) and arm-repeat domain (99.2%) were also highly conserved between two species (Tanahashi and Tabira, 1999). These results validate the feasibility of utilizing Myc/ $\delta$ -catenin mutant mice for PCa studies.

In this chapter, we demonstrated that while Myc/ $\delta$ -cat double transgenic mice show mild phenotype, Myc/ $\delta$ -catenin mutant mice develop mouse prostatic intraepithelial neoplasia (mPIN) followed by prostatic adenocarcinoma. In particular, Myc/ $\delta$ -catenin homozygous (Myc/ $\delta$ <sup>-/-</sup>) mutants not only exhibit dramatic cell proliferation, but also increased expression of  $\beta$ -catenin, GSK-3 $\beta$ , and Myc, which are correlated to decreased phosphorylated  $\beta$ -catenin, implicating its role in Wnt/ $\beta$ -catenin signaling pathway. Furthermore, expression level of HIF-1 $\alpha$  is positively correlated with the level of Myc activity, leading to alteration of their common effectors in glycolytic pathway (i.e., Glut-1 and PKM<sub>2</sub>). In summary, our results further support the hypothesis that  $\delta$ -catenin mutations play a key role in PCa development by interacting with other signaling pathways including Wnt/ $\beta$ -catenin and glucose metabolism *in vivo*.

## **C. Experimental procedures**

### C1. Generation of transgenic mouse models

Generation and characterization of Myc transgenic mice (ARR<sub>2</sub>PB-Myc; also known as Hi-Myc) and  $\delta$ -catenin heterozygous ( $\delta$ -cat<sup>+/-</sup>) mutation have been described previously (Ellwood-Yen et al., 2003; Israely et al., 2004). Mice were genotyped by PCR on tail genomic DNA or by reverse transcription-PCR post-birth as illustrated in Figure 3.1 and Figure 3.5 using protocols and primer sets described below.

### C2. DNA extraction and genotyping PCR-based analysis

Mouse-tail genomic DNA was extracted by the following steps: each tail snip was put into a clean eppendorf tube, 300  $\mu$ l of warm TNES buffer was added to each sample tube, then 8.5  $\mu$ l of 20 mg/mL Proteinase K was added and incubated in a water-bath at 55°C overnight to dissolve the mouse tail. On the next day, 83  $\mu$ l of 6 M NaCl was added and vortexed for 15 sec. Each sample was then centrifuged at 14,000 rpm for 15 min at room temperature. The supernatant was transferred into a clean, properly labeled eppendorf tube. Each supernatant was centrifuged again at 14,000 rpm for 15 min at room temperature. The supernatant was poured into a new, properly labeled eppendorf tube and then cold 95% ethanol was added to the supernatant at a 1:1 concentration. The tube was gently inverted several times to precipitate the DNA. After DNA precipitation, all tubes were centrifuged for 15 min at 14,000 rpm at 4°C and then the supernatant (ethanol) was poured off. The pellet was washed with cold 70% ethanol, and then centrifuged at 14,000 rpm at room temperature for 5 min. All residual ethanol was carefully removed and then the pellet was air-dried. Finally, the pellet was resuspended in 50  $\mu$ l sterile, de-ionized water. Samples can be stored at 4°C if the samples are not being tested right away.

Extracted mouse-tail genomic DNA was subjected to a PCR-based screening assay for genotyping. For the Myc transgenic mouse genotype, primers were selected as follows: MO45 (5'AAACATGATGACTA CCAAGCTTGGC3') is specific for the ARR<sub>2</sub>PB promoter element and MO47 (5'ATGATAGCATCTTGGTCTTAGTCTTTTTCTTAATAGGG3') is specific for the non-coding region upstream to the probasin promoter, resulting in a PCR product of 100-200 base pairs (bp). For genotyping  $\delta$ -catenin transgenic mice (ARR<sub>2</sub>PB- $\delta$ -cat), the primer 5H1 (5'ATGT TTGCGAGGAAGCCGC3'), and 3H530 (5'GTCTGGTTGCTATGGTAGCTGGC3') were used to generate a PCR product of 600 bp. For  $\delta$ -catenin mutant mice, two different primers were used as follows: primer sets for wild-type  $\delta$ -catenin ( $\delta$ -cat<sup>+/+</sup>) includes F1 (5'GACGTTT GGTTTTCCGAATG3') and R3 (5'AGAGTCAACGGAGGCACAAT3'), and primer sets for homozygous  $\delta$ -catenin mutation ( $\delta$ -cat<sup>-/-</sup>) include Ex9 forward (5'AACCGTTTCTGTGAGCAG GTCC3') and GFP1300 reverse (5'GCTCGTCCATGCCGAGAGTG3'), resulting in PCR product 2000 and 800 bp, respectively.

### C3. Mouse tissue preparation

Mice were kept under pathogen free conditions according to the guidelines of East Carolina University Animal Use Protocol. Animals were deeply anesthetized with 3% isoflurane vapor and euthanized by cervical dislocation at the appropriate time point. The prostate tissues were harvested and either fresh frozen on liquid nitrogen (for protein analysis) or fixed in 4% paraformaldehyde (for histological analysis) and stored at -4°C overnight. For immunofluorescent analysis, mouse prostate tissues were embedded in OCT and rapidly frozen with chilled isopentane. The 5  $\mu$ m thick cryostat sections were affixed to Superfrost slides (Fisher Scientific, Pittsburgh, PA).

#### C4. Histopathological analysis of mouse prostate tissue

Serial tissue sections (5 µm thick) were cut from paraffin-embedded blocks, placed on charged-glass slides, and subjected to Hematoxylin and Eosin (H&E) staining. Sections were deparaffinized in citrisol 2 times (5 min each) and then rehydrated through graded ethanol; 100% ethanol (5 min), 100% ethanol (5 min), 95% ethanol (3 min), 95% ethanol (3 min), and 80% ethanol (3 min). Sections were rinsed in distilled water (5 min). Slides were stained with hematoxylin for 6 minutes followed by immersing slides in running tap water for 10 min. Decolorization in acid alcohol was done for 1 sec and the sections were immediately dipped in tap water, and then immersed in Lithium Carbonate about 1 sec. Slides were rinsed in tap water for 5 min and counterstained in Eosin for 1 min. The sections were dehydrated through graded ethanol; 80% ethanol (2 min), 95 % ethanol (2 min), 95% ethanol (2 min) 100 % ethanol (2 min), 100 % ethanol (2 min), and were cleared in citrisol 2 times (5 min each). Finally, the sections were covered with Permount. All slides were analyzed by light microscopy using a Zeiss Axiovert S100 light microscope (Carl Zeiss, Thornwood, NY).

#### C5. Immunofluorescent analysis of prostate tissue

For immunostaining, frozen sections were incubated with 0.2% Triton X-100 for 15 min at room temperature, 20 min at room temperature with 100 mM glycine and blocked 30 min at 37°C with 10% bovine serum albumin (BSA). Primary antibodies (rabbit anti-Ki67 antibody 1:100, Abcam, Cambridge, MA; rabbit anti-Myc (N-term) antibody 1:100, Epitomics, Burlingame, CA) were incubated 1 h at room temperature. After appropriate secondary antibody labeling, Hoechst was applied to stain all nuclei. For detecting cell apoptosis, tissues were incubated with TUNEL reaction 1:50 (Roche Applied Science, Indianapolis, IN) for 45 min at

37°C. Immunofluorescent images were captured and analyzed with a Zeiss Axiovert S100 fluorescent microscope (Carl Zeiss, Thornwood, NY).

#### C6. Protein analysis of prostate tissue

Harvested prostate tissues were frozen on liquid nitrogen, crushed, and homogenized with RadioImmuno Precipitation Assay (RIPA) buffer (150 mM NaCl, 10 mM 4-(2-hydroxyethyl)-1-piperazineethanesulfonic acid (HEPES), pH 7.3, 2 mM EDTA, 0.2% SDS, 0.5% Sodium deoxycholate, 1% Triton X-100) supplemented with a protease inhibitor cocktail (Roche Applied Science, Indianapolis, IN). Following prostate tissue homogenization, tissues were incubated on ice for 30 min. Cell debris was removed by centrifugation at 14,000 rpm at 4°C for 30 min. Protein concentration of the supernatant was determined using Pierce BCA assay kit (Rockford, IL). After determination of protein concentrations, equal amounts of protein were loaded onto 8-16% tris-glycine gel (Invitrogen, Carlsbad, CA), transferred to nitrocellulose membrane (Optitran, Germany) and subjected to Western blot analysis. Blots were blocked and probed with rabbit histone-H3 1:1000 (Santa Cruz Biotechnology, Santa Cruz, CA), rabbit PARP 1:1000 (Cell Signaling Technology, Danvers, MA), rabbit  $\beta$ -catenin 1:1000 (BD transduction laboratories, Lexington, KY), rabbit phosphorylated  $\beta$ -catenin (Ser33/37Thr4) 1:1000 (Cell Signaling Technology, Danvers, MA), mouse GSK-3 $\beta$  1:1000 (BD transduction laboratories, Lexington, KY), rabbit Myc (N-term) 1:1000 (Epitomics, Burlingame, CA), rabbit HIF-1 $\alpha$  1:500 (Santa Cruz Biotechnology, Santa Cruz, CA), rabbit Glut-1 1:1000 (ThermoScientific, Philadelphia, PA), and rabbit PKM<sub>2</sub> 1:500 (Cell Signaling Technology, Danvers, MA). GAPDH (mouse, 1:2000; Calbiochem, San Diego, CA) was used as a loading control. After applied appropriate secondary, which is conjugated to horseradish peroxidase, immunoreactive protein

bands were then detected by enhanced chemiluminescence (ECL) western blot detection reagent (GE healthcare, Pittsburgh, PA) according to the manufacture's protocol.

The ChemiDoc™ XRS+ system (Bio-Rad, Hercules, CA) was used for the quantitative measurement of Western blot analyses. Films were scanned and visualized with ChemiDoc XRS program. The area of the protein bands including proteins of interest (POI) and loading control were selected within defined boxes and the same size box were selected in the clear space of the same film as a background. The  $[\text{band intensity (POI)} * \text{band area (POI)} - \text{background intensity} * \text{background area}] / [\text{band intensity (loading control)} * \text{band area (loading control)} - \text{background intensity} * \text{background area}]$  was used to define expression levels of the POI in both control and test samples. Data were then normalized to control samples and statistical analysis was conducted.

#### C7. Statistical analysis

Student's t-test Analysis was performed using SigmaPlot 10.0 (Systat Software Inc., San Jose, CA) and p-values were designated for each experiment, each of which was repeated a minimum of two times. Any null hypothesis with probability level less than 95% was rejected.

### **D. Results**

#### D1. Generation of Myc/ $\delta$ -cat double transgenic mouse model of PCa

Generation of Myc transgenic mice (ARR<sub>2</sub>PB-Myc) has been previously described (Ellwood-Yen et al., 2003). Briefly, human *Myc* is driven, in prostate-specific manner, by a derivative of the rat probasin gene promoter (ARR<sub>2</sub>PB). Similarly, human- $\delta$ -catenin is conditionally overexpressed in prostate epithelial cells by ARR<sub>2</sub>PB. The presence of the human

*δ-catenin* transgene in mice was confirmed by reverse transcription-PCR together with gel electrophoresis at 3 weeks of age. Results revealed that *δ-catenin* cDNAs were detectable indicating that we succeeded in generating *δ-catenin* transgene-positive mice (Fig. 3.1A, lanes 1 and 2). Wild-type animals served as experimental controls (Fig. 3.1A, lanes 3 and 4). Those mice overexpressing *δ-catenin* transgene were then subjected to further experiment.

In order to determine the effect of overexpression of *δ-catenin* and *Myc in vivo*, the double transgenic mice were generated by crossing ARR<sub>2</sub>PB-*Myc* with ARR<sub>2</sub>PB-*δ-cat* mice. First generation littermates (F1) were then intercrossed resulting in wild-type and *Myc/δ-cat* double transgenic mice, which are the genotypes of interest (Fig. 3.1B). *Myc/δ-cat* double transgenic offsprings were screened by PCR using genomic DNA isolated from tail snips.

#### D2. Gross anatomy of *Myc/δ-cat* double transgenic mouse prostate displays mild phenotype

To investigate the phenotype of *Myc/δ-cat* double transgenic mice, we first examined the gross anatomy of 6 month-old animals as representative data of adult mice. We found that prostates of *Myc/δ-cat* double transgenic mice were macroscopically similar to that of wild-type animals in terms of their prostate size and shape (Fig. 3.2A). The quantification of prostate area (cm<sup>2</sup>) measured by the width and length of prostate tissues further confirmed that there was no significant increased *Myc/δ-cat* double transgenic mouse prostate area when compared to wild type (Fig. 3.2B).

D3. *Myc/δ-cat* double transgenic mouse prostate exhibits mouse prostatic intraepithelial neoplasia (mPIN) lesions

Prostate tissues were harvested from 6 week-old and 6 month-old mice. They were fixed in 4% paraformaldehyde, paraffin-embedded, and then 5 μm cross-sections were subjected to histology analysis by H&E staining. Since the dorsal lateral prostate (DLP) and ventral prostate (VP) prostate were susceptible lobes in development of mouse prostatic intraepithelial neoplasia (mPIN) in our mouse models, they were chosen as the focus of most of our studies presented herein. As shown in Fig. 3.3A, the morphological characteristics of *Myc/δ-cat* double transgenic mouse prostate were quite similar to the wild-type animal at 6 weeks of age. The DLP was lined by one to two layers of simple columnar and slightly stratified and tufting epithelium. The VP, on the other hand, had flatter luminal edges and only focal epithelial tufting or in-folding with abundant luminal surface. By 6 months, *Myc/δ-cat* double transgenic prostates displayed mPIN lesions in both DLP and VP (Fig. 3.3B). At higher magnification, characteristic changes of mPIN lesions were recognized by epithelial hyperplasia, nuclear atypia (Fig. 3.3B, yellow arrow heads), and tufting growth patterns of epithelial cells (Fig. 3.3B, arrows).

δ-Catenin overexpression has been previously described as a mediator in PCa progression in tumor xenograft growth in nude mice (Zeng et al., 2009). Moreover, *Myc*-driven murine prostate is sufficient to cause the development of invasive adenocarcinoma by 6 months (Ellwood-Yen et al., 2003). Therefore, we originally hypothesized that the ectopic co-expression of *Myc* and δ-catenin could promote prostate tumor *in vivo*. We addressed this hypothesis by investigating the histology of mouse overexpressing *Myc*. Histopathologically, our Hi-*Myc* transgenic mice displayed invasive adenocarcinoma by 8 months old (Fig. 3.4A and Fig. 3.4B), predominantly in VP (Fig. 3.4B). *Myc/δ-cat* double transgenic prostates, however, continued to

exhibit mPIN lesions in both DLP and VP at 18 months (Fig. 3.4E and Fig. 3.4F). Note that non-transgenic mouse prostates showed normal-appearing epithelia and an enlargement of luminal spaces (Fig. 3.4C and Fig. 3.4D) with abundant intraluminal secretion in VP (Fig. 3.4D, arrows). These data indicated that  $\delta$ -catenin overexpression did not elicit prostatic adenocarcinoma in transgenic mice as seen in human cancer cell xenograft studies.

#### D4. Generation of *Myc*/ $\delta$ -catenin mutant mouse model of PCa

Previous studies have primarily established neuronal functions of  $\delta$ -catenin. The study by Israely et al (2004) demonstrated that targeted deletion of  $\delta$ -catenin in mice results in severe cognitive impairments.  $\delta$ -Catenin homozygous ( $\delta$ -cat<sup>-/-</sup>) mutant mice are viable, but display a range of abnormalities in hippocampal short-term and long-term synaptic plasticity, indicating a critical role of  $\delta$ -catenin in brain function (Israely et al., 2004). In order to gain a better understanding of  $\delta$ -catenin mutation in prostate pathological aspects, we generated and characterized *Myc*/ $\delta$ -catenin mutant mice. We utilized ARR<sub>2</sub>PB-*Myc* transgenic mice as our initiating event. ARR<sub>2</sub>PB-*Myc* transgenic mice were further cross-bred with  $\delta$ -catenin heterozygous ( $\delta$ -cat<sup>+/-</sup>) mutant mice whose one allele was disrupted at exon 9, thereby preventing transcription of the functional region of  $\delta$ -catenin gene (Israely et al., 2004). Of note, this mutant showed expression of  $\delta$ -catenin with the intact amino-terminal 435 amino acids after a targeted disruption of exon 9 (not a complete null). The genotype of  $\delta$ -cat<sup>+/-</sup> mice was confirmed by PCR using genomic DNA isolated from tail snips. PCR products of  $\delta$ -cat<sup>+/+</sup> and  $\delta$ -cat<sup>-/-</sup> were approximately 2000 bp (Fig. 3.5A, lanes 1 and 2) and 800 bp (Fig. 3.5A, lanes 3 and 4). The offspring generation 1 (F1) was intercrossed to obtain genotypes of interest in generation 2 littermates (F2) including wild type (WT), *Myc* with  $\delta$ -catenin wild-type (*Myc*/ $\delta$ <sup>+/+</sup>), *Myc* with

$\delta$ -catenin heterozygous mutation ( $Myc/\delta^{+/-}$ ), and  $Myc$  with  $\delta$ -catenin homozygous mutation ( $Myc/\delta^{-/-}$ ) (Fig. 3.5B).

D5. Gross anatomy of  $Myc/\delta$ -catenin mutant mice display significant increased prostate size

After successfully generating  $Myc/\delta$ -catenin mutant mice, we harvested prostate tissues at 6 weeks and 6 months of ages for further analyses. Macroscopically, prostate shape irregularity was noticeable and enlargement of the prostate was progressively increased from wild-type to  $Myc/\delta^{-/-}$  mice (Fig. 3.6A). The progressive phenotype of  $Myc/\delta$ -catenin mutant mice was further evident by mouse prostate area ( $\text{cm}^2$ ) analysis, in which  $Myc/\delta^{+/-}$ , and  $Myc/\delta^{-/-}$  mice displayed a statistically significant increased prostate area when compared to wild-type mice (Fig. 3.6B, \*  $p < 0.05$  and \*\*  $p < 0.01$ )

D6.  $Myc/\delta$ -catenin mutant mice promote prostate tumor development in a mutation dose-dependent manner

As mentioned previously, we intend to address the effect of mutant  $\delta$ -catenin in mice overexpressing  $Myc$  oncogene. To this end, we are interested in examining the histopathological changes in 3 different genotypes;  $Myc/\delta^{+/+}$ ,  $Myc/\delta^{+/-}$ , and  $Myc/\delta^{-/-}$  comparing wild type mice at 6 weeks and 6 months of ages. At 6 weeks, the DLP and VP of  $Myc/\delta^{+/+}$ ,  $Myc/\delta^{+/-}$ , and  $Myc/\delta^{-/-}$  prostates exhibited multilayering of cells partially filling the lumen, characterization of mPIN lesions (Fig. 3.7A). In addition to multi-layering of cells, these changes in  $Myc/\delta^{+/-}$  and  $Myc/\delta^{-/-}$  mutant mice included prominent nucleoli, nuclear shape variability, and intraepithelial space formation (Fig. 3.7A, b-d, f-h, j-l, and n-p, asterisks). Additionally,  $Myc/\delta$ -catenin mutant mice displayed the loss of polarity, which can be characterized by a variation in the location of nuclei

within the mPIN cells rather than basally located nuclei observed in wild-type animals (indicated by arrows). Striking differences were observed in the prostates of  $Myc/\delta^{+/+}$ ,  $Myc/\delta^{+/-}$ , and  $Myc/\delta^{-/-}$  at 6 months of age.  $Myc/\delta^{-/-}$  mice progressed to develop invasive adenocarcinoma (Fig. 3.7B, p) whereas  $Myc/\delta^{+/+}$  and  $Myc/\delta^{+/-}$  mice continued to exhibit mPIN at the same time point (Fig. 3.7B, f-g and n-o).  $Myc/\delta^{-/-}$  also showed histological signs of local invasion, with tumor cells disrupting the basement membrane of the gland and invading into the surrounding stroma, especially in VP (Fig 3.8, red arrows). These findings indicate that a homozygous mutation in  $\delta$ -catenin exacerbates prostate tumor progression in *Myc* transgenic mice. The results of these studies are consistent with our previous data demonstrating  $\delta$ -catenin displays exonic mutations in human PCa (Nopparat et al., 2014). Since the phenotype of *Myc*/ $\delta$ -catenin mutant mice was much more pronounced than that of *Myc*/ $\delta$ -cat double transgenic mice, the *Myc*/ $\delta$ -catenin mutant mouse model was chosen for analysis in the experiments described herein.

#### D7. $\delta$ -Catenin mutations promote cell proliferation and apoptosis in *Myc*/ $\delta$ -catenin mutant mice

It is well known that *Myc* overexpression can lead to cell growth and proliferation, angiogenesis, cell fate transition, DNA damage responses, and cell apoptosis (Ellwood-Yen et al., 2003; Gurel et al., 2008; Koh et al., 2010; Wang et al., 2010). Due to the rapid development of mPIN and prostatic adenocarcinoma in  $Myc/\delta^{-/-}$  mice, we further investigated whether cell proliferation or cell death is the major underlying cellular mechanism. We performed immunofluorescent staining for proliferation using anti-Ki67 antibody and apoptosis using TUNEL assay. Anti-Ki67 and TUNEL staining was quantified by counting the positive staining cells in a total of 500 cells under the fluorescent microscope. We demonstrated that there were two non-overlapping cellular populations which were the anti-Ki67 positive cells (green) and

TUNEL positive cells (red), suggesting an early determination of cell fate either entering proliferative or undergoing apoptotic pathways as a result of the rapidly dividing tumor cell condition. In addition, the mouse prostate tissues progressively increased anti-Ki67 positive cells from wild type, *Myc/δ<sup>+/+</sup>*, *Myc/δ<sup>+/-</sup>*, to *Myc/δ<sup>-/-</sup>* in both DLP and VP (Fig. 3.9A and Fig. 3.9C). Prostatic TUNEL staining was also elevated and showed significant differences in prostate tissues from *Myc/δ<sup>-/-</sup>* when compared to wild-type mice. Strikingly, the proliferative labelling index was approximately 4-fold and 5-fold greater than apoptotic labeling index in DLP and VP, respectively (Fig. 3.9B and Fig. 3.9D). Since there were many more cells undergoing proliferation than apoptosis, the net effect was increased tumor growth as depicted in Fig. 3.6A and Fig. 3.6B.

Additional analysis of protein expression in lysates prepared from 6 month-old mouse prostate tissues was performed. The protein banding patterns were analyzed by Western blot using histone-H3, a marker for proliferation, and PARP antibodies, a marker of apoptosis. As depicted in Fig. 3.10A (upper panel) histone-H3 were significantly increased in mutant  $\delta$ -catenin (Fig. 3.10B, \*  $p < 0.05$ ). PARP protein expression levels were shown to be similar in *Myc/δ*-catenin mutant and wild-type mice. However, lower amounts of cleavage product of PARP by caspase pathway, which is an active form of PARP, were also observed at a smaller molecular weight (89 kilodaltons) in *Myc/δ*-catenin mutations, but not in wild type (Fig. 3.10A, second panel). A quantification of protein bands was performed using densitometry and ratio of cleaved-PARP to full-PARP was determined. The data revealed that *Myc/δ<sup>+/+</sup>* resulted in (not statistically significant) an increase in cells undergoing apoptosis when compared to *Myc/δ<sup>-/-</sup>* (Fig. 3.10C). These findings were not consistent with the TUNEL staining analysis (Fig. 3.9). We speculated that the heterogeneity of whole mouse tissue lysates could contribute to these inconsistent

results. Overall, these results suggested that mutations of the  $\delta$ -catenin gene mediated the effect of Myc by giving a proliferative advantage that overcomes the apoptotic effect of Myc, leading to mouse prostatic adenocarcinoma.

D8. Myc/ $\delta$ -catenin mutant mice reveal a dramatic increase in cells overexpressing Myc

Promoter element of the rat probasin has been proven to be successful in target *Myc* gene expression in VP and DLP (Abate-Shen and Shen, 2000; Ellwood-Yen et al., 2003; Greenberg et al., 1995). Moreover, Myc overexpression is reported to localize within luminal epithelial cells correlated with the onset of morphological transformation of mPIN lesions in Myc transgenic mouse models (Iwata et al., 2010). To determine and compare Myc expression profiles in prostatic epithelial cell in our Myc/ $\delta$ -catenin mutant mouse model, we performed immunofluorescent analysis of frozen mouse prostate cross sections with anti-Myc antibody. As depicted in Fig. 3.11A (left panel) immunofluorescent analysis revealed a distinct pattern of Myc expression, in which not all prostatic epithelial cells showed positive anti-Myc staining. Myc/ $\delta^{+/+}$  and Myc/ $\delta^{+/-}$ , with a well-defined luminal-basal compartment, demonstrated anti-Myc positive cells being localized predominantly in luminal epithelial cells (white asterisks indicate lumina), whereas Myc/ $\delta^{-/-}$  epithelial cells staining positively for Myc were located all over tumor lesions. Additionally, wild-type prostates were completely negative for Myc staining. We also observed that number of cells expressing Myc was significantly increased in Myc/ $\delta^{-/-}$  (Fig3.11B, \*  $p < 0.01$ , relative to wild type and  $\Delta p < 0.05$ , relative to Myc/ $\delta^{+/+}$ ). These findings strongly suggested that luminal epithelial cells were susceptible to Myc-induced morphological alteration which was consistent with the study by Iwata et al (2010).

D9. Myc overexpression does not mediate apoptosis in Myc/ $\delta$ -catenin mutant mice

In order to determine whether induction of Myc overexpression in mouse epithelial cells leads to the induction of apoptosis as seen in Fig. 3.9, Fig. 3.10, and Fig. 3.11, double immunofluorescent staining was performed on prostate sections from 6-month-old Myc/ $\delta$ -catenin mutant mice using anti-Myc antibody (green) and TUNEL assay (red). Immunofluorescent analysis revealed that the area, where Myc was positively staining, was negative for TUNEL staining (Fig. 3.12). However, only a few cells were positively staining by both Myc and TUNEL (indicated by white arrows in merged images). These data indicated that Myc overexpression did not exert function as apoptotic induction in Myc/ $\delta$ -catenin mutant mice.

D10.  $\delta$ -Catenin mutations enhance  $\beta$ -catenin and Myc expression in Myc/ $\delta$ -catenin mutant mice

Many studies have primarily compared  $\delta$ -catenin to other p120<sup>ctn</sup> subfamily members due to structural similarities and their shared binding partners (Kosik et al., 2005). Fewer studies have directly addressed the shared functional properties between  $\beta$ -catenin and  $\delta$ -catenin (McCrea and Park, 2007; Paffenholz and Franke, 1997). However, a recent study by Kim et al (2012) reported  $\delta$ -catenin ectopically overexpressed in human cancer cells mediates nuclear accumulation of  $\beta$ -catenin, resulting in the transcription of genes involved in cell cycle (i.e., cyclin D1 and cdc34), and cell proliferation (e.g., Myc) (Kim et al., 2012). Thus, aberrant signaling in this pathway is associated with overproliferation of cells, a fundamental capability of cancer cells (Hanahan and Weinberg, 2011). In addition,  $\delta$ -catenin has been reported to be potentially regulated in the same way as that of  $\beta$ -catenin by which GSK-3 $\beta$ , a destructive complex molecule in the Wnt/ $\beta$ -catenin pathway, interacts with the phosphorylated  $\delta$ -catenin resulting in its ubiquitination and subsequent proteasome degradation (Bareiss et al., 2010; Oh et

al., 2009). Therefore, we intended to address whether  $\delta$ -catenin mutations could cause alteration of  $\beta$ -catenin in *Myc*/ $\delta$ -catenin mutant mouse model of PCa as previously demonstrated.

In order to investigate the effect of  $\delta$ -catenin mutations on  $\beta$ -catenin expression, 6-month-old mouse prostate tissues were lysed and subjected to Western blot analysis. The protein banding patterns revealed significantly increased  $\beta$ -catenin expression, which was correlated with significant decreased phosphorylated  $\beta$ -catenin (Fig 3.13A, upper first and upper second panels, and Fig. 3.13B, \*  $p < 0.01$  and  $\phi$   $p < 0.01$ ). Phosphorylated  $\beta$ -catenin is indicative of targeted- $\beta$ -catenin for ubiquitin-dependent degradation in the proteasome. These results suggested that few stabilized  $\beta$ -catenin in cytoplasm underwent the degradation process, implying the translocation of excess  $\beta$ -catenin into the nucleus. However, the expression pattern of GSK-3 $\beta$  protein was unexpected. In a sense, with a higher phosphorylated  $\beta$ -catenin level, one would expect to see an induction of GSK-3 $\beta$  activity, but *Myc*/ $\delta^{+/+}$  showed a reduction of GSK-3 $\beta$  level, while phosphorylated  $\beta$ -catenin was higher when compared to *Myc*/ $\delta^{+/-}$  and *Myc*/ $\delta^{-/-}$  (Fig. 3.13A, upper third panel). The potential explanation for this finding is that, as mentioned earlier,  $\delta$ -catenin was shown to be negatively regulated by the GSK-3 $\beta$  proteasome signaling pathway in the same way as  $\beta$ -catenin. Therefore, the greater level of endogenous  $\delta$ -catenin in *Myc*/ $\delta^{+/+}$  mice than that of *Myc*/ $\delta^{+/-}$  and *Myc*/ $\delta^{-/-}$  mice could cause further reduction of GSK-3 $\beta$ . In summary, increased phosphorylated  $\beta$ -catenin, together with higher endogenous  $\delta$ -catenin, could lead to decreased GSK-3 $\beta$  in *Myc*/ $\delta^{+/+}$  mice.

Furthermore, *Myc*, a downstream effector of Wnt/ $\beta$ -catenin signaling pathway, increased dramatically, corresponding with  $\beta$ -catenin expression (Fig. 3.13A, bottom second panel). Quantification of protein banding density in Fig. 3.13B confirmed the visual comparison and demonstrated mutant  $\delta$ -catenin not only significantly increased *Myc* in *Myc*/ $\delta^{-/-}$  as compared to

wild type (\*  $p < 0.01$ ), but also to  $\text{Myc}/\delta^{+/+}$  and  $\text{Myc}/\delta^{+/-}$  ( $\Delta$   $p < 0.01$ ). Interestingly, these findings support that mutations of  $\delta$ -catenin facilitated tumorigenesis by altering  $\beta$ -catenin and Myc protein level expression, leading to mouse prostate tumor growth.

#### D11. $\delta$ -Catenin mutations promote HIF-1 $\alpha$ resulting in metabolic adaptation

In order to determine the relationship between HIF-1 $\alpha$ , Glut-1, and PKM<sub>2</sub> in  $\text{Myc}/\delta$ -catenin mutant mouse model in respect of cancer cell energy metabolism, the expression profiles of HIF-1 $\alpha$ , Glut-1, and PKM<sub>2</sub> in mouse prostate were examined. Western blot analysis of prostate tissue from 6-month-old mice showed that the density of the HIF-1 $\alpha$  protein band exhibited a minimal induction in wild type (Fig. 3.14A, top panel). This is consistent with previous studies showing that HIF-1 $\alpha$  is kept at low level due to its constant degradation via oxygen-dependent hydroxylation under normoxic conditions in non-transformed tissues (Jiang et al., 2007; Kaidi et al., 2007; Zhang et al., 2013). However, HIF-1 $\alpha$  was significantly increased, which was correlated to a dosage of  $\delta$ -catenin mutations (Fig. 3.14B, \*  $p < 0.01$ , relative to wild type and  $\Delta$   $p < 0.01$ , relative to  $\text{Myc}/\delta^{+/+}$ ).

The reduction of Glut-1 activity was observed when Myc is ectopically expressed alone versus wild type (Fig. 3.14A, upper second panel, lane 2). However, Glut-1 was significantly upregulated in  $\text{Myc}/\delta^{-/-}$  mice (Fig. 3.14A, upper second panel, lanes 3 and 4, \*  $p < 0.01$ ). Furthermore,  $\delta$ -catenin mutation resulted in the alteration of PKM<sub>2</sub>, in which homozygous  $\delta$ -catenin mutation led to unexpected reduction of PKM<sub>2</sub>, while  $\text{Myc}/\delta^{+/+}$  and  $\text{Myc}/\delta^{+/-}$  showed increased PKM<sub>2</sub> expression (Fig. 3.14A, bottom second panel). A possible mechanism explaining less PKM<sub>2</sub> in  $\text{Myc}/\delta^{-/-}$  might involve the ability of Myc to drive other metabolic pathways such as glutamine metabolism, which also facilitates the metabolism of cancer cells as

reviewed by (Dang et al., 2009; Koppenol et al., 2011; Vander Heiden et al., 2009). Future experiments are required to determine whether other pathways of glutamine metabolism via glutaminase (GLS) are affected in this particular mouse model. In summary, we demonstrated that increased HIF-1 $\alpha$  signaling was correlated to an upregulated Myc expression and degree of  $\delta$ -catenin mutation. Additionally,  $\delta$ -catenin mutation potentially induced metabolic reprogramming by altering expression profiles of Glut-1 and PKM<sub>2</sub>, common effectors of HIF-1 $\alpha$  and Myc.

## **E. Discussion**

In this study we described the novel mouse models for prostate cancer based on inducible overexpression of oncogenic *Myc* combined with either conditionally overexpressed  $\delta$ -catenin or  $\delta$ -catenin mutations. We demonstrated that *Myc*/ $\delta$ -cat double transgenic mice did not, as expected, develop prostate tumor, and only mPIN lesions were observed (Fig. 3.3 and Fig. 3.4), implying that  $\delta$ -catenin suppresses *Myc* effect on tumorigenesis. These results are in contrast to the situation in which human PCa cells derived from prostatic tumor xenografts overexpress  $\delta$ -catenin promote tumor growth in nude mice (Zeng et al., 2009). Future studies will be needed to further dissect the mechanism by which  $\delta$ -catenin does not cooperate with *Myc*-induced prostate tumor in the double transgenic lines. Surprisingly,  $\delta$ -catenin mutations promote ARR<sub>2</sub>PB-*Myc*-induced mouse prostate tumor development, eventually leading to locally invasive adenocarcinoma in a dose dependent manner (*Myc*/ $\delta$ <sup>+/+</sup> < *Myc*/ $\delta$ <sup>+/-</sup> < *Myc*/ $\delta$ <sup>-/-</sup>) (Fig. 3.7). In addition, *Myc*/ $\delta$ <sup>-/-</sup> mutations displayed prostate enlargement and enhanced cell proliferation, which are accompanied by the increased expressions of  $\beta$ -catenin, *Myc* and, HIF-1 $\alpha$ . Since the  $\delta$ -catenin mutant mice were not a complete null, we cannot rule out that  $\delta$ -catenin-induced

prostate tumorigenic effect in Myc mice could possibly be due to either deletion of a tumor suppressive region in the carboxyl-terminal sequence or gaining of oncogenic properties of truncated  $\delta$ -catenin (the remaining amino-terminal sequence). Nevertheless, our current findings have ultimately provided new insight into the importance of amino- and carboxyl- termini in regulating biological effect and the association of  $\delta$ -catenin mutations and Myc in promoting prostate tumor *in vivo*. Myc/ $\delta$ -catenin mutation shows a more pronounced phenotype than that of double transgenic mice; therefore we chose this model for further analysis.

Alteration of Myc oncogenic transcription factor is well-documented in several types of cancers. In particular, amplification of a region encompassing the Myc locus (8q24) is reported in late stage/aggressive prostate cancer (Koh et al., 2010). Upregulated Myc can cause numerous effects such as increased cell proliferation, and regulating cell growth and apoptosis (Iwata et al., 2010; Koh et al., 2010). Our analyses have revealed that  $\delta$ -catenin mutations promote Myc-induced cell proliferation and apoptosis (Fig. 3.9). Myc/ $\delta^{-/-}$  displayed significantly increased cell proliferation markers including anti-Ki67 and anti-histone-H3 (Fig. 3.9 and Fig. 3.10). A significant induction of cell apoptosis was also observed, but did not outweigh cell proliferation. Therefore, overall outcome of  $\delta$ -catenin mutations clearly contributed to tumorigenesis in Myc/ $\delta$ -cat<sup>-/-</sup> mutant mice. In addition, previous reports indicated that Myc overexpression occurs within luminal epithelial cells in human cells similar to that of Myc transgenic mouse model, suggesting that luminal epithelia were highly subjected to Myc-induced transformation into mPIN lesions (Bonkhoff et al., 1994; Bostwick et al., 1996; Iwata et al., 2010). In this study we showed that Myc abundantly localized in cells residing towards the lumina (Fig. 3.11, white asterisks indicate lumina), which are consistent with anti-Ki67 immunofluorescent analyses showing that highly proliferative cells were prone to localize closer

to the lumen (Fig. 3.9A and 3.9C, white asterisks indicate lumina). Moreover, our data revealed that mouse prostatic epithelial cells overexpressing Myc did not undergo apoptosis, which further suggested that Myc gave proliferative advantage to the mouse prostate. Taken together, luminal prostatic epithelium is the target of Myc-induced transformation into hyperplasia, mPIN lesions, followed by prostate tumor in Myc/ $\delta$ -catenin mutant mouse model.

Several lines of evidence reveals that aberration of  $\delta$ -catenin expression not only plays an important role in neuronal function (namely synaptic plasticity, dendritic arborization, and cognitive deficits) but that it is also implicated in cancer pathological events (Burger et al., 2002; Lu et al., 2005; Medina et al., 2000; Zeng et al., 2009; Zhou et al., 1997). Studies showed that PCa cells overexpressing  $\delta$ -catenin promote cell-cluster formation, E-cadherin processing, nuclear  $\beta$ -catenin accumulation, and angiogenesis through increasing HIF-1 $\alpha$  (He et al., 2013b; Kim et al., 2012). Early studies by Bareiss et al (2010) and Oh et al (2009) found that  $\delta$ -catenin is negatively regulated by GSK-3 $\beta$  and promotes  $\beta$ -catenin turnover in neurons, suggesting that  $\delta$ -catenin is a new member of the destruction complex.  $\delta$ -Catenin could mediate regulation of  $\beta$ -catenin levels by increasing the GSK-3 $\beta$ / $\beta$ -catenin interaction, leading to enhanced ubiquitination and degradation of  $\beta$ -catenin in the Wnt/ $\beta$ -catenin pathway (Bareiss et al., 2010; Oh et al., 2009). These reports raise the possibility that  $\delta$ -catenin and  $\beta$ -catenin may be controlled by similar mechanisms.

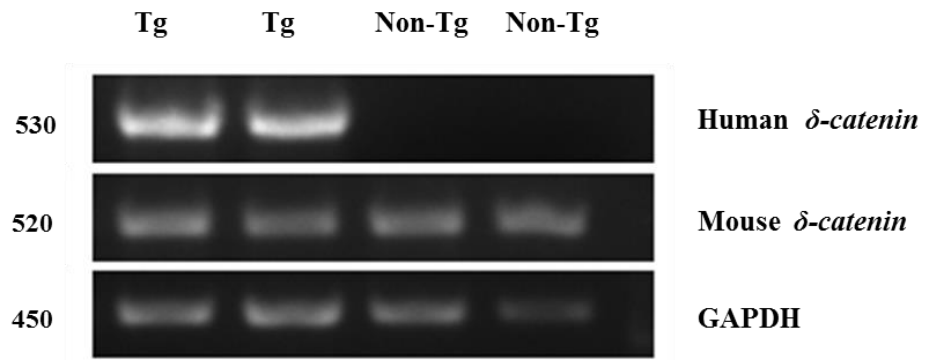
Our analyses *in vivo* revealed that  $\delta$ -catenin mutations promoted total  $\beta$ -catenin expression, which is concomitant with a reduction of phosphorylated  $\beta$ -catenin level. In addition, the degree of  $\delta$ -catenin mutations was negatively correlated with GSK-3 $\beta$  activity (Fig. 3.13). Therefore, these studies were consistent with reports in the literature that  $\delta$ -catenin could be a new member of the Wnt/ $\beta$ -catenin pathway. In support of this hypothesis, we further examined

Myc expression, a major downstream effector of nuclear  $\beta$ -catenin in the Wnt/ $\beta$ -catenin pathway. Interestingly, Myc activity was dramatically increased in a  $\delta$ -catenin gene-dosage-sensitive manner (Fig. 3.13). In summary, our findings support the hypothesis that mutation of  $\delta$ -catenin promotes tumorigenesis through an increase of  $\beta$ -catenin and Myc activities, further supporting a key role of  $\delta$ -catenin in the Wnt/ $\beta$ -catenin pathway.

It is well recognized that rapidly dividing tumor cells can cause an inability of local vasculature to supply enough oxygen and nutrient to tumor mass, resulting in hypoxic areas. Since we have shown that high levels of Myc led to rapid proliferation of luminal cells, we speculated that these cells have found a way to survive under cellular stress by switching to aerobic glycolysis. There is growing evidence that supports the findings that ectopically expressed Myc associates with HIF-1 $\alpha$  to alter their common downstream targets, such as glucose transporter 1 (Glut-1) and pyruvate kinase isoform M2 (PKM<sub>2</sub>) (Bensinger and Christofk, 2012; Dang et al., 2009; Koppenol et al., 2011). In addition, He et al (2013b) reported for the first time that  $\delta$ -catenin overexpressed in human PCa cells promotes HIF-1 $\alpha$  expression under hypoxic conditions, particularly in the nucleus, which, in turn, increases VEGF production, resulting in angiogenesis and promotion of tumor cell growth (He et al., 2013b). Results in this chapter are in agreement with those of He et al (2013b) and show that the effect of  $\delta$ -catenin mutation had a strong effect on metabolic reprogramming.  $\delta$ -Catenin mutations dramatically promoted HIF-1 $\alpha$  protein expression in which HIF-1 $\alpha$  was minimal in wild-type animal and its expression was progressively induced by Myc/ $\delta$ -catenin mutations. Furthermore, the coexpression of Myc and  $\delta$ -catenin mutations altered Glut-1 and PKM<sub>2</sub> activities compared with that of Myc effect alone (Fig. 3.14).

In summary, we showed that  $\delta$ -catenin mutations led to the upregulation in the members of the Wnt/ $\beta$ -catenin pathway. These changes include upregulation of  $\beta$ -catenin and Myc, thereby providing proliferative advantages in the Myc/ $\delta$ -cat mutant mouse model. In addition, activated Myc could interact with HIF-1 $\alpha$  in metabolic pathways, resulting in adaption of cancer cells in hypoxic conditions, which, in turn, favors aerobic glycolysis and/or survival pathways, leading to prostate tumor formation *in vivo* (Fig. 3.15).

**A.**



**B.**

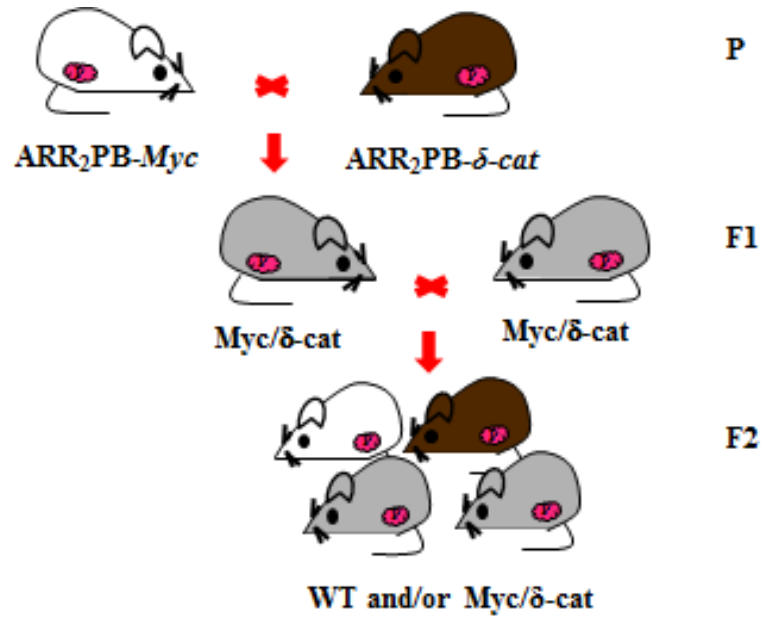
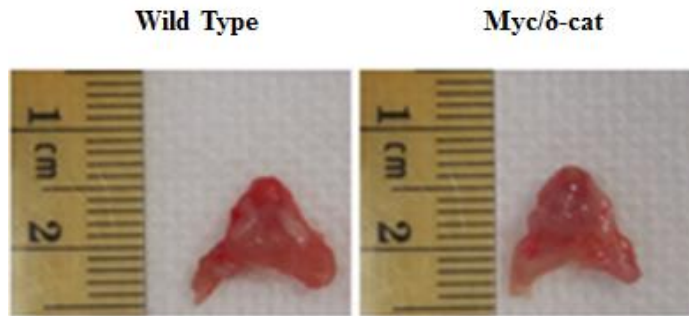


**Figure 3.1 Production and analysis of Myc/ $\delta$ -cat double transgenic mice. (A).** Comparative expression between human- $\delta$ -catenin transgene and endogenous mouse  $\delta$ -catenin between 3-week-old transgenic and non-transgenic mice was determined by RT-PCR. Lanes 1 and 2 revealed the presence of human  $\delta$ -catenin transgene. Conversely, lanes 3 and 4 showed negatively human  $\delta$ -catenin transgene expression, indicating these mice are wild type. GAPDH was used as a loading control. **(B).** Breeding scheme used to produce a Myc/ $\delta$ -cat double transgenic mouse. In parent generation, Myc transgenic mice were bred with  $\delta$ -catenin transgenic mice. In order to obtain genotypes of interest in F2 offsprings, which are wild-type and Myc/ $\delta$ -cat double transgene, the F1 progenies were intercrossed. P: Parents; F1: Offspring generation 1; F2: Offspring generation 2; Tg: transgenic mice.

**A.**



**B.**

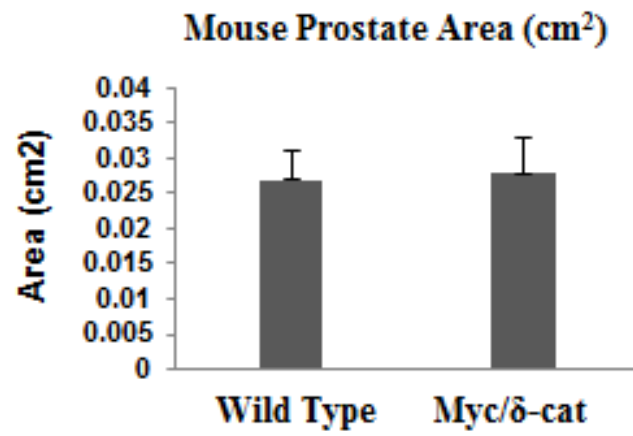
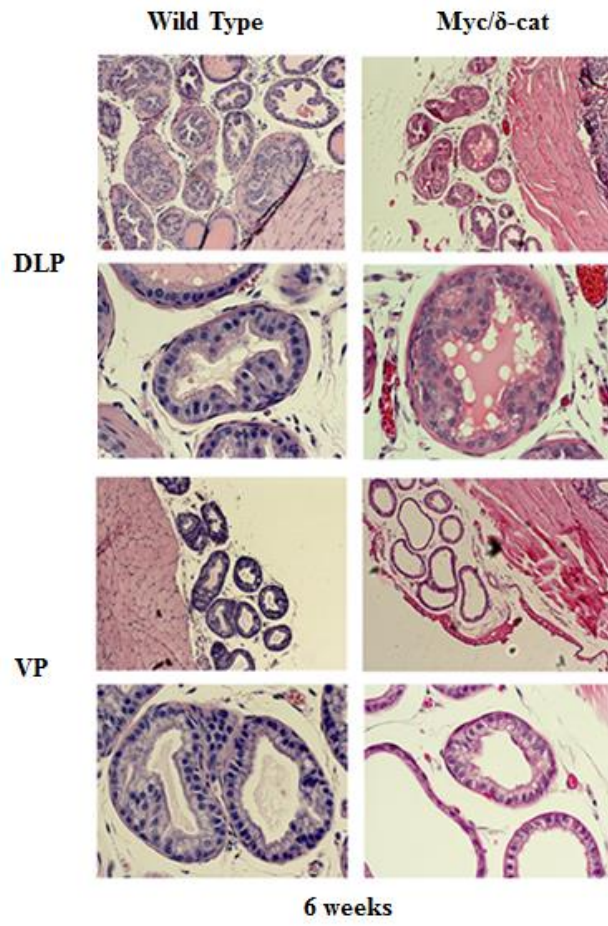


**Figure 3.2 Gross anatomy of Myc/ $\delta$ -cat double transgenic mouse prostate. (A).** Macroscopic view of the Myc/ $\delta$ -cat double transgenic prostates displayed relatively unchanged prostate size compared to normal-sized prostate in wild type. **(B).** Quantification of Myc/ $\delta$ -cat double transgenic mice prostate areas was not significantly different from wild type. Values represent mean  $\pm$ S.E.M. n= 4/ group.

**A.**



**B.**

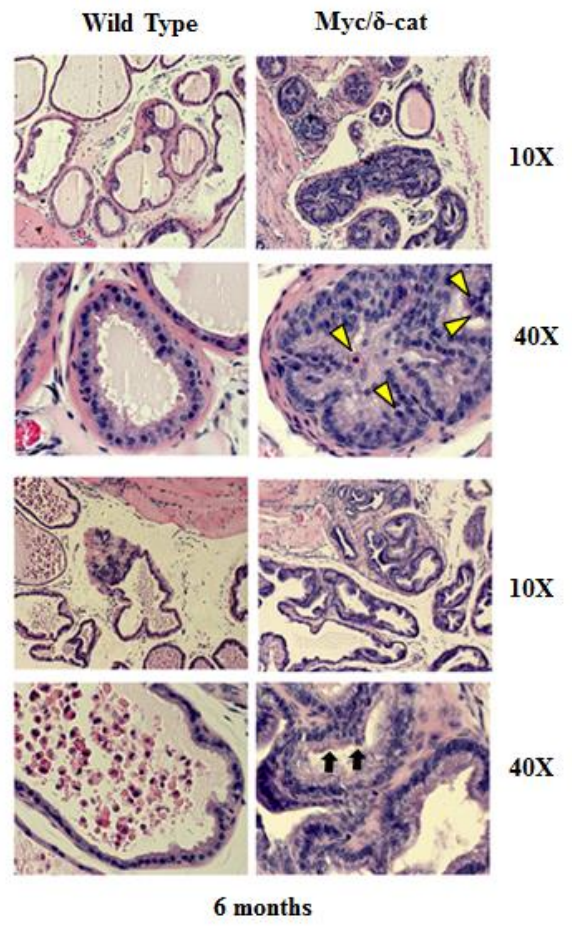
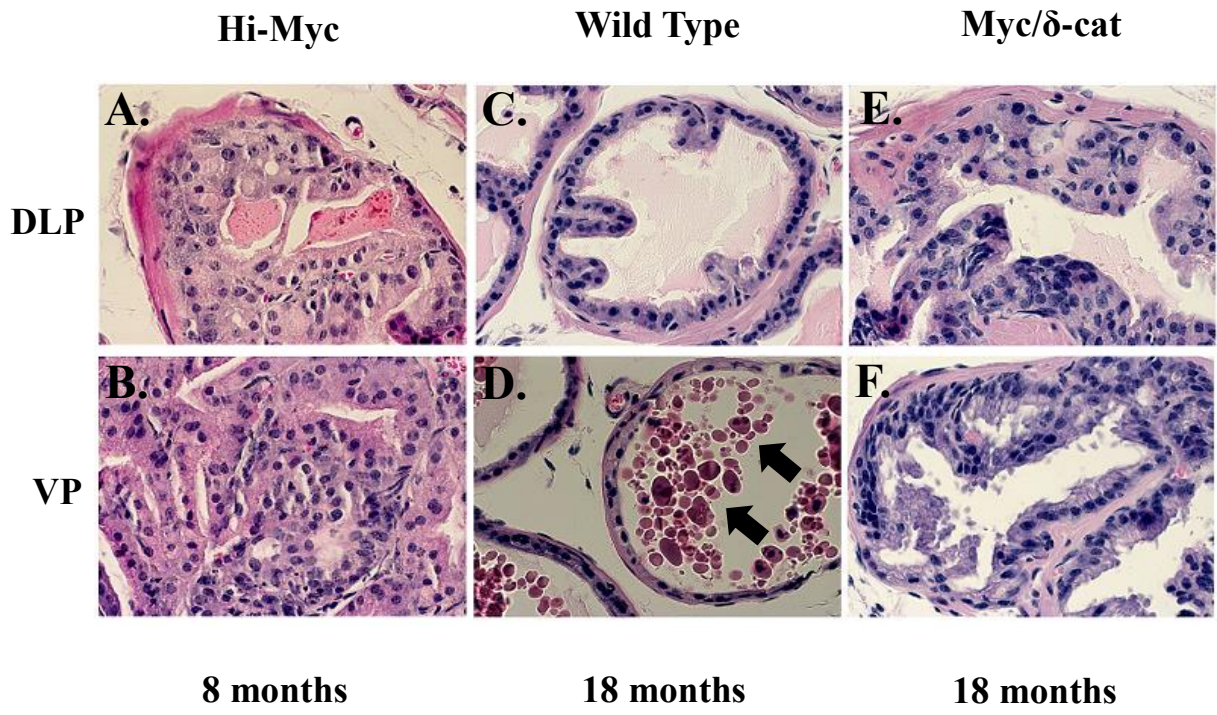


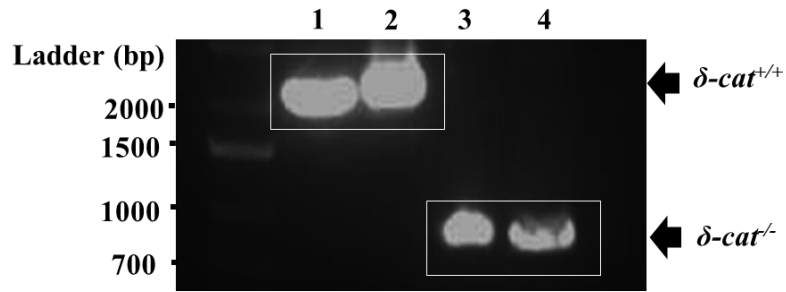
**Figure 3.3 Characteristic features of Myc/ $\delta$ -cat double transgenic mice.** (A). Histopathology analysis (H&E) performed on 6 week-old Myc/ $\delta$ -cat double transgenic prostate showed similar findings to wild type, characterized by one to two layers of prostatic epithelium. (B). Histopathology analysis (H&E) performed on 6 months-old of WT and Myc/ $\delta$ -cat double transgenic prostates. Myc/ $\delta$ -cat double transgenic mice revealed the transition from normal-appearing epithelial cells to mPIN lesions with well-demarcated basement membrane in both DLP and VP. A higher magnification of epithelia in mPIN lesions demonstrated multiple layers of cells, nuclear enlargement (indicated by yellow arrow heads) and many foldings (indicated by arrows), while age-matched wild-type tissues were lined by single layer of columnar epithelium, a characterization of normal prostate glands.



40X

**Figure 3.4  $\delta$ -Catenin overexpression in ectopically expressed *Myc* oncogene does not promote tumor progression in transgenic mice.** (A). and (B). Histological analysis of conditionally expressed *Myc* oncogene (ARR<sub>2</sub>PB-*Myc*) mouse reveals the development of prostatic adenocarcinoma by 8 months of age, predominantly in VP. (C). and (D). Histological analysis of 18 month-old wild-type prostate and (E). and (F). *Myc*/ $\delta$ -cat double transgenic prostate. While wild-type mouse prostate showed normal-looking prostatic epithelial cells with enlargement of the lumen as the mouse ages, *Myc*/ $\delta$ -cat double transgenic prostate exhibited highly proliferative epithelial cells expanded and filled prostatic lumina, but cells were still restricted within stroma, and prostate basement membrane. The arrows indicate prostate secretion in lumen.

**A.**



**B.**

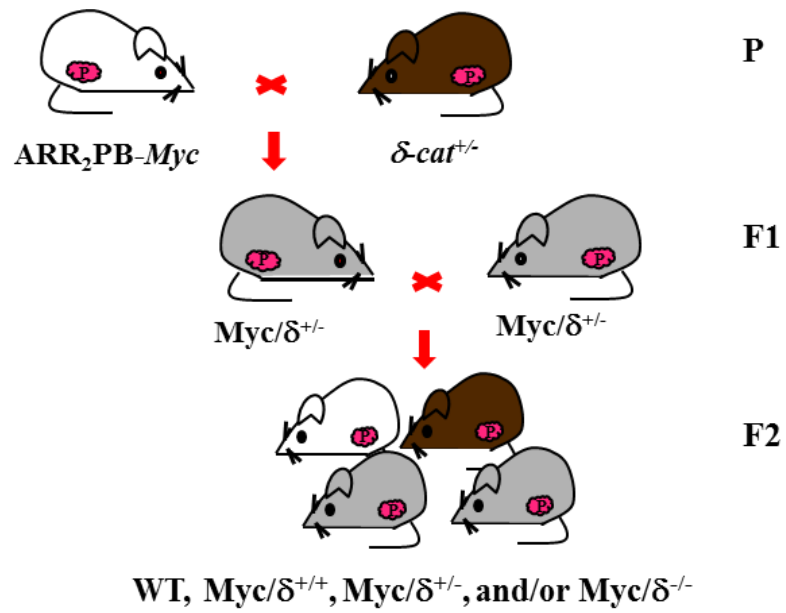
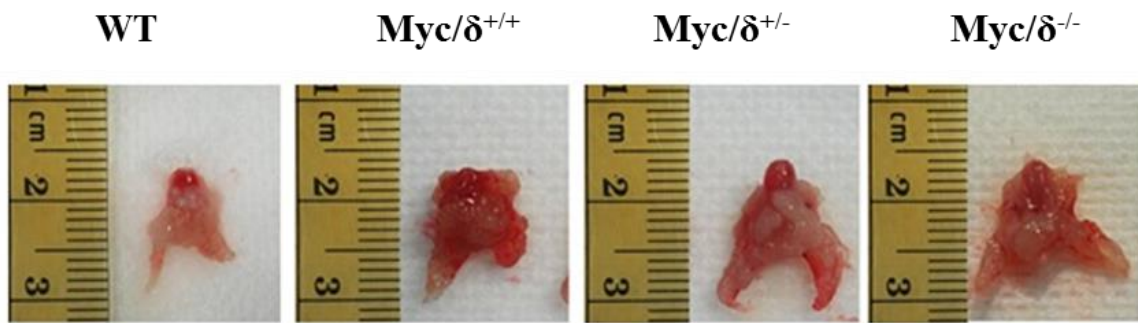
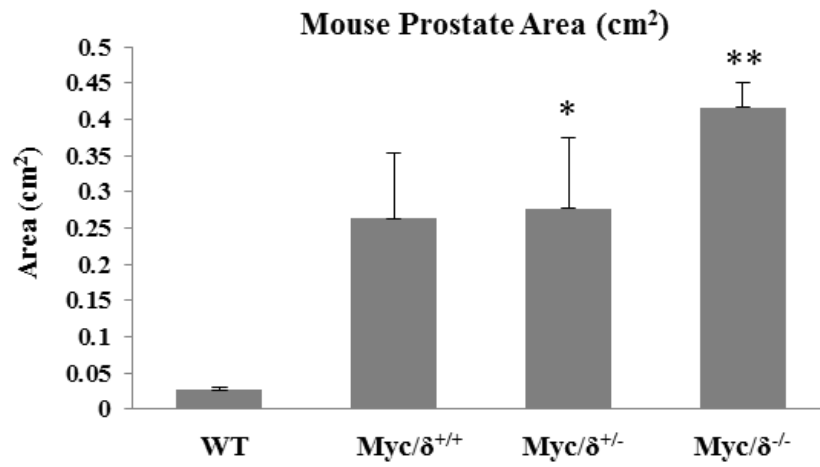


**Figure 3.5 Production and analysis of Myc/ $\delta$ -catenin mutant mice. (A).** Genotyping of mutant  $\delta$ -catenin mouse model. Lanes 1 to 4 showed PCR analysis of tail DNA of  $\delta$ -catenin homozygous ( $\delta$ -cat<sup>+/-</sup>) mutant parents, analyzed by normal  $\delta$ -catenin (lane 1 and 2) and mutant  $\delta$ -catenin (lanes 3 and 4) primers. These genomic analysis indicated that these mice were  $\delta$ -catenin heterozygous mutations and their genotypes were designated as  $\delta$ -cat<sup>+/-</sup>. **(B).** Schematic illustration of the generation of Myc/ $\delta$ -cat mutant mice. The  $\delta$ -catenin heterozygous mutant animals were mated with Myc transgenic mice and the resulting F1 progenies, Myc/ $\delta$ <sup>+/-</sup>, were intercrossed to obtain F2 mice with genotypes of interest including wild type (WT), Myc with  $\delta$ -catenin wild type (designation: Myc/ $\delta$ <sup>+/+</sup>), Myc with  $\delta$ -catenin heterozygous mutation (designation: Myc/ $\delta$ <sup>+/-</sup>), and Myc with  $\delta$ -catenin homozygous mutation (designation: Myc/ $\delta$ <sup>-/-</sup>).

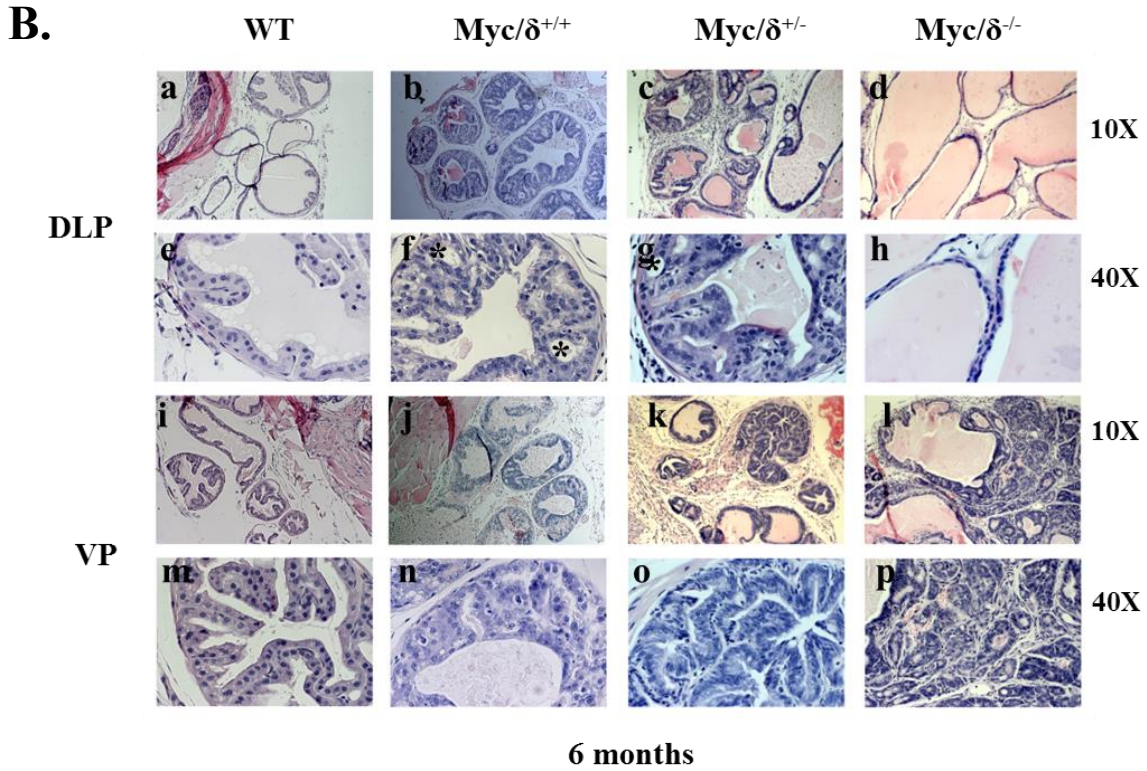
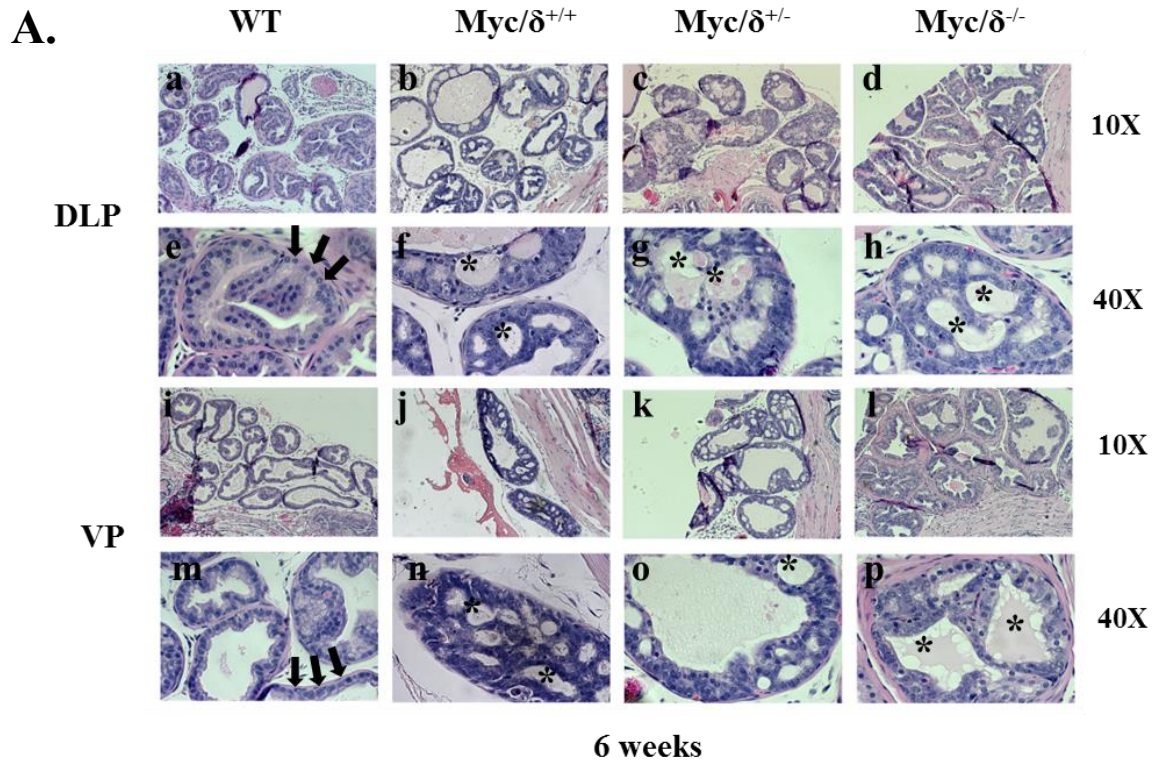
**A.**



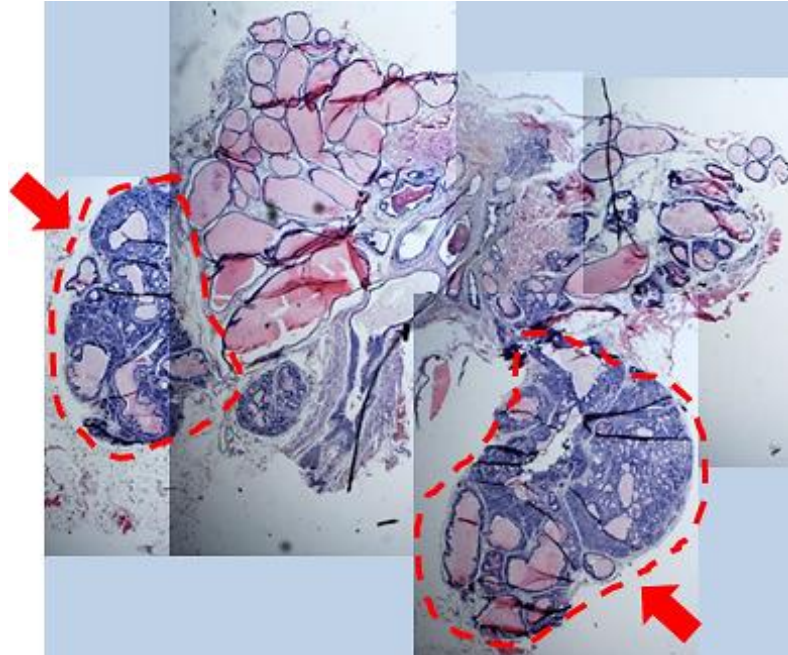
**B.**



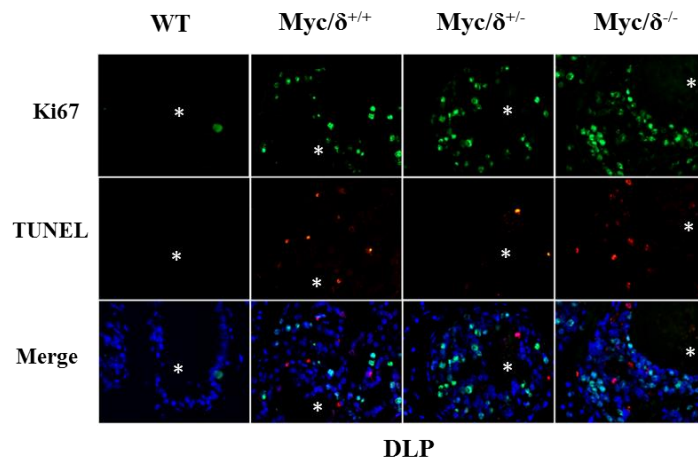
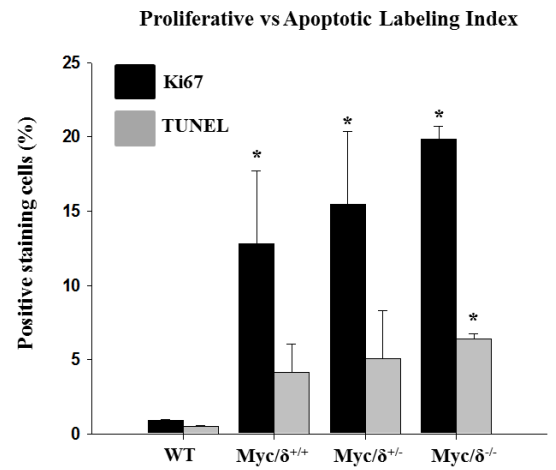
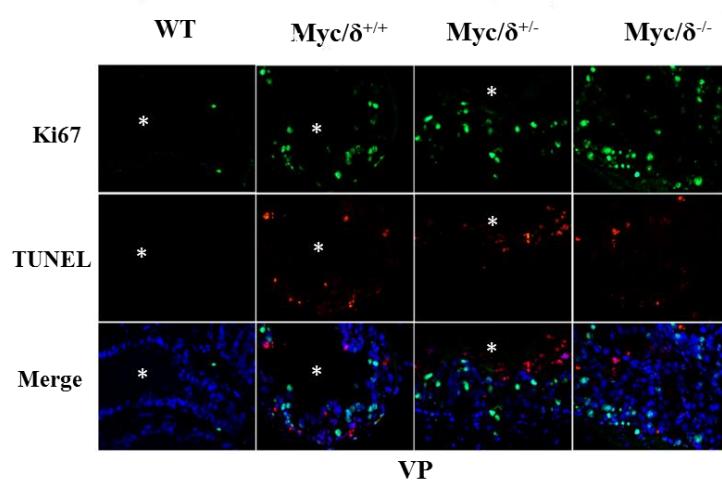
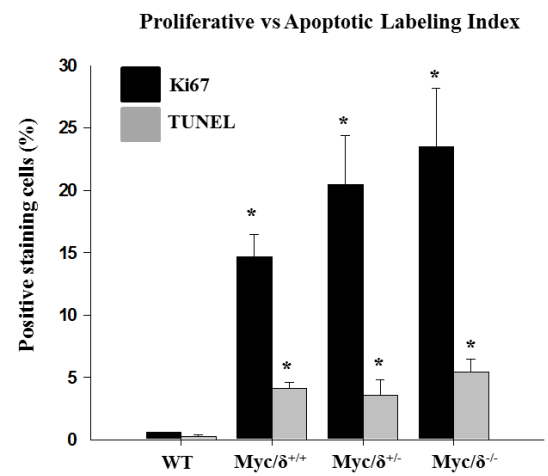
**Figure 3.6 Gross anatomy of Myc/ $\delta$ -catenin mutant mouse prostate. (A).** The prostates of Myc/  $\delta$ -catenin mutant mice displayed massive macroscopic enlargements in a  $\delta$ -catenin mutant-dosage-sensitive manner compared to normal-sized prostate in wild type (WT). **(B).** Quantification of Myc/ $\delta$ -catenin mutant prostate areas significantly increased compared to WT. Values represent mean  $\pm$  S.E.M. \*  $p < 0.05$  and \*\*  $p < 0.01$ , relative to WT. n= 3/ group.



**Figure 3.7 Characteristic features of Myc/ $\delta$ -catenin mutant mice.** (A). Histopathology analysis (H&E) of wild type (WT), Myc/ $\delta^{+/+}$ , Myc/ $\delta^{+/-}$ , and Myc/ $\delta^{-/-}$  mice prior to tumor onset (6-week-old-mice). mPIN lesions, recognized by intraepithelial space formation (indicated by asterisks), are found in transgenic animals (f-h and n-p) regardless of prostate regions. (B). Histopathology (H&E) of 6 month-old-mice from WT, Myc/ $\delta^{+/+}$ , Myc/ $\delta^{+/-}$ , and Myc/ $\delta^{-/-}$ . Note that only Myc/ $\delta^{-/-}$  mice showed diffuse, invasive prostate adenocarcinoma with large, undifferentiated tumor cells growing into stromal areas (l and p) in VP, while DP (b-c and f-g) and VP (j-k and n-o) continued to exhibit mPIN lesions at the same time point.

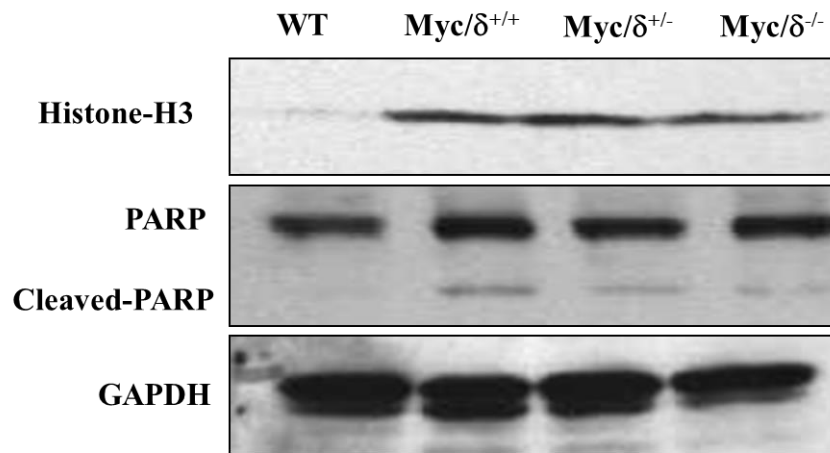


**Figure 3.8 Histopathology analysis (H&E) of *Myc/δ<sup>-/-</sup>* mice.** Cross section of a representative *Myc/δ<sup>-/-</sup>* prostate revealed the massive tumor formation in VP (Red arrows), with tumor cells disrupting the basement membrane of the gland and growing into surrounding stroma.

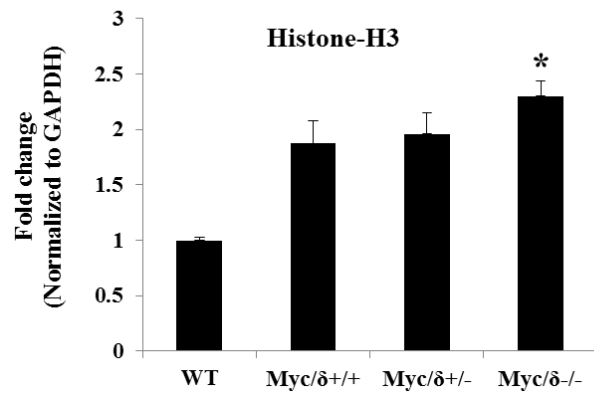
**A.****B.****C.****D.**

**Figure 3.9 An increase in cell proliferation and apoptosis labeling index in Myc/ $\delta$ -catenin mutant mice.** Frozen sections were stained for anti-Ki67, a marker of cell proliferation (green), TUNEL assay, detection of cells undergoing apoptosis (red), and Hoechst (blue), a marker for nuclei (blue). **(A).** and **(C).** Immunofluorescent images of DLP and VP. Number of Ki67 positive cells and TUNEL positive cells increased, corresponding with  $\delta$ -catenin mutations (WT < Myc/ $\delta^{+/+}$  < Myc/ $\delta^{+/-}$  < Myc/ $\delta^{-/-}$ ). **(B).** and **(D).** Quantifications of proliferative and apoptotic cells following immunofluorescent staining from **(A).** and **(C).** Note that the proliferative LI is dramatically increased in both DLP and VP, approximately four-fold higher than the LI for TUNEL staining. Values represent mean  $\pm$  S.E.M for a total of 500 cells counted from 2 sets of independent experiments. \*  $p < 0.05$ , relative to WT Ki67 or WT TUNEL. White asterisks indicate the lumen of prostate glands. LI: Labeling index. WT: wild type.

**A.**



**B.**



**C.**

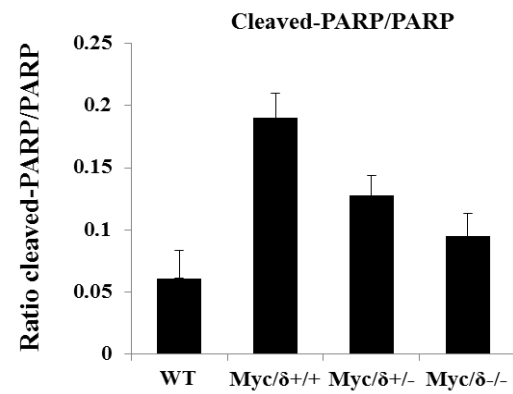
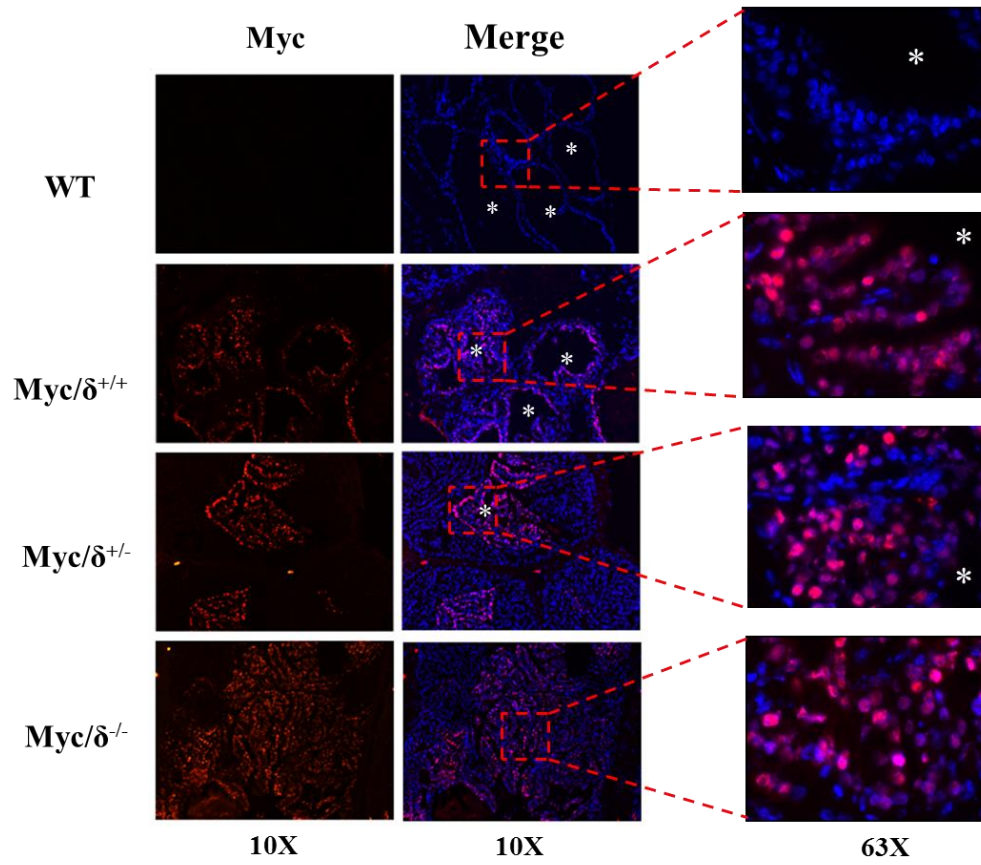
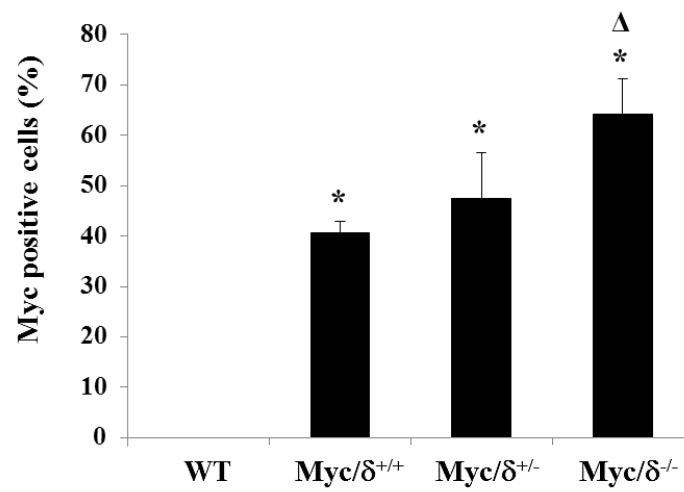


**Figure 3.10  $\delta$ -Catenin mutations promote histone-H3 activity.** (A). Representative Western blot analysis demonstrated protein banding profiles of Myc/ $\delta$ -catenin mutant prostate lysates utilizing the following antibodies: histone-H3, a marker of cell proliferation (top), PARP, a marker of cells undergoing apoptosis (middle). GAPDH served as a loading control (bottom). (B). Quantification of Myc/ $\delta$ -catenin mutant mice showed significantly increased histone-H3 compared to wild type (WT). Results shown are averaged from two independent experiments  $\pm$  S.E.M. All data was normalized to loading control and represented in fold induction relative to wild type (\*  $p < 0.05$ ). (C). Anti-PARP antibody detects full length PARP (higher molecular weight), as well as cleaved-PARP (lower molecular weight), resulting from caspase cleavage. Note that the ratio of cleaved-PARP over PARP showed that there was a reduction of cell apoptosis in Myc/ $\delta^{-/-}$  compared to Myc/ $\delta^{+/+}$ .

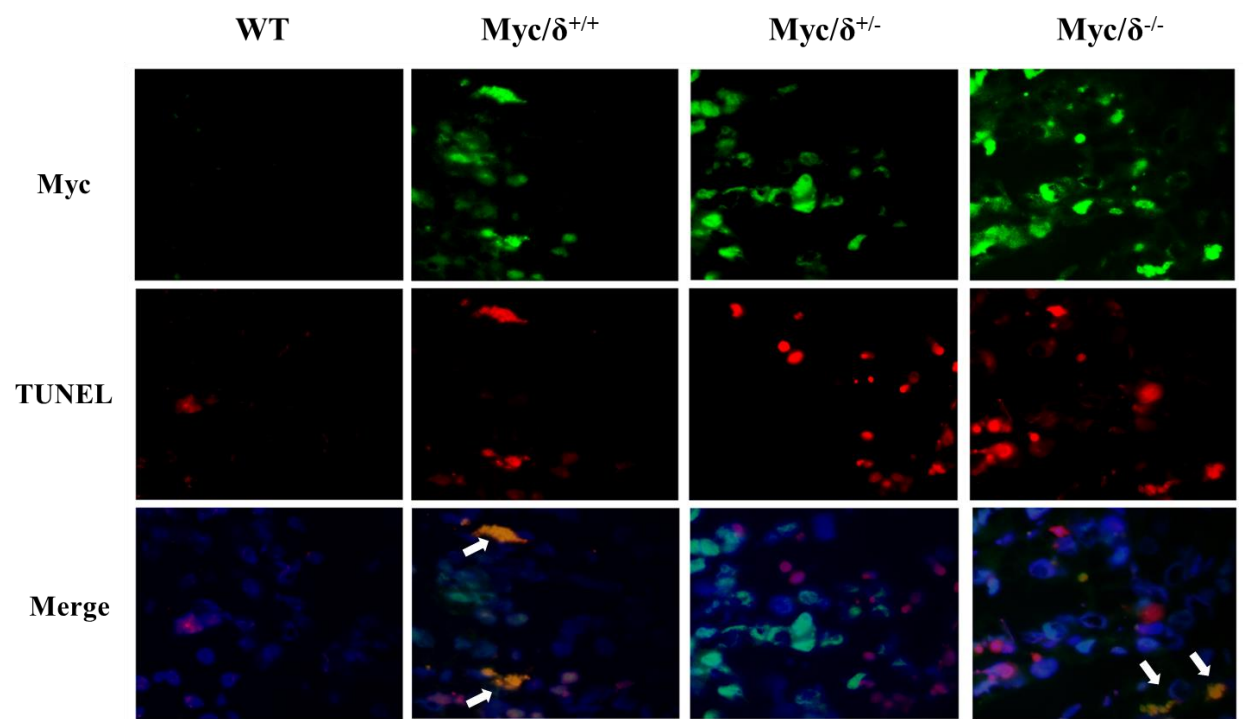
**A.**



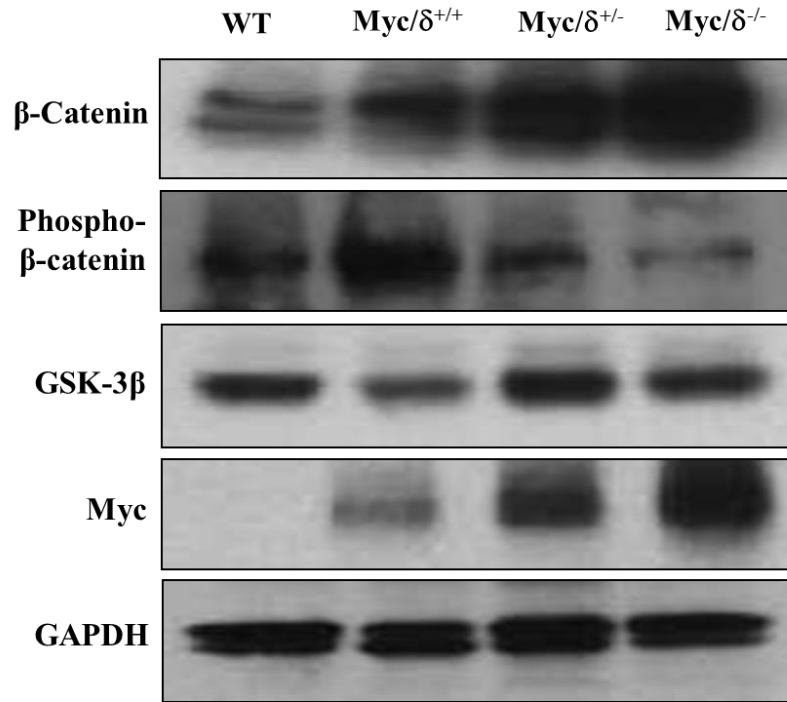
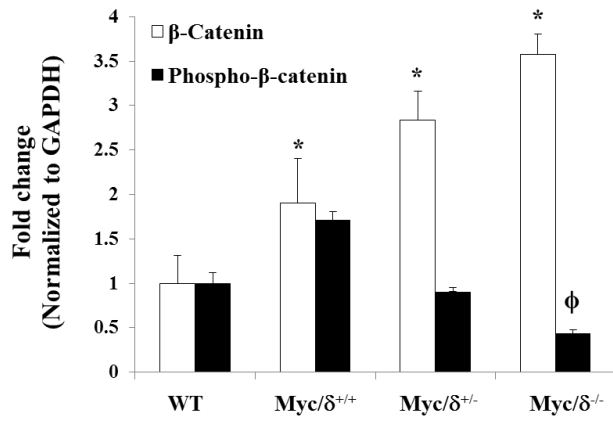
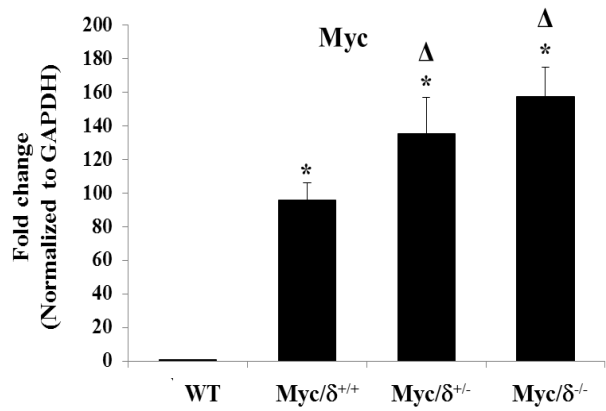
**B.**



**Figure 3.11  $\delta$ -Catenin mutations promote number of cells overexpressing Myc. (A).** Anti-Myc (red) and Hoechst (nuclei marker, blue) immunofluorescent analysis of 5  $\mu$ m mouse ventral prostate cross sections at 6 months of age from Myc/ $\delta$ -cat mutant mice. Results revealed that Myc overexpression in Myc/ $\delta^{+/+}$  and Myc/ $\delta^{+/-}$  prostates predominantly localized to luminal epithelia as indicated by white asterisks in luminal compartments of prostate glands (left and middle panels). Note that an age matched wild-type (WT) prostate was completely negative staining for Myc. **(B).** Number of cells overexpressing Myc increases dramatically, notably when prostate basement membranes were no longer intact as shown in Myc/ $\delta^{-/-}$  (right panel). Values represent mean  $\pm$  S.E.M for a total of 500 cells counted from two sets of independent experiments. \*  $p < 0.01$ , relative to WT and  $\Delta p < 0.05$ , relative to Myc/ $\delta^{+/+}$ . Boxes represent higher magnification images.



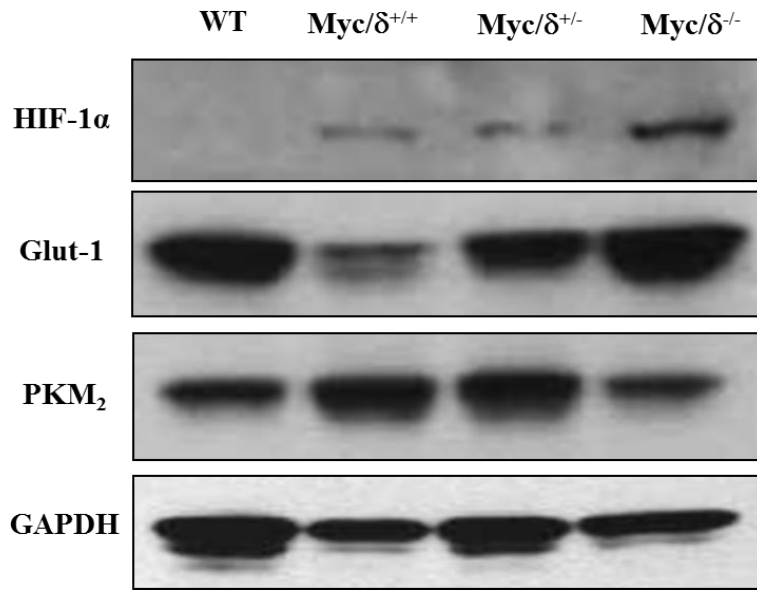
**Figure 3.12 Myc does not mediate apoptosis in Myc/ $\delta$ -catenin mutant mice.** Medium power (original magnification: 630X) view of immunofluorescent staining by anti-Myc (green), TUNEL assay, detection of cells undergoing apoptosis (red), and Hoechst, a marker for nuclei (blue) performed on six month-old Myc/ $\delta$ -catenin mutant prostate tissues. Prostatic epithelial cells, which were staining strongly positive for anti-Myc, exhibited negative staining for TUNEL and vice versa. However, merged images show that there were positive staining cells for both Myc and TUNEL (white arrows). WT: wild type.

**A.****B.****C.**

**Figure 3.13  $\delta$ -Catenin mutations enhance  $\beta$ -catenin and Myc protein expression.**

(A). Representative Western blot analysis of six month-old mouse prostate lysate probed with antibodies against  $\beta$ -catenin, phosphorylated  $\beta$ -catenin, GSK-3 $\beta$ , and Myc. GAPDH served as a loading control. (B). and (C). Graphs represent quantitative measurement of Western blot band intensities with the indicated proteins. It was shown that  $\delta$ -catenin mutations resulted in significant increased  $\beta$ -catenin and Myc expressions, but decreased phosphorylated- $\beta$ -catenin, which was associated with doses of  $\delta$ -catenin mutations. These results suggested the reduction of  $\beta$ -catenin degradation. However, only the  $\delta$ -catenin heterozygous mutant, but not homozygous mutant, increased GSK-3 $\beta$ . Results shown are mean from two independent experiments  $\pm$  S.E.M. All data was normalized to loading control and represented in fold induction versus wild type (WT) or Myc/ $\delta^{+/+}$ . (\* p< 0.01, relative to WT,  $^{\phi}$  p<0.01, relative Myc/ $\delta^{+/+}$ , and  $^{\Delta}$  p<0.01, relative Myc/ $\delta^{+/+}$ ).

**A.**



**B.**

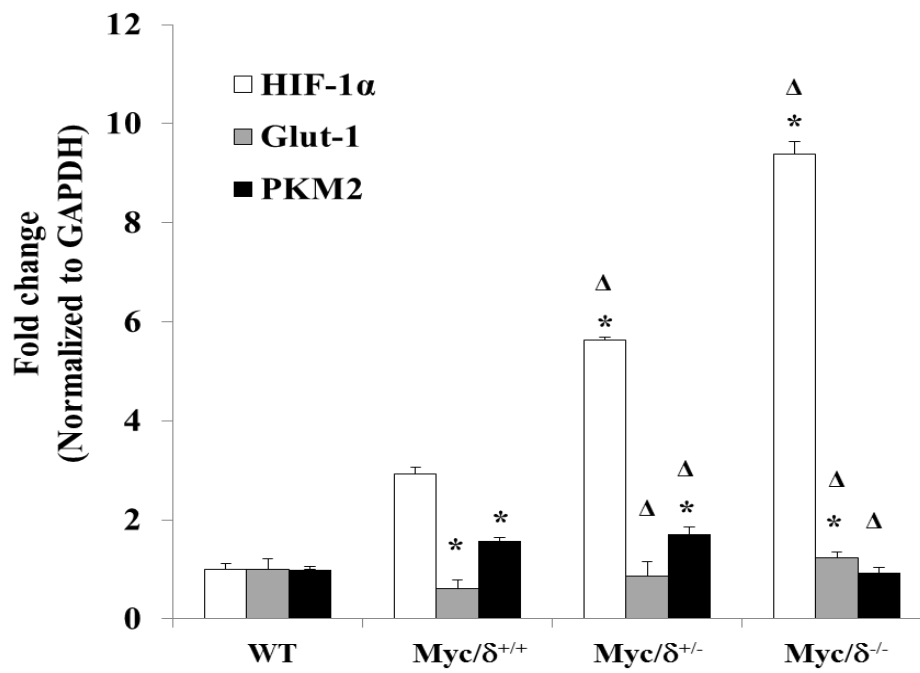


**Figure 3.14  $\delta$ -Catenin mutations induce HIF-1 $\alpha$  activity and affect expression profiles of Glut-1 and PKM<sub>2</sub>.** (A). Western blots were carried out using total protein extracts prepared from whole mouse prostates with the indicated genotypes and then the blots were probed with indicated antibodies to assess activities of HIF-1 $\alpha$ , Glut-1, and PKM<sub>2</sub>. GAPDH served as a loading control. (B). The quantitative measurements of HIF-1 $\alpha$  and Glut-1 immunoreactivities in Myc/ $\delta$ -catenin mutant mice showed significantly enhanced HIF-1 $\alpha$  and Glut-1, corresponding to degree of  $\delta$ -catenin mutants, but PKM<sub>2</sub> was reduced. Results represent averaged from two independent experiments  $\pm$  S.E.M. All data was normalized to loading control and demonstrated in fold induction versus wild type (WT) or Myc/ $\delta^{+/+}$ . (\* p<0.01, relative to WT and  $\Delta$  p<0.01, relative to Myc/ $\delta^{+/+}$ ).

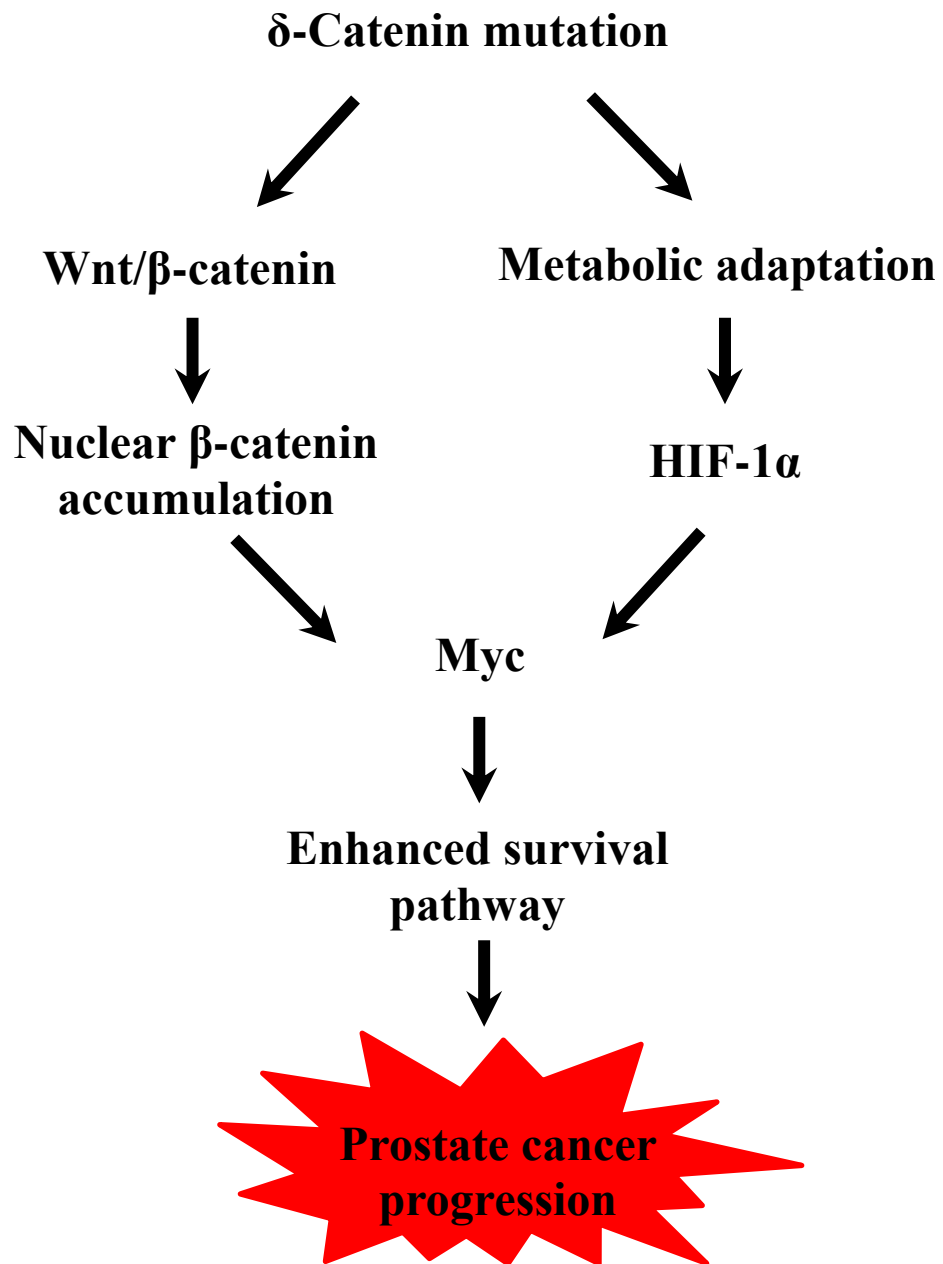


**Figure 3.15 Proposed model of  $\delta$ -catenin-induced prostate cancer progression in mouse model.**  $\delta$ -Catenin mutations could result in the activation of both Wnt/ $\beta$ -catenin and HIF-1 $\alpha$  signaling pathways, through which Myc can be activated. Activated *Myc* oncogene further contributes to survival advantage by reprogramming cellular metabolism leading to prostate cancer progression.

## **F. Acknowledgements**

We would like to acknowledge Dr. Jain-Ping Lu and Dr. Jiao Zhang for their assistance generating mouse transgenic models and Joani Zary-Oswald for her technical assistance of histological procedures.

# CHAPTER IV: CHARACTERIZATION OF PROSTATIC EPITHELIAL CELL LINES ESTABLISHED FROM $\delta$ -CATENIN MUTANT MICE OVEREXPRESSING *MYC* ONCOGENE

## A. Summary

To understand the functional interactions between *Myc* oncogene and  $\delta$ -catenin in the *Myc*/ $\delta$ -catenin mutant mouse model, two cell lines were established from heterogeneous 6 month tumors of the transgenic mouse overexpressing human *Myc* (designation: C1-*Myc*/ $\delta^{+/+}$ ) comparing with transgenic mouse overexpressing human *Myc* with  $\delta$ -catenin heterozygous mutants (designation: C2-*Myc*/ $\delta^{+/-}$ ). The *Myc* mouse model is a transgenic line harboring a construct comprised of the derivative rat probasin promoter (ARR<sub>2</sub>PB) driving prostate-specific epithelial expression of *Myc* transgene. Immunofluorescent analyses revealed that the two cell lines express PSA, E-cadherin,  $\beta$ -catenin, while vimentin only aggregates in dividing cells, suggesting an epithelial origin for the cells. In addition, C2-*Myc*/ $\delta^{+/-}$  cells show an increase of  $\beta$ -catenin, *Myc*, cyclin D1 protein levels compared to C1-*Myc*/ $\delta^{+/+}$ . While Glut-1 levels remain unchanged, protein expression levels of HIF-1 $\alpha$  and PKM<sub>2</sub>, key modulators in hypoxic and metabolic pathways, are elevated in C2-*Myc*/ $\delta^{+/-}$  compared to C1-*Myc*/ $\delta^{+/+}$ . Taken together, these results suggest that the cell lines are epithelial in origin and characteristically parallel our mouse models.

## B. Introduction

There is currently a strong interest in the application of the knowledge gained from the analyses of human prostate cancer (PCa) in modeling this disease *in vivo* and *in vitro*. For studies

of the mechanism of cancer initiation and progression, cancer cell lines are powerful tools since they can be easily manipulated *in vitro*. However, there are a limited number of human PCa cell lines derived from primary or metastatic cancers (Ittmann et al., 2013; Shappell et al., 2004). Since mouse models of PCa can readily provide tissue materials for establishing cell lines from different phases of disease progression, they have become invaluable for defining the mechanism of PCa progression for testing preventive and therapeutic regimens. However, only a few murine prostate tumor cell lines have been derived from the primary tumors to date (Shappell et al., 2004). Therefore the idea of generating murine cell lines obtained directly from early to late stage of disease has become important in understanding PCa development. Moreover, cells lines established from mouse models can be studied *in vivo* without the added complexity of using immunosuppressants in immunodeficient animals implanted with xenografts.

Several mouse models of PCa have been developed based on genetic modifications which are frequently found in human PCa in order to recapitulate its natural course of development and progression. Among these mouse models, the prostate tumor development in ARR<sub>2</sub>PB-*Myc* or Hi-*Myc* mice have been shown to closely mimic the human disease (Abate-Shen and Shen, 2002; Ellwood-Yen et al., 2003; Iwata et al., 2010). A well-refined Hi-*Myc* model was further cross-bred with  $\delta$ -catenin heterozygous ( $\delta$ -cat<sup>+/-</sup>) mutant mice in order to determine functions of  $\delta$ -catenin in mouse prostate tumors. We have successfully generated and characterized *Myc*/ $\delta$ -catenin mutant mice as previously described in chapter III. Briefly, we demonstrated that *Myc*/ $\delta$ <sup>+/+</sup> mice develop histological mPIN by 6 weeks of age that progresses to adenocarcinoma by 8 months of age. However, mPIN lesions in *Myc*/ $\delta$ <sup>+/-</sup> mice transition to adenocarcinoma by 6-7 months of age, suggesting that mutation of  $\delta$ -catenin accelerates tumor progression in this mouse model. In this report, we established and characterized two novel cell lines derived from

Myc/ $\delta^{+/+}$  mouse, designed as C1-Myc/ $\delta^{+/+}$  and Myc/ $\delta^{+/-}$  mouse, designated as C2-Myc/ $\delta^{+/+}$ . *In vitro* analysis of these cell lines demonstrates an epithelial origin. These cell lines are valuable new models for studying the mPIN stage of cancer development. This system could provide extensive data on protein correlating to cancer grade, as well as, a therapeutic model for an effective therapy.

### **C. Experimental procedures**

#### *C1. Establishment of cell lines from Myc/ $\delta^{+/+}$ and Myc/ $\delta^{+/-}$ mouse PCa models*

Mouse prostate cell lines were prepared following the method of Foster et al. and Liao et al. with minor modification (Foster et al., 1997; Liao et al., 2010). Prostate tissues used to establish the cell lines were freshly collected from either a 6 month-old Myc/ $\delta^{+/+}$  mouse or a Myc/ $\delta^{+/-}$  mouse. Prostate tumor tissues were minced with sterile scalpels, transferred to a 50-ml tube, and incubated in 5 ml of a digestion medium at 37°C on a rotator for three hours. The digestion medium contained Dulbecco's modified Eagles's medium (DMEM)/F12 (Invitrogen, Carlsbad, CA), 10% fetal bovine serum (FBS; Invitrogen, Carlsbad, CA), collagenase (1 mg/ml), hyaluronidase (1 mg/ml), and DNase I (1  $\mu$ g/ml). After low-speed centrifugation, single cells and cell clumps were collected and passed through 100- $\mu$ m cell strainers (BD Bioscience, San Jose, CA). The cell mixture was then cultured in a maintenance medium that was comprised of DMEM/F12, 10% FBS, 25  $\mu$ g/ml bovine pituitary extract (Invitrogen), 5  $\mu$ g/ml insulin, 6 ng/ml recombinant human epidermal growth factor (rhEGF), and 10<sup>-8</sup> M dihydrotestosterone. The culture medium was changed every 2-3 days. During early passage, the cells were differentially trypsinized to enrich for more adherent epithelial cells. When cell colonies with epithelial cell morphology were observed, cell were trypsinized, counted, diluted with culture medium to

obtain a concentration of approximately one cell per 100  $\mu$ l, and subsequently seeded in 96-well plates. Cells were carefully monitored under the bright field in microscopy. Wells containing single cells with the epithelial morphology were marked for expanding these cell populations in larger culture dishes, and subjected to further experiments. All other chemicals were from Sigma (St. Louis, MO) unless otherwise indicated.

### C2. PCR genotyping

Genomic DNAs from C1-Myc/ $\delta^{+/+}$  and C2-Myc/ $\delta^{+/-}$  cell lines were extracted by using DNeasy Tissue Kit (Qiagen Science, Maryland) according to manufacturer's instruction and used as templates for PCR reactions using specific primer sets for *Myc* and  $\delta$ -catenin (full-length and truncated fragment) as listed in Table 4.1. Finally, PCR reactions were run through 1% agarose gel and visualized under UV light to examine DNA bands. All images were captured by the ChemiDoc™ XRS+ system (Bio-Rad, Hercules, CA) equipped with Quantity-one 4.6.9 program.

**Table 4.1 Primer sets used in PCR-based analysis**

<b>Gene</b>	<b>Forward primer (5' to 3')</b>	<b>Reverse primer (5' to 3')</b>	<b>Product size (base pairs)</b>
<i>Myc</i>	AAACATGATGACTAC CAAGCTTGGC	ATGATAGCATCTTGTTCTT AGTCTTTTTCTTAATAGGG	100-200
$\delta$ -cat <sup>+/+</sup> (Full-length)	GACGTTTGGTTTTCCG AATG	AGAGTCAACGGAGGCAC AAT	2000
$\delta$ -cat <sup>-/-</sup> (Truncation)	AACCGTTTCTGTGAG CAGGTCC	GCTCGTCCATGCCGAGAG TG	800

### C3. RNA isolation and reverse-transcription PCR

Total RNA from C1-Myc/ $\delta^{+/+}$  and C2-Myc/ $\delta^{+/-}$  cell lines was isolated by using Qiagen RNeasy Kit (Qiagen Science, Maryland) following the manufacturer's protocol. Isolated RNA was reverse-transcribed into cDNA using RETROscript™ kit (Ambion Life Technologies, Grand Island, NY) and then it was used as templates for PCR reactions using specific primer sets to amplify human-*Myc*, and exon 13-17 of mouse- *$\delta$ -catenin* sequences as listed in Table 4.2. *GAPDH* served as a housekeeping gene. The final PRC products were run through 1% agarose gel and visualized under UV light in order to determine DNA bands. All images were captured by the ChemiDoc™ XRS+ system (Bio-Rad, Hercules, CA) equipped with Quantity-one 4.6.9 program.

**Table 4.2 Primer sets used in reverse transcription PCR-based analysis**

<b>Gene</b>	<b>Forward primer (5' to 3')</b>	<b>Reverse primer (5' to 3')</b>	<b>Product size (base pairs)</b>
human- <i>Myc</i>	GGGAGGCTGCTGCTTT	CTTCTCTGAAAGGCTC TCCT	1300
mouse- <i><math>\delta</math>-catenin</i> Exon 13-17	TACAGCTGCATTCATCA GAGGTGG	CGCATGGCATACTTGC CAATGAGT	769
mouse- <i>GAPDH</i>	TCAACAGCAACTCCCA CTCTTCCA	ACCCTGGTTGCTGTAG CCGTATTCA	~200

#### C4. Immunofluorescent analysis

C1-Myc/ $\delta^{+/+}$  or C2-Myc/ $\delta^{+/-}$  cells on coverslips were incubated with 0.2% Triton X-100 for 10 min at room temperature, 20 min at room temperature with 100 mM glycine and blocked 30 min at 37°C with 10% bovine serum albumin (BSA). Primary antibodies (rabbit E-cadherin 1:100, Santa Cruz Biotechnology, Santa Cruz, CA; rabbit  $\beta$ -catenin 1:100, BD transduction laboratories, Lexington, KY; mouse vimentin 1:100, Assay Biotech Company, Sunnyvale, CA; and mouse PSA 1:100, Santa Cruz Biotechnology, Santa Cruz, CA) were incubated one hour at room temperature. Immunofluorescent images were captured and analyzed with a Carl Zeiss microscope (Thornwood, NY) equipped with Axiovision Rel 4.8 imaging software.

#### C5. Western blot analysis

C1-Myc/ $\delta^{+/+}$  or C2-Myc/ $\delta^{+/-}$  cells were washed one time in cold PBS and then lysed in RIPA buffer. Lysates were collected by cell scrapers and homogenized on ice by passing approximately 10 times through 22-gauge needles and incubated on ice for 30 min. The cell lysates were then centrifuged at 14,000 rpm for 30 min. After centrifugation, the supernatant was transferred to new, properly labeled tubes. The total protein concentration of each sample was measured by using the BCA protein assay kit.

The cell lysates in the SDS sample buffer were separated by 8-16% Tris SDS-PAGE and transferred to nitrocellulose membranes. The membrane was then blocked in 5% non-fat dried milk in TBS plus 0.1% Tween 20 for 1 h at room temperature. Western blotting was performed with a rabbit histone-H3 antibody 1:1000 (Santa Cruz Biotechnology, Santa Cruz, CA), a rabbit PARP antibody 1:1000 (Cell Signaling Technology, Danvers, MA), a rabbit  $\beta$ -catenin antibody

1:1000 (BD transduction laboratories, Lexington, KY), a rabbit Myc (N-term) antibody 1:1000 (Epitomics, Burlingame, CA), a rabbit cyclin D1 1:250 (Santa Cruz Biotechnology, Santa Cruz, CA), a rabbit HIF-1 $\alpha$  antibody 1:500 (Santa Cruz Biotechnology, Santa Cruz, CA), a rabbit Glut-1 antibody 1:1000 (ThermoScientific, Philadelphia, PA), and a rabbit PKM<sub>2</sub> antibody 1:500 (Cell Signaling Technology, Danvers, MA). GAPDH (mouse, 1:2000; Calbiochem, San Diego, CA) was used as a loading control, followed by probing with appropriate HRP-conjugated secondary antibodies for 1 h at room temperature. Immunoreactive protein bands were detected by enhanced chemiluminescence (ECL) Western blot detection reagent from GE healthcare (Pittsburgh, PA).

#### C6. Statistical analysis

Student *t*-test analysis was performed using SigmaPlot 10.0 (Systat Software Inc., San Jose, CA) and *p*-values were designated for each experiment, each of which was repeated a minimum of two times. Any null hypothesis with probability level less than 95% was rejected.

### **D. Results**

#### D1. Characterization of the novel murine prostate tumor cell lines

We first isolated cells from Myc/ $\delta^{+/+}$  or Myc/ $\delta^{+/-}$  prostates from mice of 6 months of age. After culturing of single cells in 96-well plates, colonies with epithelial-like morphology were selected and expanded. The first cell line obtained from Myc/ $\delta^{+/+}$  was designated as C1-Myc/ $\delta^{+/+}$  and the second cell line established from Myc/ $\delta^{+/-}$  was named C2-Myc/ $\delta^{+/-}$ . The sub-confluent cultures were shown to underline the morphological differences between C1-Myc/ $\delta^{+/+}$  and C2-Myc/ $\delta^{+/-}$  cells. C1-Myc/ $\delta^{+/+}$  cells morphologically consisted of polygonal cells growing in a

tightly-packed clumps of cells, suggesting a tight intracellular adhesion (Fig. 4.1A, left panel). In contrast, C2-Myc/ $\delta^{+/+}$  generally exhibited a polygonal-shaped morphology but apparently with irregular dendritic-like extensions (indicated by arrows) (Fig. 4.1A, right panel).

To determine *Myc* and  $\delta$ -catenin gene status in these two cell lines, a genotyping analysis was performed. Genomic DNA extracted from these cell line cells was subjected to PCR-based screening with primer sets specific for human-*Myc* transgene and endogenous mouse  $\delta$ -catenin gene. Mouse-tail genomic DNA was extracted from the tail-snip Myc/ $\delta^{+/+}$  and used as a control for the PCR reactions (Fig. 4.1B, lanes 5 and 9). As illustrated in Fig. 4.1B (lanes 1, 3, and 7), C2-Myc/ $\delta^{+/+}$  exhibited appropriate DNA bands when  $\delta$ -cat<sup>+/+</sup>,  $\delta$ -cat<sup>-/-</sup>, and *Myc* primer sets were used. In contrast, PCR product from C1-Myc/ $\delta^{+/+}$  with  $\delta$ -cat<sup>-/-</sup> primer sets was undetectable (Fig. 4.1B, lane 4), indicating that there was no fragmentation of  $\delta$ -catenin as a consequence of target deletion seen in C2-Myc/ $\delta^{+/+}$ . These results revealed that the genetic profiles in epithelial cell lines were consistent with that from mouse tissues, validating the quality of C1-Myc/ $\delta^{+/+}$  and C2-Myc/ $\delta^{+/+}$  cell lines.

#### D2. Reverse-transcription PCR reveals a phenotypic difference in C1-Myc/ $\delta^{+/+}$ and C2-Myc/ $\delta^{+/+}$ cell lines

In order to confirm that C2-Myc/ $\delta^{+/+}$  is genetically different from C1-Myc/ $\delta^{+/+}$ , we performed reverse-transcription PCR using isolated RNA from these 2 cell lines. Since  $\delta$ -catenin homozygous ( $\delta$ -cat<sup>-/-</sup>) mice were generated by disrupting the  $\delta$ -catenin gene at exon 9 as previously described (Israely et al., 2004), we designed and used the primer sets to amplify the PCR templates at the exon 13 to 17 of  $\delta$ -catenin gene. As expected, single DNA band was detectable in C1-Myc/ $\delta^{+/+}$  (Fig. 4.1C, lane 1), whereas only smear DNA band was detectable in

C2-Myc/ $\delta^{+/-}$  (Fig. 4.1C, lane 2). These results further support that C2-Myc/ $\delta^{+/-}$  cells carried  $\delta$ -catenin heterozygous deletion. *GAPDH* served as a housekeeping gene (Fig. 4.1C, lanes 3 and 4).

### D.3 C1-Myc/ $\delta^{+/+}$ and C2-Myc/ $\delta^{+/-}$ cell lines are prostatic epithelial in origin

To further characterize the expression of epithelial specific-proteins in our cell lines, double immunofluorescent labeling was performed using vimentin antibody (green signal), a stromal cell marker, and PSA antibody (red signal), a prostate specific marker. As depicted in Fig. 4.2 (upper first panel) immunofluorescent analysis revealed a distinct vimentin aggregating pattern. It expressed predominantly in the nucleus of dividing cells (indicated by white arrows). However, C1-Myc/ $\delta^{+/+}$  and C2-Myc/ $\delta^{+/-}$  cells exhibited greatly distributed PSA in cytoplasm of cells (Fig. 4.2, upper second panel). Taken together, the positive immunostaining for PSA and negative immunostaining for vimentin suggested prostatic epithelial origin for C1-Myc/ $\delta^{+/+}$  and C2-Myc/ $\delta^{+/-}$  cell lines.

### D4. Loss or altered distribution of E-cadherin and $\beta$ -catenin in C2-Myc/ $\delta^{+/-}$ in comparison to that of C1-Myc/ $\delta^{+/+}$

Double immunostaining of E-cadherin and  $\beta$ -catenin, well-characterized proteins in regulating cell-cell junctions, was performed in order to elucidate their localization in our cell lines. We demonstrated that E-cadherin immunoreactivity (green signal) was detectable and showed similar distribution in both cell lines (Fig. 4.3A; upper first panel), providing further evidence that the cell lines were epithelial in origin. We also observed that the most intense staining of E-cadherin was close to the nucleus, where the cytoplasm was the thickest (white

arrows). However, most E-cadherin was either lost or redistributed to the cytoplasm, especially in C2-Myc/ $\delta^{+/-}$  cells.

Interestingly, the majority of  $\beta$ -catenin immunostaining (red signal) was localized at cell-cell junctions in C1-Myc/ $\delta^{+/+}$ , while it was expressed in the cytoplasm and nuclei as well as cell-cell contact region in C2-Myc/ $\delta^{+/-}$  (Fig 4.3A, upper second panel, white arrows). In addition, merged images of E-cadherin and  $\beta$ -catenin immunoreactivities revealed that they did not colocalize either in cytoplasm or at cell-cell junction (Fig. 4.3A, bottom panel).

A closer examination of  $\beta$ -catenin localization and distribution in cells was performed by measuring pixel intensity in three different cellular compartments including the nucleus, cytoplasm, and cell-cell junction. When expressed as a ratio of cytoplasm to cell-cell junction or nucleus to cytoplasm, the pixel intensity quantification more clearly described the localization of  $\beta$ -catenin. These data demonstrated an increase of  $\beta$ -catenin distribution in the cytoplasm and nucleus in C2-Myc/ $\delta^{+/-}$  compared to C1-Myc/ $\delta^{+/+}$  (Fig. 4.3B, cytoplasm/junction and nucleus/cytoplasm). Such results support our hypothesis that C2-Myc/ $\delta^{+/-}$  displayed a more aggressive phenotype than that of C1-Myc/ $\delta^{+/+}$ .

Additionally, we performed Western blotting analysis to determine protein expression levels of histone-H3, a proliferation marker, and PARP, a marker for cell apoptosis. The results from quantification of protein banding intensities revealed that there was a moderate increase in histone-H3 protein expression in C2-Myc/ $\delta^{+/-}$  although it was not statistically significant when compared to that of C1-Myc/ $\delta^{+/+}$  (Fig 4.4A, top panel). However, significant increases in the ratio of cleaved-PARP to PARP were shown in C2-Myc/ $\delta^{+/-}$  (Fig. 4.4A, second panel, and Fig. 4.4B). These findings support the observations of increased anti-Ki67 and TUNEL analyses in cellular level mouse tissue sections (Fig. 3.9, Chapter III), which further validates the importance

of having a complete model to study molecular mechanisms more accurately. Future studies, such as doubling time assay, cell growth on matrigel, and cell cycle regulation, will be needed to further determine the growth characteristics of these cell lines.

D5. Altered Wnt/ $\beta$ -catenin signaling pathway elements in C2-Myc/ $\delta^{+/-}$  in comparison to that of C1-Myc/ $\delta^{+/+}$

Our previous findings demonstrated that  $\delta$ -catenin mutations alter the expression of  $\beta$ -catenin and its target effectors with respect to the canonical Wnt/ $\beta$ -catenin signaling pathway. To further examine this hypothesis, analysis of protein expression in lysates prepared from cell cultures were performed. Western blot analysis revealed slower migrating  $\beta$ -catenin forms in full-length  $\delta$ -catenin containing cells (C1-Myc/ $\delta^{+/+}$ ) as compared to C2-Myc/ $\delta^{+/-}$  (Fig 4.5A, upper first panel, arrow). These higher molecular weight forms of  $\beta$ -catenin are indicative of ubiquitination (Aberle et al., 1997; Bareiss et al., 2010). These results suggest that  $\delta$ -catenin mutations affected  $\beta$ -catenin ubiquitination since reduced levels of slower migrating  $\beta$ -catenin forms (decreased ubiquitination) were observed in C2-Myc/ $\delta^{+/-}$  cells compared to C1-Myc/ $\delta^{+/+}$ . In addition, immunoblot targeting Myc (Fig. 4.5A, upper second panel) and cyclin D1 (Fig. 4.5A, bottom second panel) downstream of nuclear  $\beta$ -catenin in the canonical Wnt/ $\beta$ -catenin signaling pathway, showed enhanced levels in C2-Myc/ $\delta^{+/-}$  compared to C1-Myc/ $\delta^{+/+}$  (Fig. 4.5B). Collectively, these results further support that  $\delta$ -catenin mutations play a crucial role in PCa progression by altering the Wnt/ $\beta$ -catenin signaling pathway.

To determine whether the remarkably increased Myc expression level is due to the increased transcriptional activity of *Myc* transgene or its overexpression at the protein level, reverse transcription-PCR using human-*Myc* primer sets was conducted. 1.0 ug aliquot of RNA

isolated from C1-Myc/ $\delta^{+/+}$  and C2-Myc/ $\delta^{+/-}$  was reverse-transcribed to cDNA, followed by PCR-based tests. As depicted in Fig. 4.5C (lane 1; C1-Myc/ $\delta^{+/+}$  and lane 2; C2-Myc/ $\delta^{+/-}$ ), the PCR reactions fell in a proper molecular weight range (1300 bp), but the expression levels remained relatively unchanged. These results suggested that elevated Myc protein observed in C2-Myc/ $\delta^{+/-}$  could possibly be due to post-translational modifications (e.g., phosphorylation through Ras-MEK-ERK pathway) affecting *Myc* oncoprotein expression. Such modifications and their underlying functional significance will require future investigations. *GAPDH* served as housekeeping gene.

#### D6. C2-Myc/ $\delta^{+/-}$ promotes HIF-1 $\alpha$ and PKM<sub>2</sub> expression level

Thus far the experimental results showed that  $\delta$ -catenin mutations in C2-Myc/ $\delta^{+/-}$  cells affected  $\beta$ -catenin and its target effectors (Myc and cyclin D1). Next, the affect of  $\delta$ -catenin mutations on HIF-1 $\alpha$ , a key modulator in metabolic pathway, was examined. Cells were lysed and analyzed by Western blot analysis with antibodies to HIF-1 $\alpha$ , PKM<sub>2</sub>, and Glut-1 (Fig 4.6A). While Glut-1 level remained relatively the same, HIF-1 $\alpha$  and PKM<sub>2</sub> levels were significantly greater in C2-Myc/ $\delta^{+/-}$  than that of C1-Myc/ $\delta^{+/+}$  (Fig. 4.6B, \* p<0.05). These findings indicate that  $\delta$ -catenin mutations in the murine prostatic cell cultures activated HIF-1 $\alpha$  activity, implicating its role in metabolic reprogramming. Importantly, these results were consistent with the experimental findings shown in the transgenic mouse models (Chapter III).

## **E. Discussion**

The rationale for the current studies was that prostatic epithelial cell lines representing different genetic modifications, presumably having varying degrees of tumorigenicity, could be

isolated from the mouse model of PCa. Here we report the establishment and characterization of new and potential lines derived from two different tumors developed in the *Myc/δ*-catenin mutant mouse models.

Initially, we intended to generate three prostatic cell lines corresponding to three genotypes of *Myc/δ*-catenin mutant mouse models. However, through several attempts we found that the primary cells isolated from *Myc/δ<sup>-/-</sup>* mouse prostate did not respond to the culture condition we employed. It is possible that *Myc/δ<sup>-/-</sup>* mouse prostate cells failed to grow due to unfavorable culture medium. The future studies will be needed to determine what growth factors could enhance mouse prostatic epithelial growth. We also speculated that cells expressing homozygous deletion of *δ-catenin* gene could abolish their ability to attach to the culture dish; therefore coating culture plates with collagen, gelatin, or laminin might improve cell attachment to culture surface. Nonetheless, we succeeded in generating two new prostatic cell lines includes C1-*Myc/δ<sup>+/+</sup>*, derived from *Myc/δ<sup>+/+</sup>* mouse prostate and C2-*Myc/δ<sup>+/-</sup>*, established from *Myc/δ<sup>+/-</sup>* mouse prostate.

The detection of the epithelial cell markers such as PSA (prostatic specific antigen), E-cadherin, and  $\beta$ -catenin is conforming to the polygonal epithelial morphology of these cells in culture. In addition, the negative immunostaining for vimentin (stromal cell marker), with an exception of dividing cells, suggests epithelia in origin of the cells. We also demonstrated that E-cadherin staining was shown to be less intense in C2-*Myc/δ<sup>+/-</sup>* than in C1-*Myc/δ<sup>+/+</sup>* cells, but it was not surprising because E-cadherin is reduced or lost in invasive human PCa (Lu et al., 2005). It was interesting to note that  $\beta$ -catenin showed intense junctional staining in C1-*Myc/δ<sup>+/+</sup>* cells, whereas  $\beta$ -catenin immunoreactivity was either lost or redistributed to the cytoplasm and nuclei

in C2-Myc/ $\delta^{+/-}$ , further supporting that C2-Myc/ $\delta^{+/-}$  cell line is likely to be a more aggressive cancer cell phenotype.

An additional examination in protein expression reveals that  $\beta$ -catenin expression levels remained similar between C1-Myc/ $\delta^{+/+}$  and C2-Myc/ $\delta^{+/-}$  cells. However, C1-Myc/ $\delta^{+/+}$  showed more intense multiple bands of slower migrating forms (laddering effect) on SDS-gel previously described for  $\beta$ -catenin ubiquitination (Aberle et al., 1997) than that of C2-Myc/ $\delta^{+/-}$ . These findings suggest that full-length  $\delta$ -catenin is associated with  $\beta$ -catenin ubiquitination.

Furthermore, we demonstrated that  $\delta$ -catenin mutations in C2-Myc/ $\delta^{+/-}$  cells resulted in a statistically significant elevation in Myc (oncoprotein) and cyclin D1 (cell cycle regulation), downstream signal cascades for the Wnt/ $\beta$ -catenin pathway, when compared to C1-Myc/ $\delta^{+/+}$  cells containing full length  $\delta$ -catenin. Since we found a dramatic increase of Myc protein expression in C2-Myc/ $\delta^{+/-}$ , we further questioned whether the ectopic overexpression of human-Myc in these cells was altered at mRNA level. A reverse-transcription PCR analysis reveals that C1-Myc/ $\delta^{+/+}$  and C2-Myc/ $\delta^{+/-}$  cell lines showed similarly accumulated amounts of human-Myc mRNA, implying that  $\delta$ -catenin mutations in C2-Myc/ $\delta^{+/-}$  promote elevation of Myc in protein level. Although, we cannot rule out that the upregulations of Myc and cyclin D1 were a consequence from increased  $\beta$ -catenin nuclear localization, these finding revealed a pivotal relationship between  $\delta$ -catenin and  $\beta$ -catenin in promoting PCa progression. Further study is needed to confirm the mechanism of  $\delta$ -catenin-induced Myc and cyclin D1 upregulation in the cell lines.

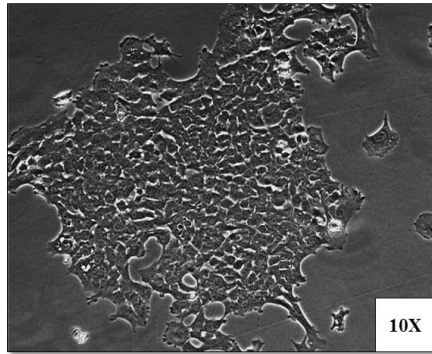
HIF-1 $\alpha$  is well-established as a key molecule upregulated under hypoxic conditions in solid tumors. However, several lines of evidence indicate that HIF-1 $\alpha$  can be activated independently of hypoxia for example through PI3K, mTOR, p53, or Wnt/ $\beta$ -catenin pathways (Podar and Anderson, 2010; Poon et al., 2009; Yeung et al., 2008). Upon HIF-1 $\alpha$  activation, it

alters several biological processes. In particular, HIF-1 $\alpha$  has been reported in facilitating cancer cell metabolic reprogramming, thereby allowing cancer cells to adapt, survive, and grow in a tumor microenvironment. There is emerging evidence to support that HIF-1 $\alpha$  enhances aerobic glycolysis, also known as the Warburg effect, by directly upregulating the expression of glycolytic proteins such as HK, LDH-A, Glut-1, and PKM<sub>2</sub>. Many of the proteins regulated by HIF-1 $\alpha$  are known to be regulated by Myc as well (Dang et al., 2009; Podar and Anderson, 2010). In this report, we demonstrated that C2-Myc/ $\delta^{+/-}$  exhibited induction of HIF-1 $\alpha$  and PKM<sub>2</sub>, but it did not induce Glut-1 level compared to C1-Myc/ $\delta^{+/+}$ . Therefore, our results are consistent with reports that the increased expression of Myc is closely related to elevated HIF-1 $\alpha$  in response to the tumor microenvironment. Collectively, these studies indicate that  $\delta$ -catenin mutations have important implications in PCa progression by promoting Myc and HIF-1 $\alpha$  activities, thereby promoting cancer cell adaptation and survival.

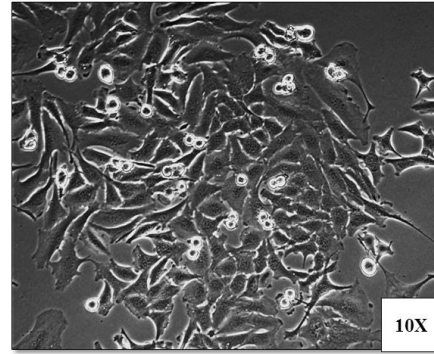
In summary, we have successfully established two innovative mouse prostate tumor cell lines. The establishment of these cell lines provides a culture system derived from the Myc/ $\delta$ -catenin compound transgenic mouse model to make possible molecular manipulation. These *in vitro* cultures in conjunction with their parent transgenic mouse models will provide an effective system to investigate for new innovative therapeutic approaches. Moreover, it is anticipated that the cell lines will also be useful to identify pathways that regulate and/or associate with  $\delta$ -catenin, leading to a better understanding of its functions in PCa progression.

**A.**

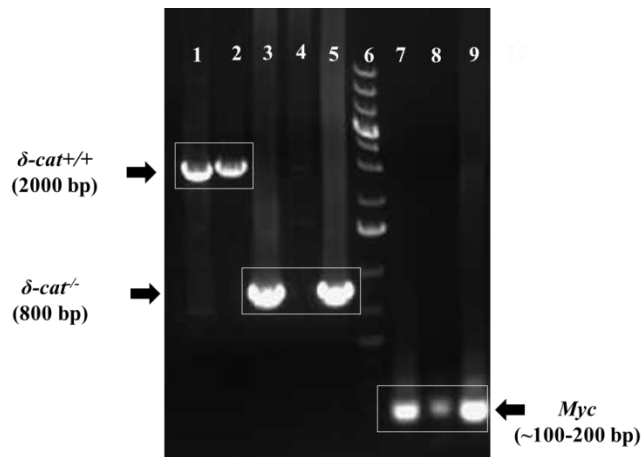
**C1-Myc/ $\delta^{+/+}$**



**C2-Myc/ $\delta^{+/-}$**

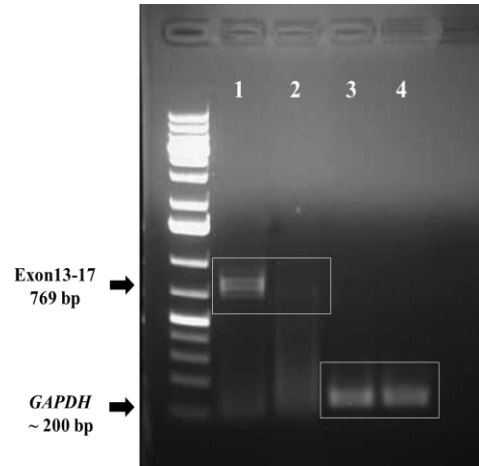


**B.**



Lanes 2, 4 and 8: C1-Myc/ $\delta^{+/+}$  cell line  
Lanes 1, 3, and 7: C2-Myc/ $\delta^{+/-}$  cell line  
Lanes 5 and 9: Myc/ $\delta^{+/-}$  tail tissue  
Lane 6: DNA ladder

**C.**



Lanes 1 and 3: C1-Myc/ $\delta^{+/+}$   
Lanes 2 and 4: C2-Myc/ $\delta^{+/-}$

**Figure 4.1 Characterization of the C1-Myc/ $\delta^{+/+}$  and C2-Myc/ $\delta^{+/-}$  cell lines.** (A). Comparison of the morphology of cells under the bright field in microscopy. While all cell lines appeared to exhibit polygonal-shaped cells that are indicative of epithelial cells, some cells in C2-Myc/ $\delta$ -cat $^{+/-}$  displayed elongated cell morphology (white arrows). (B). PCR genotyping of the cell lines using full-length  $\delta$ -catenin ( $\delta$ -cat $^{+/+}$ ), truncated  $\delta$ -catenin ( $\delta$ -cat $^{+/-}$ ), and Myc specific primers. Mouse tail genomic-DNA was used as a positive control (lanes 5 and 9). (C). Comparative reverse-transcription PCR analysis of mRNA level of  $\delta$ -catenin, exons 13-17. C1-Myc/ $\delta^{+/+}$  showed higher amounts of mRNA than C2-Myc/ $\delta^{+/-}$ , indicating that exon 13-17 of  $\delta$ -catenin in C2-Myc/ $\delta^{+/-}$  was disrupted.

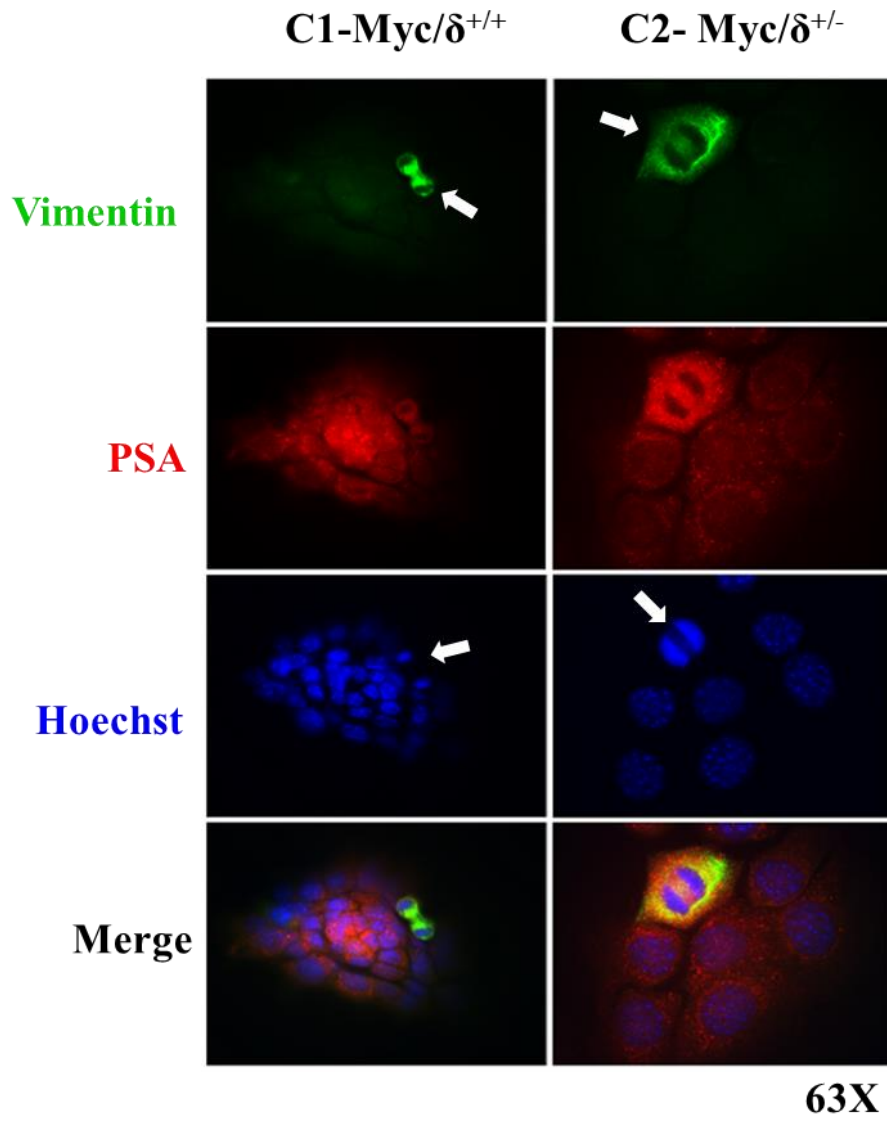
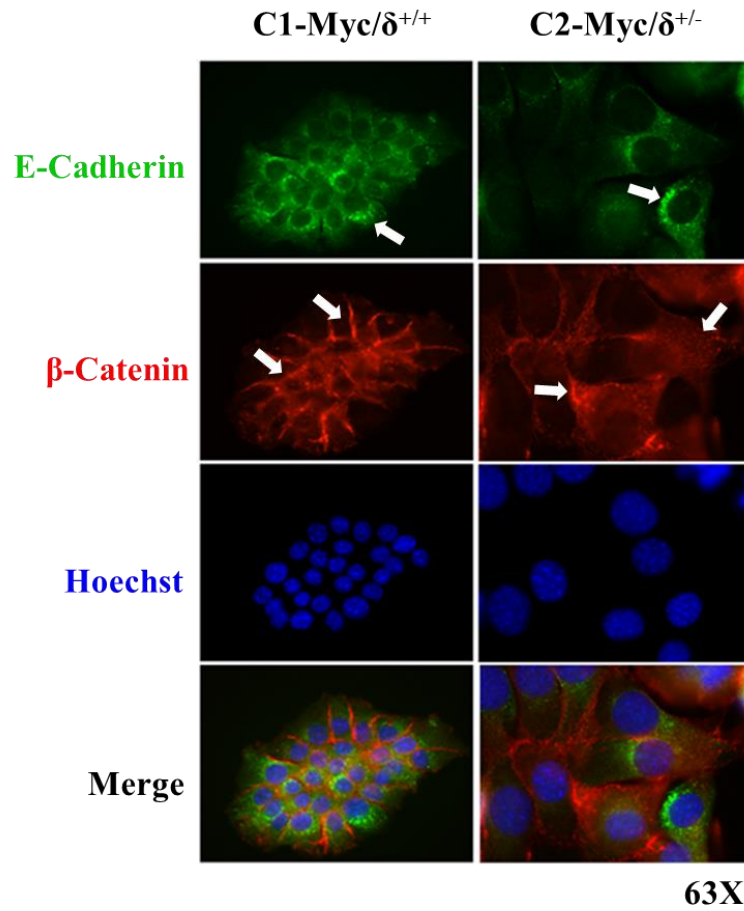


**Figure 4.2 C1-Myc/ $\delta^{+/+}$  and C2-Myc/ $\delta^{+/-}$  cell lines are epithelia in origin.** Vimentin and PSA immunofluorescent analysis of cells grown on cover slips. Results revealed that most cells were negative for vimentin staining (green signal, upper panel), except cells undergoing division (white arrows). In contrast, cells showed positive staining for PSA, indicating that these cells were derived from epithelia. Original magnification: 630x.

**A.**



**B.**

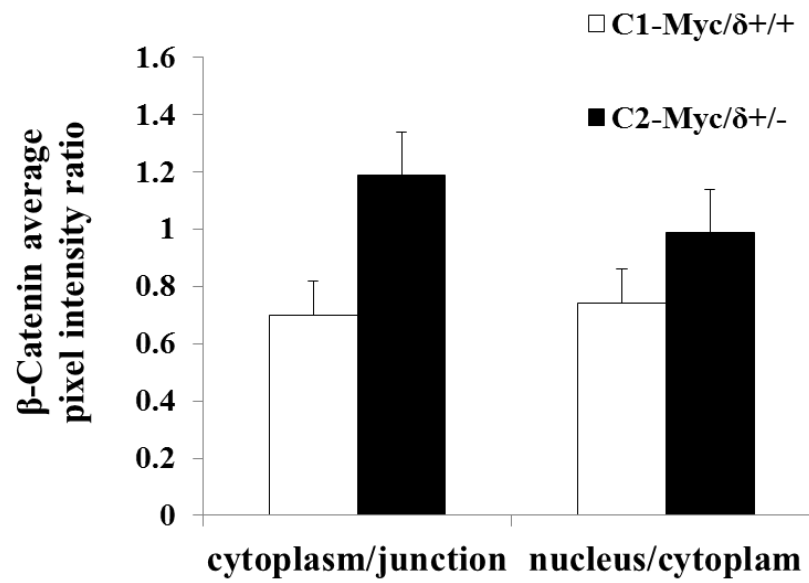
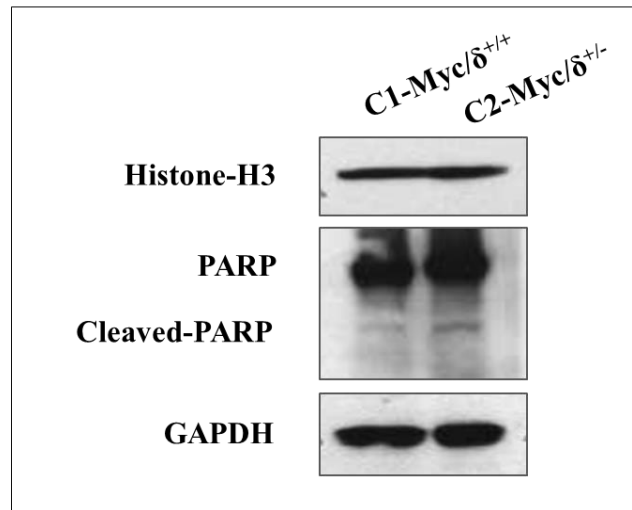


**Figure 4.3 C2-Myc/ $\delta^{+/-}$  reveals the reductions of E-cadherin and  $\beta$ -catenin immunoreactivities.** (A). After growing on the coverslips until reaching approximately 80% confluency, cells were fixed with 4% paraformaldehyde and stained with E-cadherin and  $\beta$ -catenin. White arrows indicate that the aggregation of E-cadherin in the cytoplasm accumulated near the nucleus, similarly in both cell lines (upper first panel). However, while  $\beta$ -catenin in C1-Myc/ $\delta^{+/+}$  showed strong junctional staining, it was disrupted and relocalized to the cytoplasm in C2-Myc/ $\delta^{+/-}$  (upper second panel). The cell nuclei were stained by Hoechst (bottom second panel). (B). Quantification of pixel intensity of  $\beta$ -catenin distribution in 3 cellular pools including nucleus, cytoplasm, cell-cell junction, were measured. The ratios of  $\beta$ -catenin pixel intensity in cytoplasm to junction and nucleus to cytoplasm were determined. Note that, although not significant, there was the induction of cytoplasmic and nuclear  $\beta$ -catenin in C2-Myc/ $\delta^{+/-}$  compared to that of C1-Myc/ $\delta^{+/+}$ . Values represent mean  $\pm$  S.E.M. n=25 cells/group.

**A.**



**B.**

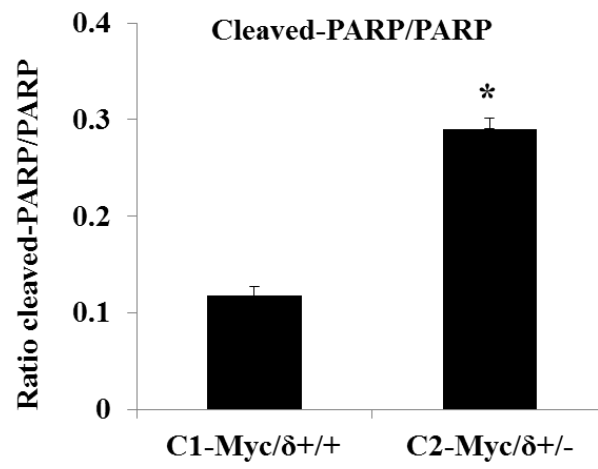
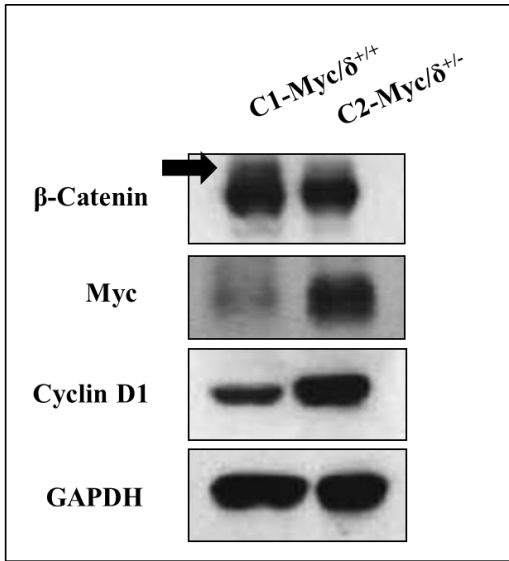
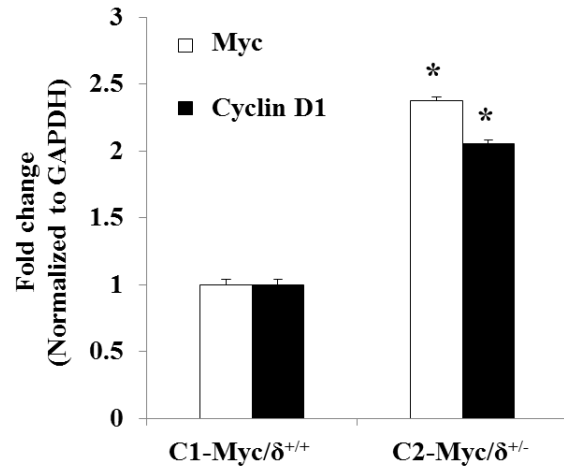


**Figure 4.4 C2-Myc/ $\delta^{+/-}$  cells reveal increased cell apoptosis.** C1-Myc/ $\delta^{+/+}$  and C2-Myc/ $\delta^{+/-}$  cells were lysed, homogenized and subjected to Western blot analysis. **(A).** Blots were probed with histone-H3, proliferative cell marker, and PARP, cell apoptosis marker, antibodies. The protein banding profiles of histone-H3 showed a moderate increase (not significant) in C2-Myc/ $\delta^{+/-}$  when compared to that of C1-Myc/ $\delta^{+/+}$ . GAPDH was used as a loading control. **(B).** Quantification of PARP detected by western blotting was performed using densitometry and ratio of cleaved-PARP to PARP was determined. Statistical analysis revealed the significant differences in the ratio of cleaved-PARP to PARP between C1-Myc/ $\delta^{+/+}$  and C2-Myc/ $\delta^{+/-}$  (\*  $p < 0.05$ ), suggesting the induction of apoptotic cells in C2-Myc/ $\delta^{+/-}$ . Results are representative of two independent experiments.

**A.**



**B.**



**C.**

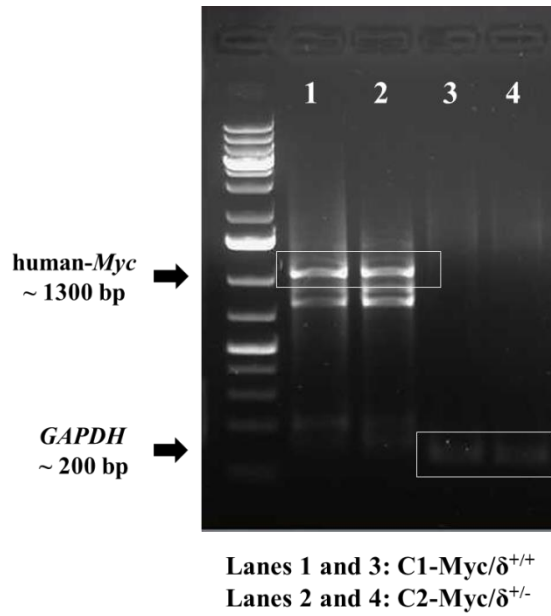
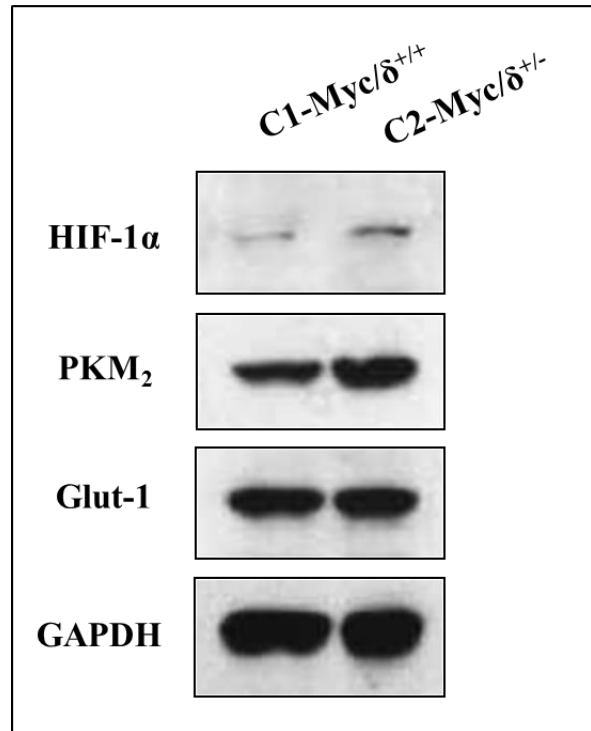


**Figure 4.5  $\delta$ -Catenin mutations in C2-Myc/ $\delta^{+/-}$  are correlated with upregulated Myc and cyclin D1. (A).** C1-Myc/ $\delta^{+/+}$  and C2-Myc/ $\delta^{+/-}$  cell lysates were analyzed by Western blotting with antibodies against  $\beta$ -catenin, Myc, and cyclin D1. The C1-Myc/ $\delta^{+/+}$  showed more intense slower migrating  $\beta$ -catenin patterns (arrow), indicative of  $\beta$ -catenin ubiquitination, than that of C2-Myc/ $\delta^{+/-}$ . Additionally, C2-Myc/ $\delta^{+/-}$  enhanced Myc and cyclin D1 protein expression levels. GAPDH was used as a loading control **(B).** Quantification of protein banding intensities. Bar graphs of representative Western blot in panel **(A)** show mean values of relative densitometry of Myc and cyclin D1. Results are representative of two independent experiments (\*  $p < 0.05$ ). **(C).** A comparison of human-Myc mRNA amounts between C1-Myc/ $\delta^{+/+}$  and C2-Myc/ $\delta^{+/-}$  was carried out by reverse-transcription PCR using human-Myc specific primers. No significant different amounts were found in ectopic overexpression human-Myc in mRNA level in these two cell lines. *GAPDH* served as a housekeeping gene.

**A.**



**B.**

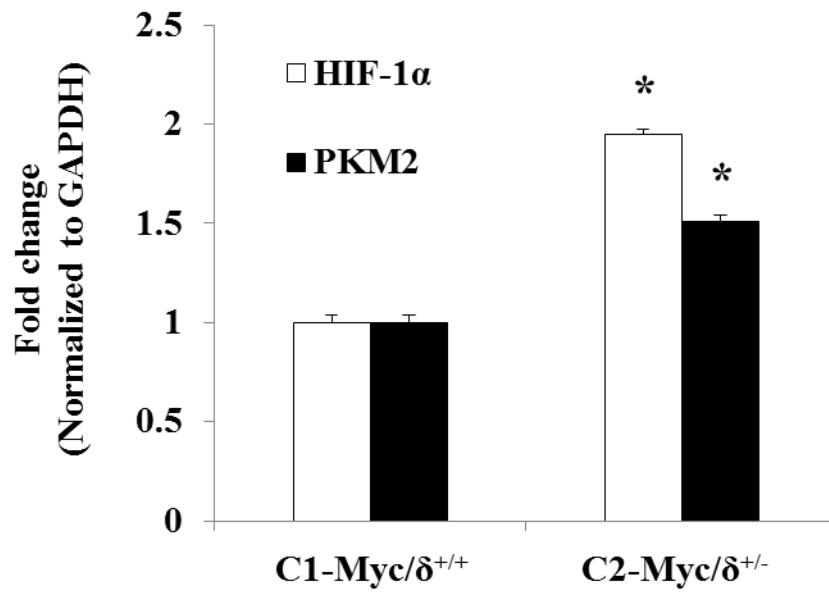


**Figure 4.6  $\delta$ -Catenin mutations in C2-Myc/ $\delta^{+/-}$  promote HIF-1 $\alpha$  and PKM<sub>2</sub> expressions.**

(A). Western blot analysis showed that  $\delta$ -catenin mutations in C2-Myc/ $\delta^{+/-}$  increased HIF-1 $\alpha$  and PKM<sub>2</sub>. GAPDH was used as a loading control (B). Quantification of protein banding intensities. Bar graphs of representative Western blot in panel (A) show mean values of relative densitometry of HIF-1 $\alpha$  and PKM<sub>2</sub>. Results are representative of two independent experiments. (\* p<0.05).

## CHAPTER V: CONCLUSIONS AND GENERAL DISCUSSION

Upon the discovery and identification of  $\delta$ -catenin full-length gene nearly 15 years ago through a variety of clinical and experimental studies,  $\delta$ -catenin has been reported to be a critical modulator in many cellular functions which lead to its validated and important roles in pathological conditions ranging from neurological dysfunctions and genetic disorders, to cancer progression (Lu et al., 2011; Lu et al., 2005; Medina et al., 2000). Initially, most studies focused exclusively on the involvement of  $\delta$ -catenin in neuronal function. Several lines of evidence demonstrate that appropriate levels of  $\delta$ -catenin are crucial for normal cognitive function and play a powerful role in dendritic morphogenesis (Bareiss et al., 2010; Israely et al., 2004; Kim et al., 2008a). Engagement of  $\delta$ -catenin in cancer progression has emerged through the detection of its overexpression in prostate cancer in 2002 (Burger et al., 2002). To date, however, the exact mechanisms and/or signaling pathways associated with regulating and maintaining  $\delta$ -catenin expression have not yet been elucidated. In the current study, we demonstrate the novel findings indicating that mutations of  $\delta$ -catenin are correlated with increased incidence of prostate cancer development *in vitro* and *in vivo*. This conclusion was drawn according to three key observations (i) ectopic expression of  $\delta$ -catenin is highly susceptible to mutagenesis under prostate cancer cell environment; (ii) prostate cancer cells expressing  $\delta$ -catenin mutations exhibit growth and survival advantage over control cells; and (iii)  $\delta$ -catenin mutations promote prostate tumor in Myc mice, leading to activation of  $\beta$ -catenin- and HIF-1 $\alpha$ -mediated oncogenic signals. Therefore, our goal in this study was not only to elucidate  $\delta$ -catenin involvement in prostate cancer progression but to identify other major oncogenic signaling pathways associated with  $\delta$ -catenin-mediated prostate cancer development.

The data presented in Chapter II demonstrated for the first time that  $\delta$ -catenin genetic mutations were inducible when it was overexpressed in human prostate cancer cells. Initially, we transfected human prostate tumor xenograft CWR22Rv-1 or PC-3 cells of prostate cancer bone metastasis with full-length  $\delta$ -catenin (named as Rv/ $\delta$ ) or GFP vector alone (named as Rv/C) in order to determine functional roles of  $\delta$ -catenin *in vitro*. Surprisingly, we found that the full-length  $\delta$ -catenin in stable cell lines showed faster migrating variant on SDS-PAGE. A closer examination by sequencing analysis revealed that truncated  $\delta$ -catenin variant exhibited frame-shifting mutations that lead to premature termination at exon 16, suggesting that  *$\delta$ -catenin* is susceptible to cancer environment-induced genetic alterations.

Extensive genomic analyses of prostate cancer have identified a number of important somatic alterations and chromosomal rearrangements associated with prostate cancer progression. In particular, the comparative genomic hybridization (CGH) analysis reveals that gains or losses of chromosome regions including gains at 8q and losses at 3p, 8p, 10q, 13q, and 17p are associated with prostate cancer. Several key modulator genes have been mapped within these chromosomal regions for example *NKX3.1* at 8p21, *PTEN* at 10q23, and *Myc* at 8q24, which have been found to be altered, but infrequently mutated in human prostate cancer (Abate-Shen and Shen, 2000; Bostwick et al., 1996; Elo and Visakorpi, 2001; Iwata et al., 2010; Koh et al., 2010). Our findings strongly raise a possibility of  *$\delta$ -catenin* located on 5p15.2 as one such somatically mutated gene in prostate cancer. However, the mechanisms driving  $\delta$ -catenin mutations in prostate cancer are not yet fully understood. One compelling explanation for this phenomenon is that ectopic  *$\delta$ -catenin* cDNA was inserted randomly into host chromosomes resulting in increasing genomic instability. Any acquisition of mutations that increases the ability of cells to proliferate and survive is selected. Thus, the mutated carboxyl-terminus of  $\delta$ -catenin

might favor cell survival so that it has been selected, replicated, and finally become predominant in prostate cancer populations.

Also of importance is our ability to understand the function of  $\delta$ -catenin by using *in vivo* model systems. We successfully generated two novel mouse models for prostate cancer; Myc/ $\delta$ -catenin double transgenic mice and Myc/ $\delta$ -catenin mutant mice as described in chapter III. Myc/ $\delta$ -catenin double transgenic mice showed mild phenotype. Conversely, mouse prostates from Myc/ $\delta$ -catenin mutant strain displayed a severe phenotype, in which Myc with  $\delta$ -catenin homozygous mutations (designated as Myc/ $\delta^{-/-}$ ) developed prostatic adenocarcinoma by 6 months. In addition, both our *in vivo* and *in vitro* studies demonstrate that  $\delta$ -catenin mutations provided a proliferative advantage over control cells. These data further support that  $\delta$ -catenin mutations play a critical role in prostate cancer progression.

The findings that  $\delta$ -catenin associates with the  $\beta$ -catenin-mediated oncogenic cascade have significant implications in prostate cancer progression. Many of the key components of the Wnt/ $\beta$ -catenin signaling pathway are overexpressed or mutated in several tumor types. For example, nearly all colon tumors arise from an initiating mutation in either  $\beta$ -catenin (15%) or APC (85%) proteins (Polakis, 2000; Harada et al., 1999). In addition, mutations in  $\beta$ -catenin have been found in many other tumors and are particularly common in ovarian cancer (Polakis, 2000; Polakis, 2007). These mutations make  $\beta$ -catenin resistant to degradation and initiate its translocation to the nucleus where it regulates transcription and promotes tumorigenesis (Polakis, 2000). It would be of great interest to determine if mutations in  $\delta$ -catenin contribute to its upregulation in cancer in a similar way to that of  $\beta$ -catenin. Collectively, the work presented in this dissertation supports a role for  $\delta$ -catenin in promoting the  $\beta$ -catenin signaling pathway. It is demonstrated that cells expressing truncated  $\delta$ -catenin variant (Rv/M1) increased the

translocation of  $\beta$ -catenin into the nucleus where it acts as a transcription factor and triggers its target gene expression such as Myc and cyclin D1. Additionally, increased  $\beta$ -catenin is correlated with the increased expression of Myc in Myc/ $\delta^{-/-}$  mice, suggesting that  $\delta$ -catenin mutations are closely related to  $\beta$ -catenin signaling. Although our study confirmed the involvement of the  $\delta$ -catenin and  $\beta$ -catenin signaling cascade in the prostate cancer models, we still lack a clear understanding of how  $\delta$ -catenin mutations facilitate  $\beta$ -catenin nuclear distribution. One possible explanation is that in late/advanced stage of prostate cancer, E-cadherin is reduced or lost and  $\delta$ -catenin and  $\beta$ -catenin are disassociated from their binding domains at E-cadherin, resulting in their accumulation in cytoplasm. There is evidence supporting that  $\delta$ -catenin and  $\beta$ -catenin are negatively regulated by the same mechanism. It was shown that GSK-3 $\beta$  phosphorylated  $\delta$ -catenin and targeted it for ubiquitin proteasome mediated degradation (Aberle et al., 1997; Chesire and Isaacs, 2003; Jiang et al., 2007; Oh et al., 2009). Hence, once  $\delta$ -catenin and  $\beta$ -catenin aggregate in cytoplasm,  $\delta$ -catenin, as a newly identified GSK-3 $\beta$  substrate, might compete with  $\beta$ -catenin to bind to GSK-3 $\beta$ . The excessive and stabilized  $\beta$ -catenin in the cytoplasm then can translocate to the nucleus and inappropriately activate the transcription of Myc and cyclin D1, thereby promoting prostate cancer development.

An important aspect of cancer survival and growth involves its adaptation to microenvironmental changes. The rapidly dividing cancer cells can cause an inability of the local vasculature to supply enough oxygen and nutrients to the tumor, resulting in hypoxic conditions. HIF-1 $\alpha$  is a key molecule that mediates cellular response to hypoxia and can activate a set of genes involved in angiogenesis, glucose uptake, and glycolysis. Clinically, HIF-1 $\alpha$  has been shown to be a marker of highly aggressive disease and has been associated with poor prognosis and treatment failure in a number of cancers (Saramaki et al., 2001). Throughout these studies

$\delta$ -catenin mutations, rather than full-length  $\delta$ -catenin, elevated HIF-1 $\alpha$  expression. Importantly, we demonstrate that HIF-1 $\alpha$  expression in the nucleus was significantly increased in  $\delta$ -catenin mutant cells under glucose-deprived condition. Additionally, the upregulated HIF-1 $\alpha$  was accompanied by enhanced Glut-1 expression observed in *Myc/ $\delta^{-/-}$*  mice. Therefore, establishment of  $\delta$ -catenin mutation-induced HIF-1 $\alpha$  expression within this report highlights an additional novel relationship between  $\delta$ -catenin and glycolytic pathway. There are number of evidence to support that HIF-1 $\alpha$  can be activated under normoxic conditions by PI3K/AKT oncogenic signaling pathway (Poon et al., 2009; Powis and Kirkpatrick, 2004). It would be of great interest to determine whether  $\delta$ -catenin-induced HIF-1 $\alpha$  expression is associated with the PI3K/AKT signaling pathway.

To develop a better understanding of the progression of mPIN to adenocarcinoma, we have established and characterized two mouse prostate cell lines, C1-*Myc/ $\delta^{+/+}$*  and C2-*Myc/ $\delta^{+/-}$* . These cell lines were derived from the prostates of 6 month-old *Myc/ $\delta$ -catenin* mutant mice, which appear to represent both early- (C1-*Myc/ $\delta^{+/+}$* ) and late- (C2-*Myc/ $\delta^{+/-}$* ) stage disease. Immunofluorescent analysis demonstrates C1-*Myc/ $\delta^{+/+}$*  and C2-*Myc/ $\delta^{+/-}$*  express PSA, prostate specific antigen marker, but not vimentin, a stromal cell marker. Importantly, protein expression profiles in these cell lines are consistent with that of mouse models, further validating their quality for future experiments. In addition to demonstrating the epithelial status, future experiments to determine their growth characteristic and invasive phenotype are needed. Due to different genetic contents in the cell lines, we anticipated that these cell lines would likely be important tools for exploring the mechanisms in prostate cancer progression and manifestation of the diverse histopathological phenotypes.

In summary, we have now successfully established a complete model system for prostate cancer research involving *Myc* oncogene and  $\delta$ -catenin. By utilizing these models, we proposed that  $\delta$ -catenin exhibits tumor suppressive function in normal cells. In particular, upon carboxyl-terminus deletions or mutations, the remaining truncated  $\delta$ -catenin displays oncogenic properties. This study highlights the functional role of  $\delta$ -catenin in prostate cancer and raises a possibility of  $\delta$ -catenin-targeted therapy.

## REFERENCES

- Abate-Shen, C., and Shen, M.M. (2000). Molecular genetics of prostate cancer. *Genes Dev*, *14*, 2410-2434.
- Abate-Shen, C., and Shen, M.M. (2002). Mouse models of prostate carcinogenesis. *Trends Genet*, *18*, S1-5.
- Aberle, H., Bauer, A., Stappert, J., Kispert, A., and Kemler, R. (1997). Beta-catenin is a target for the ubiquitin-proteasome pathway. *EMBO J*, *16*, 3797-3804.
- Abu-Elneel, K., Ochiishi, T., Medina, M., Remedi, M., Gastaldi, L., Caceres, A., and Kosik, K.S. (2008). A delta-catenin signaling pathway leading to dendritic protrusions. *J Biol Chem*, *283*, 32781-32791.
- Anastasiadis, P.Z. (2007). p120-ctn: a nexus for contextual signaling via Rho GTPases. *J Biol Chem*, *1773*, 34-46.
- Anastasiadis, P.Z., and Reynolds, A.B. (2000). The p120 catenin family: complex roles in adhesion, signaling and cancer. *J Cell Sci*, *113*, 1319-1334.
- Bareiss, S., Kim, K., and Lu, Q. (2010). Delta-catenin/NPRAP: A new member of the glycogen synthase kinase-3beta signaling complex that promotes beta-catenin turnover in neurons. *J Neurosci Res*, *88*, 2350-2363.
- Baum, C., von Kalle, C., Staal, F.J.T., Li, Z.X., Fehse, B., Schmidt, M., Weerkamp, F., Karlsson, S., Wagemaker, G., and Williams, D.A. (2004). Chance or necessity? Insertional mutagenesis in gene therapy and its consequences. *Mol Ther*, *9*, 5-13.
- Bensinger, S.J., and Christofk, H.R. (2012). New aspects of the Warburg effect in cancer cell biology. *Semin Cell Devel Biol*, *23*, 352-361.
- Bonkhoff, H., Stein, U., and Remberger, K. (1994). The proliferative function of basal cells in the normal and hyperplastic human prostate. *Prostate*, *24*, 114-118.
- Bostwick, D.G., Pacelli, A., and Lopez-Beltran, A. (1996). Molecular biology of prostatic intraepithelial neoplasia. *Prostate*, *29*, 117-134.
- Burger, M.J., Tebay, M.A., Keith, P.A., Samaratunga, H.M., Clements, J., Lavin, M.F., and Gardiner, R.A. (2002). Expression analysis of delta-catenin and prostate-specific membrane antigen: their potential as diagnostic markers for prostate cancer. *Int J Cancer*, *100*, 228-237.

- Bussemakers, M.J., Van Bokhoven, A., Tomita, K., Jansen, C.F., and Schalken, J.A. (2000). Complex cadherin expression in human prostate cancer cells. *Int J Cancer*, 85, 446-450.
- Cairns, R.A., Harris, I.S., and Mak, T.W. (2011). Regulation of cancer cell metabolism. *Nat Rev Cancer*, 11, 85-95.
- Cancer Facts & Figures. American Cancer Society. (2013). <http://www.cancer.org/acs/groups/content/@epidemiologysurveillance/documents/document/acspc-036845.pdf>.
- Carlsson, S., Vickers, A.J., Roobol, M., Eastham, J., Scardino, P., Lilja, H., and Hugosson, J. (2012). Prostate cancer screening: facts, statistics, and interpretation in response to the US Preventive Services Task Force Review. *J Clin Oncol*, 30, 2581-2584.
- Cheshire, D.R., and Isaacs, W.B. (2003). Beta-catenin signaling in prostate cancer: an early perspective. *Endocr Relat Cancer*, 10, 537-560.
- Dai, S.D., Wang, Y., Zhang, J.Y., Zhang, D., Zhang, P.X., Jiang, G.Y., Han, Y., Zhang, S., Cui, Q.Z., and Wang, E.H. (2011). Upregulation of delta-catenin is associated with poor prognosis and enhances transcriptional activity through Kaiso in non-small-cell lung cancer. *Cancer Sci*, 102, 95-103.
- Dang, C.V., Kim, J.W., Gao, P., and Yuste, J. (2008). The interplay between MYC and HIF in cancer. *Nat Rev Cancer*, 8, 51-56.
- Dang, C.V., Le, A., and Gao, P. (2009). MYC-induced cancer cell energy metabolism and therapeutic opportunities. *Clin Cancer Res*, 15, 6479-6483.
- Das, S., and Zain, J.M. (2011). Prostate cancer: some interesting facts. *Int J Clin Pract*, 65, 514-515.
- Davis, M.A., Ireton, R.C., and Reynolds, A.B. (2003). A core function for p120-catenin in cadherin turnover. *J Cell Biol*, 163, 525-534.
- DeBusk, L.M., Boelte, K., Min, Y.F., and Lin, P.C. (2010). Heterozygous deficiency of delta-catenin impairs pathological angiogenesis. *J Exp Med*, 207, 669-669.
- Deguchi, M., Iizuka, T., Hata, Y., Nishimura, W., Hirao, K., Yao, I., Kawabe, H., and Takai, Y. (2000). PAPIN. A novel multiple PSD-95/Dlg-A/ZO-1 protein interacting with neural plakophilin-related armadillo repeat protein/delta-catenin and p0071. *J Biol Chem*, 275, 29875-29880.
- Deng, W., Tsao, S.W., Lucas, J.N., Leung, C.S., and Cheung, A.L. (2003). A new method for improving metaphase chromosome spreading. *Cytometry Part A*, 51, 46-51.
- Ding, L., Getz, G., Wheeler, D.A., Mardis, E.R., McLellan, M.D., Cibulskis, K., Sougnez, C., Greulich, H., Muzny, D.M., Morgan, M.B., Fulton, L., Fulton, R.S., Zhang, Q.Y., Wendl,

- M.C., Lawrence, M.S., Larson, D.E., Chen, K., Dooling, D.J., Sabo, A., Hawes, A.C., Shen, H., Jhangiani, S.N., Lewis, L.R., Hall, O., Zhu, Y.M., Mathew, T., Ren, Y.R., Yao, J.Q., Scherer, S.E., Clerc, K., Metcalf, G.A., Ng, B., Milosavljevic, A., Gonzalez-Garay, M.L., Osborne, J.R., Meyer, R., Shi, X.Q., Tang, Y.Z., Koboldt, D.C., Lin, L., Abbott, R., Miner, T.L., Pohl, C., Fewell, G., Haipek, C., Schmidt, H., Dunford-Shore, B.H., Kraja, A., Crosby, S.D., Sawyer, C.S., Vickery, T., Sander, S., Robinson, J., Winckler, W., Baldwin, J., Chirieac, L.R., Dutt, A., Fennell, T., Hanna, M., Johnson, B.E., Onofrio, R.C., Thomas, R.K., Tonon, G., Weir, B.A., Zhao, X.J., Ziaugra, L., Zody, M.C., Giordano, T., Orringer, M.B., Roth, J.A., Spitz, M.R., Wistuba, I.I., Ozenberger, B., Good, P.J., Chang, A.C., Beer, D.G., Watson, M.A., Ladanyi, M., Broderick, S., Yoshizawa, A., Travis, W.D., Pao, W., Province, M.A., Weinstock, G.M., Varmus, H.E., Gabriel, S.B., Lander, E.S., Gibbs, R.A., Meyerson, M., and Wilson, R.K. (2008). Somatic mutations affect key pathways in lung adenocarcinoma. *Nature*, *455*, 1069-1075.
- Duparc, R.H., Boutemmine, D., Champagne, M.P., Tetreault, N., and Bernier, G. (2006). Pax6 is required for delta-catenin/neurojugin expression during retinal, cerebellar and cortical development in mice. *Dev Biol*, *300*, 647-655.
- Ellwood-Yen, K., Graeber, T.G., Wongvipat, J., Iruela-Arispe, M.L., Zhang, J.F., Matusik, R., Thomas, G.V., and Sawyers, C.L. (2003). Myc-driven murine prostate cancer shares molecular features with human prostate tumors. *Cancer Cell*, *4*, 223-238.
- Elo, J.P., and Visakorpi, T. (2001). Molecular genetics of prostate cancer. *Ann Med*, *33*, 130-141.
- Foster, B.A., Gingrich, J.R., Kwon, E.D., Madias, C., and Greenberg, N.M. (1997). Characterization of prostatic epithelial cell lines derived from transgenic adenocarcinoma of the mouse prostate (TRAMP) model. *Cancer Res*, *57*, 3325-3330.
- Fujita, T., Okada, T., Hayashi, S., Jahangeer, S., Miwa, N., and Nakamura, S. (2004). Delta-catenin/NPRAP (neural plakophilin-related armadillo repeat protein) interacts with and activates sphingosine kinase 1. *Biochem J*, *382*, 717-723.
- Gopalkrishnan, R.V., Kang, D.C., and Fisher, P.B. (2001). Molecular markers and determinants of prostate cancer metastasis. *J Cell Physiol*, *189*, 245-256.
- Greenberg, N.M., DeMayo, F., Finegold, M.J., Medina, D., Tilley, W.D., Aspinall, J.O., Cunha, G.R., Donjacour, A.A., Matusik, R.J., and Rosen, J.M. (1995). Prostate cancer in a transgenic mouse. *Proc Natl Acad Sci USA*, *92*, 3439-3443.
- Gumbiner, B.M. (2005). Regulation of cadherin-mediated adhesion in morphogenesis. *Nat Rev Mol Cell Biol*, *6*, 622-634.
- Gurel, B., Iwata, T., Koh, C.M., Jenkins, R.B., Lan, F., Van Dang, C., Hicks, J.L., Morgan, J., Cornish, T.C., Sutcliffe, S., Isaacs, W.B., Luo, J., and De Marzo, A.M. (2008). Nuclear MYC protein overexpression is an early alteration in human prostate carcinogenesis. *Mod Pathol*, *21*, 1156-1167.

- Hanahan, D., and Weinberg, R.A. (2011). Hallmarks of cancer: the next generation. *Cell*, *144*, 646-674.
- Harrison, O.J., Jin, X., Hong, S., Bahna, F., Ahlsen, G., Brasch, J., Wu, Y., Vendome, J., Felsovalyi, K., Hampton, C.M., Troyanovsky, R.B., Ben-Shaul, A., Frank, J., Troyanovsky, S.M., Shapiro, L., and Honig, B. (2011). The extracellular architecture of adherens junctions revealed by crystal structures of type I cadherins. *Structure*, *19*, 244-256.
- Hartsock, A., and Nelson, W.J. (2008). Adherens and tight junctions: structure, function and connections to the actin cytoskeleton. *Biochim Biophys Acta*, *1778*, 660-669.
- Harvard Medical School 2013 annual report on prostate diseases. (2013). <http://www.cpcce-polyu.edu.hk/lib/eresource/harvard/ProstateAnnual13.pdf>.
- Hatzfeld, M. (2005). The p120 family of cell adhesion molecules. *Eur J Cell Biol*, *84*, 205-214.
- He, Y., Han, J.R., Chang, O., Oh, M., James, S.E., Lu, Q., Seo, Y.W., Kim, H., and Kim, K. (2013a). 14-3-3varepsilon/zeta affects the stability of delta-catenin and regulates delta-catenin-induced dendrogenesis. *FEBS Open Bio*, *3*, 16-21.
- He, Y., Kim, H., Ryu, T., Kang, Y., Kim, J.A., Kim, B.H., Lee, J.H., Kang, K., Lu, Q., and Kim, K. (2013b). Delta-Catenin overexpression promotes angiogenic potential of CWR22Rv-1 prostate cancer cells via HIF-1alpha and VEGF. *FEBS Lett*, *587*, 193-199.
- Hirsch, D., Kemmerling, R., Davis, S., Camps, J., Meltzer, P.S., Ried, T., and Gaiser, T. (2013). Chromothripsis and focal copy number alterations determine poor outcome in malignant melanoma. *Cancer Res*, *73*, 1454-1460.
- Ho, C., Zhou, J., Medina, M., Goto, T., Jacobson, M., Bhide, P.G., and Kosik, K.S. (2000). Delta-catenin is a nervous system-specific adherens junction protein which undergoes dynamic relocalization during development. *J Comp Neurol*, *420*, 261-276.
- Huang, X., Hu, J., Hu, X., Zhang, C., Zhang, L., Wang, S., Lu, W., and Bao, Z. (2007). Cytogenetic characterization of the bay scallop, *Argopecten irradians irradians*, by multiple staining techniques and fluorescence in situ hybridization. *Genes Genet Syst*, *82*, 257-263.
- Huber, A.H., Nelson, W.J., Weis, and W.I. (1997). Three-dimensional structure of the armadillo repeat region of beta-catenin. *Cell*, *90*, 871-882.
- Ide, N., Hata, Y., Deguchi, M., Hirao, K., Yao, I., and Takai, Y. (1999). Interaction of S-SCAM with neural plakophilin-related Armadillo-repeat protein/delta-catenin. *Biochem Biophys Res Commun*, *256*, 456-461.

- Inoki, K., Ouyang, H., Zhu, T., Lindvall, C., Wang, Y., Zhang, X., Yang, Q., Bennett, C., Harada, Y., Stankunas, K., Wang, C.Y., He, X., MacDougald, O.A., You, M., Williams, B.O., and Guan, K.L. (2006). TSC2 integrates Wnt and energy signals via a coordinated phosphorylation by AMPK and GSK3 to regulate cell growth. *Cell*, *126*, 955-968.
- Israely, I., Costa, R.M., Xie, C.W., Silva, A.J., Kosik, K.S., and Liu, X. (2004). Deletion of the neuron-specific protein delta-catenin leads to severe cognitive and synaptic dysfunction. *Curr Biol*, *14*, 1657-1663.
- Ittmann, M., Huang, J., Radaelli, E., Martin, P., Signoretti, S., Sullivan, R., Simons, B.W., Ward, J.M., Robinson, B.D., Chu, G.C., Loda, M., Thomas, G., Borowsky, A., and Cardiff, R.D. (2013). Animal models of human prostate cancer: the consensus report of the New York meeting of the mouse models of human cancers consortium prostate pathology committee. *Cancer Res*, *73*, 2718-2736.
- Iwata, T., Schultz, D., Hicks, J., Hubbard, G.K., Mutton, L.N., Lotan, T.L., Bethel, C., Lotz, M.T., Yegnasubramanian, S., Nelson, W.G., Dang, C.V., Xu, M., Anele, U., Koh, C.M., Bieberich, C.J., and De Marzo, A.M. (2010). MYC overexpression induces prostatic intraepithelial neoplasia and loss of Nkx3.1 in mouse luminal epithelial cells. *PLoS ONE* *5*, e9427.
- Izawa, I., Nishizawa, M., Ohtakara, K., and Inagaki, M. (2002). Densin-180 interacts with delta-catenin/neural plakophilin-related armadillo repeat protein at synapses. *J Biol Chem*, *277*, 5345-5350.
- Jaulin-Bastard, F., Arsanto, J.P., Le Bivic, A., Navarro, C., Vely, F., Saito, H., Marchetto, S., Hatzfeld, M., Santoni, M.J., Birnbaum, D., and Borg, J.P. (2002). Interaction between Erbin and a catenin-related protein in epithelial cells. *J Biol Chem*, *277*, 2869-2875.
- Jeanes, A., Gottardi, C.J., and Yap, A.S. (2008). Cadherins and cancer: how does cadherin dysfunction promote tumor progression? *Oncogene*, *27*, 6920-6929.
- Jiang, Y.G., Luo, Y., He, D.L., Li, X., Zhang, L.L., Peng, T., Li, M.C., and Lin, Y.H. (2007). Role of Wnt/beta-catenin signaling pathway in epithelial-mesenchymal transition of human prostate cancer induced by hypoxia-inducible factor-1alpha. *Int J Urol*, *14*, 1034-1039.
- Jones, S.B., Lanford, G.W., Chen, Y.H., Morabito, M., Kim, K., and Lu, Q. (2002). Glutamate-induced delta-catenin redistribution and dissociation from postsynaptic receptor complexes. *Neuroscience*, *115*, 1009-1021.
- Jun, G., Moncaster, J.A., Koutras, C., Seshadri, S., Buros, J., McKee, A.C., Levesque, G., Wolf, P.A., St George-Hyslop, P., Goldstein, L.E., and Farrer, L.A. (2012). Delta-catenin is genetically and biologically associated with cortical cataract and future Alzheimer-related structural and functional brain changes. *PLoS ONE* *7*, e43728.

- Kaidi, A., Williams, A.C., and Paraskeva, C. (2007). Interaction between beta-catenin and HIF-1 promotes cellular adaptation to hypoxia. *Nat Cell Biol*, 9, 210-217.
- Kaseb, A.O., Chinnakannu, K., Chen, D., Sivanandam, A., Tejwani, S., Menon, M., Dou, Q.P., and Reddy, G.P. (2007). Androgen receptor and E2F-1 targeted thymoquinone therapy for hormone-refractory prostate cancer. *Cancer Res*, 67, 7782-7788.
- Kim, H., Han, J.R., Park, J., Oh, M., James, S.E., Chang, S., Lu, Q., Lee, K.Y., Ki, H., Song, W.J., and Kim, K. (2008a). Delta-catenin-induced dendritic morphogenesis. An essential role of p190RhoGEF interaction through Akt1-mediated phosphorylation. *J Biol Chem*, 283, 977-987.
- Kim, H., He, Y., Yang, I., Zeng, Y., Kim, Y., Seo, Y.W., Murnane, M.J., Jung, C., Lee, J.H., Min, J.J., Kwon, D.D., Kim, K.K., Lu, Q., and Kim, K. (2012). Delta-catenin promotes E-cadherin processing and activates beta-catenin-mediated signaling: implications on human prostate cancer progression. *Biochim Biophys Acta*, 1822, 509-521.
- Kim, H., Oh, M., Lu, Q., and Kim, K. (2008b). E-Cadherin negatively modulates delta-catenin-induced morphological changes and RhoA activity reduction by competing with p190RhoGEF for delta-catenin. *Biochem Biophys Res Commun*, 377, 636-641.
- Kim, J.S., Bareiss, S., Kim, K.K., Tatum, R., Han, J.R., Jin, Y.H., Kim, H., Lu, Q., and Kim, K. (2006). Presenilin-1 inhibits delta-catenin-induced cellular branching and promotes delta-catenin processing and turnover. *Biochem Biophys Res Commun*, 351, 903-908.
- Kim, K., Oh, M., Ki, H., Wang, T., Bareiss, S., Fini, M.E., Li, D., and Lu, Q. (2008c). Identification of E2F1 as a positive transcriptional regulator for delta-catenin. *Biochem Biophys Res Commun*, 369, 414-420.
- Kim, K., Sirota, A., Chen, Y.H., Jones, S.B., Dudek, R., Lanford, G.W., Thakore, C., and Lu, Q. (2002). Dendrite-like process formation and cytoskeletal remodeling regulated by delta-catenin expression. *Exp Cell Res*, 275, 171-184.
- Kim, S.W., Park, J.I., Spring, C.M., Sater, A.K., Ji, H., Otchere, A.A., Daniel, J.M., and McCrea, P.D. (2004). Non-canonical Wnt signals are modulated by the Kaiso transcriptional repressor and p120-catenin. *Nat Cell Biol*, 6, 1212-1220.
- Koh, C.M., Bieberich, C.J., Dang, C.V., Nelson, W.G., Yegnasubramanian, S., and De Marzo, A.M. (2010). MYC and Prostate Cancer. *Genes Cancer*, 1, 617-628.
- Koppenol, W.H., Bounds, P.L., and Dang, C.V. (2011). Otto Warburg's contributions to current concepts of cancer metabolism. *Nat Rev Cancer*, 11, 325-337.
- Kosik, K.S., Donahue, C.P., Israely, I., Liu, X., and Ochiishi, T. (2005). Delta-catenin at the synaptic-adherens junction. *Trends Cell Biol*, 15, 172-178.

- Kouchi, Z., Barthet, G., Serban, G., Georgakopoulos, A., Shioi, J., and Robakis, N.K. (2009). p120-Catenin recruits cadherins to gamma-secretase and inhibits production of Abeta peptide. *J Biol Chem*, 284, 1954-1961.
- Lamberti, C., Lin, K.M., Yamamoto, Y., Verma, U., Verma, I.M., Byers, S., and Gaynor, R.B. (2001). Regulation of beta-catenin function by the IkappaB kinases. *J Biol Chem*, 276, 42276-42286.
- Laura, R.P., Witt, A.S., Held, H.A., Gerstner, R., Deshayes, K., Koehler, M.F., Kosik, K.S., Sidhu, S.S., and Lasky, L.A. (2002). The Erbin PDZ domain binds with high affinity and specificity to the carboxyl termini of delta-catenin and ARVCF. *J Biol Chem*, 277, 12906-12914.
- Li, Y.J., Goh, L., Khor, C.C., Fan, Q., Yu, M., Han, S., Sim, X., Ong, R.T., Wong, T.Y., Vithana, E.N., Yap, E., Nakanishi, H., Matsuda, F., Ohno-Matsui, K., Yoshimura, N., Seielstad, M., Tai, E.S., Young, T.L., and Saw, S.M. (2011). Genome-wide association studies reveal genetic variants in CTNND2 for high myopia in Singapore Chinese. *Ophthalmology*, 118, 368-375.
- Liao, C.P., Liang, M., Cohen, M.B., Flesken-Nikitin, A., Jeong, J.H., Nikitin, A.Y., and Roy-Burman, P. (2010). Mouse prostate cancer cell lines established from primary and postcastration recurrent tumors. *Horm Cancer*, 1, 44-54.
- Logan, C.Y., and Nusse, R. (2004). The Wnt signaling pathway in development and disease. *Ann Rev Cell Dev Biol*, 20, 781-810.
- Lu, B., Jiang, D., Wang, P., Gao, Y., Sun, W., Xiao, X., Li, S., Jia, X., Guo, X., and Zhang, Q. (2011). Replication study supports CTNND2 as a susceptibility gene for high myopia. *Invest Ophthalmol Vis Sci*, 52, 8258-8261.
- Lu, J.P., Zhang, J., Kim, K., Case, T.C., Matusik, R.J., Chen, Y.H., Wolfe, M., Nopparat, J., and Lu, Q. (2010). Human homolog of Drosophila Hairy and enhancer of split 1, Hes1, negatively regulates delta-catenin (CTNND2) expression in cooperation with E2F1 in prostate cancer. *Mol Cancer*, 9, 304.
- Lu, Q. (2010). Delta-catenin dysregulation in cancer: interactions with E-cadherin and beyond. *J Pathol*, 22, 119-123.
- Lu, Q., Dobbs, L.J., Gregory, C.W., Lanford, G.W., Revelo, M.P., Shappell, S., and Chen, Y.H. (2005). Increased expression of delta-catenin/neural plakophilin-related armadillo protein is associated with the down-regulation and redistribution of E-cadherin and p120ctn in human prostate cancer. *Hum Pathol*, 36, 1037-1048.
- Lu, Q., Mukhopadhyay, N.K., Griffin, J.D., Paredes, M., Medina, M., and Kosik, K.S. (2002). Brain armadillo protein delta-catenin interacts with Abl tyrosine kinase and modulates cellular morphogenesis in response to growth factors. *J Neurosci Res*, 67, 618-624.

- Lu, Q., Paredes, M., Medina, M., Zhou, J., Cavallo, R., Peifer, M., Orecchio, L., and Kosik, K.S. (1999). Delta-catenin, an adhesive junction-associated protein which promotes cell scattering. *J Cell Biol*, *144*, 519-532.
- Lu, Q., Zhang, J., Allison, R., Gay, H., Yang, W.X., Bhowmick, N.A., Frelix, G., Shappell, S., and Chen, Y.H. (2009). Identification of extracellular delta-catenin accumulation for prostate cancer detection. *Prostate*, *69*, 411-418.
- Mackie, S., and Aitken, A. (2005). Novel brain 14-3-3 interacting proteins involved in neurodegenerative disease. *FEBS J*, *272*, 4202-4210.
- Makrilia, N., Kollias, A., Manolopoulos, L., and Syrigos, K. (2009). Cell adhesion molecules: role and clinical significance in cancer. *Cancer Invest*, *27*, 1023-1037.
- Martinez, M.C., Ochiishi, T., Majewski, M., and Kosik, K.S. (2003). Dual regulation of neuronal morphogenesis by a delta-catenin-cortactin complex and Rho. *J Cell Biol*, *162*, 99-111.
- Mathupala, S.P., Ko, Y.H., and Pedersen, P.L. (2006). Hexokinase II: Cancer's double-edged sword acting as both facilitator and gatekeeper of malignancy when bound to mitochondria. *Oncogene*, *25*, 4777-4786.
- McCrea, P.D., and Park, J.I. (2007). Developmental functions of the p120-catenin sub-family. *Biochim Biophys Acta*, *1773*, 17-33.
- McNeal, J.E. (1988). Normal histology of the prostate. *Am J Surg Pathol*, *12*, 619-633.
- Medina, M., Marinescu, R.C., Overhauser, J., and Kosik, K.S. (2000). Hemizyosity of delta-catenin (CTNND2) is associated with severe mental retardation in cri-du-chat syndrome. *Genomics*, *63*, 157-164.
- Mikuz, G. (1997). Pathology of prostate cancer. Old problems and new facts. *Adv Clin Path*, *1*, 21-34.
- Munoz, J.P., Huichalaf, C.H., Orellana, D., and Maccioni, R.B. (2007). Cdk5 modulates beta- and delta-catenin/Pin1 interactions in neuronal cells. *J Cell Biochem*, *100*, 738-749.
- Nopparat, J., Zhang, J., Lu, J.P., Chen, Y.H., Zheng, D., Neuffer, D., Fan, J., Hong, H., Boykin, C., and Lu, Q. (2014).  $\delta$ -Catenin, a Wnt/ $\beta$ -Catenin modulator, reveals inducible mutagenesis promoting cancer cell survival adaptation and metabolic reprogramming. *Oncogene*. In press.
- Ochiishi, T., Futai, K., Okamoto, K., Kameyama, K., and Kosik, K.S. (2008). Regulation of AMPA receptor trafficking by delta-catenin. *Mol Cell Neurosci*, *39*, 499-507.

- Oh, M., Kim, H., Yang, I., Park, J.H., Cong, W.T., Baek, M.C., Bareiss, S., Ki, H., Lu, Q., No, J., Kwon, I., Choi, J.K., and Kim, K. (2009). GSK-3 phosphorylates delta-catenin and negatively regulates its stability via ubiquitination/proteasome-mediated proteolysis. *J Biol Chem*, 284, 28579-28589.
- Paffenholz, R., and Franke, W.W. (1997). Identification and localization of a neurally expressed member of the plakoglobin/armadillo multigene family. *Differentiation*, 61, 293-304.
- Pan, Y., Lui, W.O., Nupponen, N., Larsson, C., Isola, J., Visakorpi, T., Bergerheim, U.S., and Kytola, S. (2001). 5q11, 8p11, and 10q22 are recurrent chromosomal breakpoints in prostate cancer cell lines. *Genes Chromosomes Cancer*, 30, 187-195.
- Papadopoulos, N., Kinzler, K.W., and Vogelstein, B. (2006). The role of companion diagnostics in the development and use of mutation-targeted cancer therapies. *Nat Biotechnol*, 24, 985-995.
- Paredes, J., Correia, A.L., Ribeiro, A.S., Albergaria, A., Milanezi, F., and Schmitt, F.C. (2007). P-Cadherin expression in breast cancer: a review. *Breast Cancer Res*, 9, 214.
- Patiar, S., and Harris, A.L. (2006). Role of hypoxia-inducible factor-1alpha as a cancer therapy target. *Endocr Relat Cancer*, 1, S61-75.
- Peifer, M., Pai, L.M., and Casey, M. (1994). Phosphorylation of the Drosophila adherens junction protein Armadillo: roles for wingless signal and zeste-white 3 kinase. *Dev Biol*, 166, 543-556.
- Podar, K., and Anderson, K.C. (2010). A therapeutic role for targeting c-Myc/HIF-1-dependent signaling pathways. *Cell cycle*, 9, 1722-1728.
- Poon, E., Harris, A.L., and Ashcroft, M. (2009). Targeting the hypoxia-inducible factor (HIF) pathway in cancer. *Expert Rev Mol Med*, 11, e26.
- Poore, C.P., Sundaram, J.R., Pareek, T.K., Fu, A., Amin, N., Mohamed, N.E., Zheng, Y.L., Goh, A.X., Lai, M.K., Ip, N.Y., Pant, H.C., and Kesavapany, S. (2010). Cdk5-mediated phosphorylation of delta-catenin regulates its localization and GluR2-mediated synaptic activity. *J Neurosci*, 30, 8457-8467.
- Powis, G., and Kirkpatrick, L. (2004). Hypoxia inducible factor-1alpha as a cancer drug target. *Mol Cancer Ther*, 3, 647-654.
- Reynolds, A.B., and Carnahan, R.H. (2004). Regulation of cadherin stability and turnover by p120ctn: implications in disease and cancer. *Semin Cell Dev Biol*, 15, 657-663.
- Rios-Doria, J., Day, K.C., Kuefer, R., Rashid, M.G., Chinnaiyan, A.M., Rubin, M.A., and Day, M.L. (2003). The role of calpain in the proteolytic cleavage of E-cadherin in prostate and mammary epithelial cells. *J Biol Chem*, 278, 1372-1379.

- Rodova, M., Kelly, K.F., VanSaun, M., Daniel, J.M., and Werle, M.J. (2004). Regulation of the rapsyn promoter by Kaiso and delta-catenin. *Mol Cell Biol*, *24*, 7188-7196.
- Saramaki, O.R., Savinainen, K.J., Nupponen, N.N., Bratt, O., and Visakorpi, T. (2001). Amplification of hypoxia-inducible factor 1alpha gene in prostate cancer. *Cancer Genet Cytogenet*, *128*, 31-34.
- Shappell, S.B., Thomas, G.V., Roberts, R.L., Herbert, R., Ittmann, M.M., Rubin, M.A., Humphrey, P.A., Sundberg, J.P., Rozengurt, N., Barrios, R., Ward, J.M., and Cardiff, R.D. (2004). Prostate pathology of genetically engineered mice: definitions and classification. The consensus report from the Bar Harbor meeting of the Mouse Models of Human Cancer Consortium Prostate Pathology Committee. *Cancer Res*, *64*, 2270-2305.
- Shen, M.M., and Abate-Shen, C. (2007). Pten inactivation and the emergence of androgen-independent prostate cancer. *Cancer Res*, *67*, 6535-6538.
- Shen, M.M., and Abate-Shen, C. (2010). Molecular genetics of prostate cancer: new prospects for old challenges. *Genes Dev*, *24*, 1967-2000.
- Silverman, J.B., Restituto, S., Lu, W., Lee-Edwards, L., Khatri, L., and Ziff, E.B. (2007). Synaptic anchorage of AMPA receptors by cadherins through neural plakophilin-related arm protein AMPA receptor-binding protein complexes. *J Neurosci*, *27*, 8505-8516.
- Tanahashi, H., and Tabira, T. (1999). Isolation of human delta-catenin and its binding specificity with presenilin 1. *Neuroreport*, *10*, 563-568.
- Vander Heiden, M.G., Cantley, L.C., and Thompson, C.B. (2009). Understanding the Warburg effect: the metabolic requirements of cell proliferation. *Science*, *324*, 1029-1033.
- Vogelstein, B., and Kinzler, K.W. (2004). Cancer genes and the pathways they control. *Nat Med*, *10*, 789-799.
- Wang, J., Kim, J., Roh, M., Franco, O.E., Hayward, S.W., Wills, M.L., and Abdulkadir, S.A. (2010). Pim1 kinase synergizes with c-MYC to induce advanced prostate carcinoma. *Oncogene*, *29*, 2477-2487.
- Wang, T., Chen, Y.H., Hong, H., Zeng, Y., Zhang, J., Lu, J.P., Jeansonne, B., and Lu, Q. (2009). Increased nucleotide polymorphic changes in the 5'-untranslated region of delta-catenin (CTNND2) gene in prostate cancer. *Oncogene*, *28*, 555-564.
- Warburg, O. (1956). Origin of cancer cells. *Science*, *123*, 309-314.
- Westbrook, T.F., Martin, E.S., Schlabach, M.R., Leng, Y.M., Liang, A.C., Feng, B., Zhao, J.J., Roberts, T.M., Mandel, G., Hannon, G.J., DePinho, R.A., Chin, L., and Elledge, S.J.

- (2005). A genetic screen for candidate tumor suppressors identifies REST. *Cell*, *121*, 837-848.
- Wildenberg, G.A., Dohn, M.R., Carnahan, R.H., Davis, M.A., Lobdell, N.A., Settleman, J., and Reynolds, A.B. (2006). p120-Catenin and p190RhoGAP regulate cell-cell adhesion by coordinating antagonism between Rac and Rho. *Cell*, *127*, 1027-1039.
- Willert, K., and Jones, K.A. (2006). Wnt signaling: is the party in the nucleus? *Genes Dev*, *20*, 1394-1404.
- Wilson, K.F., Erickson, J.W., Antonyak, M.A., and Cerione, R.A. (2013). Rho GTPases and their roles in cancer metabolism. *Trends Mol Med*, *19*, 74-82.
- Wolf, A., Keil, R., Gotzl, O., Mun, A., Schwarze, K., Lederer, M., Huttelmaier, S., and Hatzfeld, M. (2006). The armadillo protein p0071 regulates Rho signalling during cytokinesis. *Nat Cell Biol*, *8*, 1432-1440.
- Wu, M., Neilson, A., Swift, A.L., Moran, R., Tamagnine, J., Parslow, D., Armistead, S., Lemire, K., Orrell, J., Teich, J., Chomicz, S., and Ferrick, D.A. (2007). Multiparameter metabolic analysis reveals a close link between attenuated mitochondrial bioenergetic function and enhanced glycolysis dependency in human tumor cells. *Am J Physiol Cell Physiol*, *292*, C125-C136.
- Yang, I., Chang, O., Lu, Q., and Kim, K. (2010). Delta-catenin affects the localization and stability of p120-catenin by competitively interacting with E-cadherin. *Mol Cells*, *29*, 233-237.
- Yeung, S.J., Pan, J., and Lee, M.H. (2008). Roles of p53, MYC and HIF-1 in regulating glycolysis - the seventh hallmark of cancer. *Cell Mol Life Sci*, *65*, 3981-3999.
- Yu, X., Wang, Y., DeGraff, D.J., Wills, M.L., and Matusik, R.J. (2011). Wnt/beta-catenin activation promotes prostate tumor progression in a mouse model. *Oncogene*, *30*, 1868-1879.
- Yuan, H., Perry, C.N., Huang, C.Q., Iwai-Kanai, E., Carreira, R.S., Glembotski, C.C., and Gottlieb, R.A. (2009). LPS-induced autophagy is mediated by oxidative signaling in cardiomyocytes and is associated with cytoprotection. *Am J Physiol Heart Circ Physiol*, *296*, 470-479.
- Yun, J.Y., Rago, C., Cheong, I., Pagliarini, R., Angenendt, P., Rajagopalan, H., Schmidt, K., Willson, J.K.V., Markowitz, S., Zhou, S.B., Diaz, L.A., Velculescu, V.E., Lengauer, C., Kinzler, K.W., Vogelstein, B., and Papadopoulos, N. (2009). Glucose Deprivation Contributes to the Development of KRAS Pathway Mutations in Tumor Cells. *Science*, *325*, 1555-1559.

- Zeng, Y., Abdallah, A., Lu, J.P., Wang, T., Chen, Y.H., Terrian, D.M., Kim, K., and Lu, Q. (2009). Delta-catenin promotes prostate cancer cell growth and progression by altering cell cycle and survival gene profiles. *Mol Cancer*, 8, 19.
- Zhang, J., Chen, Y.H., and Lu, Q. (2010a). Pro-oncogenic and anti-oncogenic pathways: opportunities and challenges of cancer therapy. *Future Oncol*, 6, 587-603.
- Zhang, J., Lu, J.P., Suter, D.M., Krause, K.H., Fini, M.E., Chen, B., and Lu, Q. (2010b). Isoform- and dose-sensitive feedback interactions between paired box 6 gene and delta-catenin in cell differentiation and death. *Exp Cell Res*, 316, 1070-1081.
- Zhang, J.Y., Wang, Y., Zhang, D., Yang, Z.Q., Dong, X.J., Jiang, G.Y., Zhang, P.X., Dai, S.D., Dong, Q.Z., Han, Y., Zhang, S., Cui, Q.Z., and Wang, E.H. (2010c). Delta-catenin promotes malignant phenotype of non-small cell lung cancer by non-competitive binding to E-cadherin with p120ctn in cytoplasm. *J Pathol*, 222, 76-88.
- Zhang, Q., Bai, X., Chen, W., Ma, T., Hu, Q., Liang, C., Xie, S., Chen, C., Hu, L., Xu, S., and Liang, T. (2013). Wnt/beta-catenin signaling enhances hypoxia-induced epithelial-mesenchymal transition in hepatocellular carcinoma via crosstalk with HIF-1alpha signaling. *Carcinogenesis*, 34, 962-973.
- Zheng, M., Simon, R., Mirlacher, M., Forster, T., Diener, P.A., Mihatsch, M.J., Sauter, G., and Schraml, P. (2004). TRIO amplification and abundant mRNA expression is associated with invasive tumor growth and rapid tumor cell proliferation in urinary bladder cancer. *Am J Pathol*, 165, 63-69.
- Zhou, J., Liyanage, U., Medina, M., Ho, C., Simmons, A.D., Lovett, M., and Kosik, K.S. (1997). Presenilin 1 interaction in the brain with a novel member of the Armadillo family. *Neuroreport*, 8, 2085-2090.

## APPENDIX A: Animal use protocol



Animal Care and  
Use Committee

212 Ed Warren Life  
Sciences Building  
East Carolina University  
Greenville, NC 27834

252-744-2436 office  
252-744-2355 fax

October 16, 2012

Qun Lu, Ph.D.  
Department of Anatomy  
Brody 7N-100  
ECU Brody School of Medicine

Dear Dr. Lu:

Your Animal Use Protocol entitled, "Studies of Delta-Catenin Function Using Gene Targeting Approaches" (AUP #A173b) was reviewed by this institution's Animal Care and Use Committee on 10/16/12. The following action was taken by the Committee:

"Approved as submitted"

**\*Please contact Dale Aycock at 744-2997 prior to hazard use\***

A copy is enclosed for your laboratory files. Please be reminded that all animal procedures must be conducted as described in the approved Animal Use Protocol. Modifications of these procedures cannot be performed without prior approval of the ACUC. The Animal Welfare Act and Public Health Service Guidelines require the ACUC to suspend activities not in accordance with approved procedures and report such activities to the responsible University Official (Vice Chancellor for Health Sciences or Vice Chancellor for Academic Affairs) and appropriate federal Agencies.

Sincerely yours,

A handwritten signature in cursive script that reads 'S. McRae'.

Susan McRae, Ph.D.  
Chair, Animal Care and Use Committee

SM/jd

enclosure

## APPENDIX B: Permission policy from NPG



RightsLink®

Home

Account Info

Help



**Title:** -Catenin, a Wnt-catenin modulator, reveals inducible mutagenesis promoting cancer cell survival adaptation and metabolic reprogramming

**Author:** J Nopparat, J Zhang, J-P Lu, Y-H Chen, D Zheng, P D Neufer, J M Fan, H Hong, C Boykin, Q Lu

**Publication:** Oncogene

**Publisher:** Nature Publishing Group

**Date:** Apr 14, 2014

Logged in as:  
Jongdee Nopparat  
Account #:  
3000779423

LOGOUT

Copyright © 2014, Rights Managed by Nature Publishing Group

### Author Request

If you are the author of this content (or his/her designated agent) please read the following. If you are not the author of this content, please click the Back button and select an alternative [Requestor Type](#) to obtain a quick price or to place an order.

Ownership of copyright in the article remains with the Authors, and provided that, when reproducing the Contribution or extracts from it, the Authors acknowledge first and reference publication in the Journal, the Authors retain the following non-exclusive rights:

- To reproduce the Contribution in whole or in part in any printed volume (book or thesis) of which they are the author(s).
- They and any academic institution where they work at the time may reproduce the Contribution for the purpose of course teaching.
- To reuse figures or tables created by them and contained in the Contribution in other works created by them.
- To post a copy of the Contribution as accepted for publication after peer review (in Word or Text format) on the Author's own web site, or the Author's institutional repository, or the Author's funding body's archive, six months after publication of the printed or online edition of the Journal, provided that they also link to the Journal article on NPG's web site (eg through the DOI).

NPG encourages the self-archiving of the accepted version of your manuscript in your funding agency's or institution's repository, six months after publication. This policy complements the recently announced policies of the US National Institutes of Health, Wellcome Trust and other research funding bodies around the world. NPG recognises the efforts of funding bodies to increase access to the research they fund, and we strongly encourage authors to participate in such efforts.

Authors wishing to use the published version of their article for promotional use or on a web site must request in the normal way.

If you require further assistance please read NPG's online [author reuse guidelines](#).

For full paper portion: Authors of original research papers published by NPG are encouraged to submit the author's version of the accepted, peer-reviewed manuscript to their relevant funding body's archive, for release six months after publication. In addition, authors are encouraged to archive their version of the manuscript in their institution's repositories (as well as their personal Web sites), also six months after original publication.

v2.0

